HISTORY MATCHING PRESSURE

RESPONSE FUNCTIONS FROM PRODUCTION DATA

A Dissertation

by

MAZHER HASSAN IBRAHIM

Submitted to the Office of Graduate Studies of
Texas A&M University
in partial fulfillment of the requirements for the degree of

DOCTOR OF PHILOSOPHY

December 2004

Major Subject: Petroleum Engineering

HISTORY MATCHING PRESSURE

RESPONSE FUNCTIONS FROM PRODUCTION DATA

A Dissertation

by

MAZHER HASSAN IBRAHIM

Submitted to Texas A&M University
in partial fulfillment of the requirements
for the degree of

DOCTOR OF PHILOSOPHY

Approved as to style and content by:

_____
Robert A. Wattenbarger
(Chair of Committee)

_____
Richard A. Startzman
(Member)

_____
J. Bryan Maggard
(Member)

_____
Jianxin Zhou
(Member)

_____
Stephen A. Holditch
(Head of Department)

December 2004

Major Subject: Petroleum Engineering

ABSTRACT

History Matching Pressure

Response Functions from Production Data. (December 2004)

Mazher Hassan Ibrahim, B.S., Suez Canal University, Egypt;

M.S., Suez Canal University, Egypt

Chair of Advisory Committee: Dr. Robert A. Wattenbarger

This dissertation presents several new techniques for the analysis of the long-term production performance of tight gas wells. The main objectives of this work are to determine pressure response function for long-term production for a the slightly compressible liquid case, to determine the original gas in place (OGIP) during pseudosteady state (*PSS*), to determine OGIP in the transient period, and to determine the effects of these parameters on linear flow in gas wells.

Several methods are available in the industry to analyze the production performance of gas wells. One common method is superposition time. This method has the advantage of being able to analyze variable-rate and variable-pressure data, which is usually the nature of field data. However, this method has its shortcomings.

In this work, simulation and field cases illustrate the shortcomings of superposition. I present a new normalized pseudotime plotting function for use in the superposition method to smooth field data and more accurately calculate OGIP. The use of this normalized pseudotime is particularly important in the analysis of highly depleted reservoirs with large change in total compressibility where the superposition errors are largest.

The new tangent method presented here can calculate the OGIP with current reservoir properties for both constant rate and bottomhole flowing pressure (p_{wf}) production.

In this approach pressure-dependent permeability data can be integrated into a modified real gas pseudopressure, $\widetilde{m}(p)$, which linearizes the reservoir flow equations and provides correct values for permeability and skin factor. But if the customary real-gas pseudopressure, $m(p)$ is used instead, erroneous values for permeability and skin factor will be calculated. This method uses an exponential equation form for permeability vs. pressure drop.

Simulation and field examples confirm that the new correction factor for the rate dependent problem improves the linear model for both *PSS* and transient period, whether plotted on square-root of time or superposition plots.

DEDICATION

To my wife, Shimaa Ahmed, for her patience and support…to my mother and my father for their love, encouragement, and support….for my brothers and sisters for their encouragement.

ACKNOWLEDGMENTS

The author wishes to express his sincere appreciation to Dr. Robert A. Wattenbarger, chair of the advisory committee, for his valuable guidance, intellectual contributions, and his patience in helping bring this research to completion. Dr. Wattenbarger spent endless hours with the author discussing and correcting the directions of his work. Dr. Wattenbarger diligently and meticulously reviewed and corrected each and every piece of the work and continuously added his fresh and great ideas and experience to the final product. Whatever words are used to express thanks to Dr. Wattenbarger they are not enough.

The author wishes also to thank Dr. R.A. Startzman and Dr. Bryan Maggard for serving as members of the advisory committee and for their advice to produce the dissertation in this form.

The author wishes also to thank Dr. Jianxin Zhou for serving as a member of the advisory committee and for his contributions in correcting the dissertation contents.

The author also is grateful to his father, Hassan Ibrahim, his mother, Fathia Ahmed, his wife, Shimaa Ahmed, and his two babies, Mohand and Mostafa. He has been able to finish his studies and his research only through their understanding and continuous encouragement.

TABLE OF CONTENTS

LIST OF TABLES

LIST OF FIGURES

CHAPTER I

INTRODUCTION

Problem Description

Tight gas reservoirs are those with permeability less than 0.1 md. Tight gas reservoirs are usually found in deeper formations with high initial reservoir pressure, which assists gas production through the low permeability reservoir. Higher initial reservoir pressure gives lower values of B_g, which translates into a large quantity of gas at surface conditions. The low viscosity of gas (μ_g) leads to high mobility ratio (k/μ_g), which also helps the gas flow easily through the reservoir. Economic exploitation of tight gas reservoirs requires large amounts of original gas in place, which requires large areal expanse of reservoir and thick net pays. The most common method to determine these reservoir parameters is from long-term production data.

Pressure transient testing is an excellent method for determining reservoir characteristics under normal *in-situ* conditions. However, in tight gas reservoirs pressure transient testing can be unreliable and impractical. These gas reservoirs frequently require months or years to reach the middle, late-transient, or boundary-dominated flow periods.

Instead long-term production data can be used to analyze tight gas reservoirs. Production analysis in tight gas reservoirs allows an estimation of the following information: formation conductivity, *kh*, formation damage; earlier flow effect; permeability-thickness $\sqrt{k}\,A_C$ product, permeability of the formation, *k*, cross-sectional area to flow, A_c, drainage distance investigated, y_{inv}, drainage area, *A*; formation volume, *FV*; pore volume, V_p; original gas in place, and OGIP.

This dissertation follows the style of *SPE Reservoir Evaluation & Engineering.*

An accurate and dependable method used to analyze production performance of gas wells is superposition time. This method has the advantage of being able to analyze variable-rate and variable-pressure data, which is usually the nature of field data. However, this method has its shortcomings. Simulation and field cases used to illustrate the shortcomings of the superposition method to analyze long-term production data in transient linear flow and the pseudosteady state (*PSS)* period to calculate accurate reservoir parameters.

The linear flow regime generally associated with tight gas reservoirs is defined as flow for which the cross-sectional area to flow is perpendicular to the flow paths and has a constant area. Linear flow in tight gas reservoirs may be occur under conditions of, anisotropy, linear or elongated reservoirs (channel sands, bar sands), high-permeability streaks, hydraulic fractures, and natural fractures, therefore linear flow analysis is important in determining reservoir parameters like $\sqrt{k}A_C$, k, A_c, y_{inv}, A, V_p, OGIP, and reserves.

Arévalo[1-3] modified the constant-rate and p_{wf} equations to match the actual value of OGIP in simulation models but he did not mention the reason for the error in these equations. To identify the source of error, we investigated the effect of different values of drawdown pressures on linearity of the plot of the square root of time $\sqrt{t}$; and superposition time for long-term production. Our equation will correct the plot for each method.

Objectives and Procedures

The objectives of this research are:

(1)   To present a new method for determing the pressure response function for long-term oil production by using superposition.

(2)   To use simulation and field cases to review and compare the application of the superposition method and illustrate its shortcomings.

(3)   To present a new normalized pseudotime to smooth field data and more accurately calculate OGIP.

(4)   To present a new normalized pseudotime and superposition to calculate OGIP for variable rate and pressures for gas wells.

(5)   To present a new tangent method to calculate the OGIP with current reservoir properties for both constant-rate and bottomhole flowing pressure production.

(6)   To present the parameters affecting on the non linearity of rectilinear flow in gas wells.

(7)   To present a new correction factor equation to correct the effect of drawdown on the accuarcy of the slope in plot of $\sqrt{t}$ and superposition time.

Reservoir simulation techniques are used in combination with analytical and field data to achieve our objectives.

Organization of This Dissertation

The outline and organization of this dissertation are as follows:

I begin my work in the introductory Chapter I, in which I present the objectives and deliverables of this research.

In Chapter II, I present a comprehensive literature review describing the technology of determining OGIP, decline-curve, linear-flow and superposition methods.

In Chapter III, I present the shortcomings of the superposition method through analysis of simulation cases for oil wells.

In Chapter IV, I discuss the determining of OGIP at *PSS*. We present new equation for determining OGIP with current properties for constant-rate and pressure production. Also, we present a new normalized pseudotime and superposition equation use in calculating OGIP accurately.

In Chapter V, I discuss ways to determine OGIP at *PSS* including permeability-dependent pressure. We update the pseudotime equation for determining OGIP with current properties for constant-rate and pressure production.

In Chapter VI, I discuss the parameters affecting the non linearity problem in constant-p_{wf} production for the $\sqrt{t}$ plot and superposition time plot. A correction factor will adjust for the two plots at each drawdown value, which will correct the effect of non linearity.

In Chapter VII, I use the methods developed in Chapter III, Chapter IV, and V to analyze and interpret production data from field data in producing gas wells. I estimate the accurate reservoir properties and show validation of our by using numerical simulation.

In Chapter VIII, I present summary, conclusions, and some recommendations for future research work.

Finally, I present the nomenclature, references, and some appendixes developed in this research.

CHAPTER II

LITERATURE REVIEW

Determination of OGIP

If the average reservoir pressure is known from field measurements, a plot of p/z versus cumulative gas production (G_p) is the commonly accepted method used to obtain OGIP in closed gas reservoirs.[4, 5] A straight line is fitted to the data, and OGIP is determined from the material balance equation:

$$\frac{\bar{p}}{z}[1 - \frac{\Delta p\,(C_f + C_w\,S_{wi})}{(1 - S_{wi})}] = \frac{p_i}{z_i}\,(1 - \frac{G_p}{OGIP}) \ \dots\dots\dots\dots\dots\dots\dots\dots\dots\dots\dots\dots\dots\dots \text{(2.1)}$$

But we do not usually know the average reservoir pressure in tight gas reservoirs because of the long transient periods. So we try to estimate OGIP from long-term production data (flow rates, and wellbore flowing pressure).

The superposition time function has been used as a tool to analyze variable flow rate[6] without knowing the average reservoir pressure. The superposition time is given by

$$\frac{[m(p_i) - m(p_{wf})]}{q_{gn}} = \tilde{m}_{PSS}\,[\sum_{i=1}^{n}\frac{\Delta q_{gi}}{q_{gn}}(t_n - t_{i-1})] + b \ \dots\dots\dots\dots\dots\dots\dots\dots\dots \text{(2.2)}$$

The slope ($\tilde{m}_{PSS}$) from plotting $\dfrac{[m(p_i) - m(p_{wf})]}{q_g}$ vs. Superposition time is used to determine the OGIP by

$$OGIP = \frac{2 p_i\,S_{gi}}{z_i\,(\mu_g c_t)_i}\left(\frac{1}{\tilde{m}_{PSS}}\right) \ \dots\dots\dots\dots\dots\dots\dots\dots\dots\dots\dots\dots \text{(2.3)}$$

Where $m(p) = 2\displaystyle\int_{p_o}^{p}\frac{p}{\mu_g z}\,dp$ is the real gas pseudopressure defined by Al-Hussainy and Ramey.[7]

Note that initial properties are used in Eq. 2.3.

Blasingame and Lee[8] introduced a plotting variable called material balance time to account for variation in rate:

$$\tilde{t} = \frac{G_p}{q_g} \qquad \text{.. (2.4)}$$

This is exactly the same as the superposition time as shown in Appendix C. Agarwal[9] and Lee and Holditch[10] used pseudotime to linearize the transient analysis of gas wells with massive hydraulic fracture. They considered variations of gas viscosity and compressibility as functions of p_{wf}. Their pseudotime was defined as

$$t_a = \int_0^t \frac{1}{\mu(p_{wf}) c_t(p_{wf})} dt \qquad \text{.. (2.5)}$$

Fraim and Wattenbarger[11] proposed an iterative procedure using the OGIP to predict average reservoir-pressure. They used a normalized pseudotime function to take into account the variation of gas properties and provide an exponential decline behavior for gas wells produced at a constant-p_{wf} production. Their normalized pseudotime was defined as

$$t_n = (\mu c_t)_i \int_0^t \frac{1}{\mu(\bar{p}) c_t(\bar{p})} dt \qquad \text{.. (2.6)}$$

Palacio and Blasingame[12] developed normalized pseudotime to account for rate change and calculate OGIP from the decline-curve match, which is based on Eq. 2.6 as follows:

$$\tilde{t}_a = \frac{(\mu c_t)_i}{q_g} \int_0^t \frac{q_g}{\mu(\bar{p}) c_t(\bar{p})} dt \qquad \text{.. (2.7)}$$

In the present work, we examine the shortcoming of using superposition time and Eq. 2.3 with initial properties to calculate the OGIP. It appears that, regardless of the flow regimes exhibited by the well/reservoir system, the reservoir properties change with pressure. If the cumulative production increased by more than 10%, the superposition time plot becomes non linear, and OGIP from Eq. 2.3 can have error more than 300%. To correct this error, we include the change in reservoir properties. We also will include the change in porosity with average reservoir pressure. The change in porosity as the pressure changes can be significant especially in high-pressure gas reservoirs with high compressibility. These changes can cause error in calculating OGIP.

Decline Type Curve Analysis

Decline-curve analysis is frequently used to predict future performance when minimal data are available to analyze rate/time performance of oil and gas wells. The most popular method for this analysis is the empirical Arps[13] decline curve, which fits production rate decline when boundary effects dominate, primarily in high permeability oil and gas wells.

Fetkovich[14] presented a log-log type curve for decline-curve analysis of wells in a closed radial reservoir. He combined the analytical solution for transient radial flow (for early times) with the Arps boundary-dominated decline curves (for later times). The Fetkovich type curve includes curves for values of b from 0 to 1, corresponding the Arps' b parameter (b = 0 is exponential decline, $b > 0$ is hyperbolic decline). He showed that type curve analysis can be used very effectively when both transient and boundary-dominated effects are present in the rate/time data.

Slider[15] published a new type-curve-matching procedure based on a semi-log analysis approach to extrapolate production rate. He used a practical curve-fitting process based on Arp's equations. Slider's approach is more direct and uniform than Arp's expressions as regression relations. A disadvantage is that Slide's procedure needs a significant amount data preparation.

Gentry[16] developed a new set of type curves that simplify the solution and give a confident extrapolation of production decline. This approach gave us an effective graphical method for solving all types of production decline curves (harmonic, hyperbolic, and exponential).

Nind[17] presented graphical plotting functions that allowed unique straight-line relations for the hyperbolic decline-curve family (with the exception of the exponential case). Nind's approach is essentially a graphical regression of the Arps equations.

Maley[18] presented decline-curve equations that can be used to give accurate and theoretically valid projections for tight gas reservoirs. He used a hyperbolic equation with b value higher than one to study gas production data. He concluded that in the standard decline equations the hyperbolic equation is a better estimator that $\sqrt{t}$ plots in the cases he analyzed. He explained that a b value of two and decline factor of 0.5/month give approximately a linear flow decline.

Fetkovich *et al.*[19] presented field data from oil and gas wells to illustrate the use of the decline type curve analysis technique. This procedure has become a classic mechanism for the analysis of production data to estimate reservoir properties and to forecast rate. The authors concluded that the analysis of transient-flow production data is not possible using the Arps hyperbolic equations, since the Arps equations imply that the system is in depletion and that transient flow data should never be used to estimate reservoir volumes (as this practice generally gives optimistic forecasts). They suggested that reservoir volume in relation to related flow characteristics should not be estimated using decline curve-type-analysis techniques prior to the development of boundary-dominated flow.

Fraim and Wattenbarger[11] proposed an iterative procedure using the OGIP to predict average reservoir pressure calculations. They used a pseudotime function to take into account the variation of gas properties and provide an exponential decline behavior for gas wells produced at a constant p_{wf}. The normalized pseudopressure and pseudotime functions linearize the gas diffusivity equation, which then yields liquid flow behavior (i.e., an exponential decline during boundary-dominated flow). These pseudofunctions of pressure and time provide a procedure to analyze gas production data. The pseudotime function for this case is based on average reservoir pressure. Then an initial estimation of OGIP is required to initiate the pseudotime calculation. Refinement of the OGIP estimation occurs in the matching of production data onto the liquid type curve. After, we estimate the best OGIP, we calculate the correct pseudotime function, and hence the gas flow problem is treated like the liquid case.

Blasingame and Lee[20] developed a new theoretical approach for predicting reservoir drainage area size and shape from a well producing a single-phase liquid of small and constant compressibility at any flow rate condition. The approach uses a Cartesian plot of pressure drop/rate versus a material balance-time function (cumulative production/flow rate) where these functions yield a straight-line trend in which the slope and intercept would be used to calculate the pore volume of the reservoir and the shape factor. The model can be used for analyzing field production data that are influenced by arbitrary changes in p_{wf} and flow rate. The model is valid for boundary-dominated flow as long as changes in flow rates are relatively continuous. The authors showed the practical application of this new method to a wide range of variable-rate scenarios for wells in bounded reservoirs.

Blasingame and Lee[21] adapted their reservoir limits testing technique[20] to the general case of variable-rate/variable-pressure data from gas wells. In this case, they linearized the gas diffusivity equation using adequate pseudotime and pseudopressure functions. The procedure is similar to the material-balance time function in the liquid case where the pseudotime function also included a variable-rate term. Similar to Fraim and Wattenbarger[8] work, Blasingame and Lee's method requires the estimation of average reservoir pressure to calculate the pseudotime function. This average reservoir pressure is evaluated using an iterative procedure in which the OGIP is estimated and the pseudotime function is verified using an average reservoir pressure computed from the new estimate of OGIP. Theoretically, this method is only applicable after the initial pressure transient has reached the outer boundary of the reservoir. However, they suggested that the calculated average pressure profile may also be valid for analyzing transient gas flow data when numerical simulation is used.

Blasingame, McCray, and Lee[22] developed an approach for the analysis of production decline data where the p_{wf} varies significantly as a function of time. They tried to create an equivalent constant pressure analysis formulation (a constant pressure analog time function that could be used for the analysis of variable rate/variable pressure

drop production data). Their work used recursion-type formulas to transform variable-rate data into the constant pressure solution profile for the boundary-dominated flow condition. However, they found that these recursion formulas tend to break down when significant data noise is present.

Linear Flow Regime

Long-term linear behavior has been detected in almost all tight basins that produce gas in low permeability reservoirs.[23-35] Causes of linear flow in tight gas reservoirs are numerous: linear reservoirs; high-permeability streaks; wells between two no-flow boundaries; transient dual-porosity behavior for radial reservoirs; wells intercepted by vertical, horizontal, or diagonal fractures; horizontal wells; and horizontal wells with fractures.

Muskat[36] discussed steady-state single-phase and multiphase linear flow systems and their pressure distribution. He also showed linear flow geometries in terms of core analysis and line derive networks applied to secondary recovery.

Miller[37] gave solutions for linear flow in infinite-acting and bounded aquifers for both the constant-rate and constant-pressure solutions.

Nabor and Barham[38] generalized Miller's solutions using dimensionless variables and derived solutions for the constant-pressure outer-boundary case. In linear heat conduction, Carslaw and Jaeger[39] presented the mathematics for these solutions.

El-Banbi[23] investigated the literature and found that some authors did not use correct equations in analyzing data under constant flowing bottomhole pressure. He observed that analytical solutions for constant bottomhole flowing pressure production and constant-rate production are not the same. They mentioned that only a constant-rate production equation in gas well is well known. Then, they adapted the linear solutions of Miller[37] and Nabor and Barham[38] for fractured wells in a rectangular geometry for both the constant-rate and constant-pressure cases for linear flow in a rectangle. The authors

developed correct transient and stabilized linear equations plus infinite series solution and a methodology for estimating $\sqrt{k}\,A_c$ product and original gas in place, OGIP, for tight gas reservoirs.

El-Banbi and Wattenbarger[26] presented a practical approach to analyze both pressure (well-testing) and production (decline-curve-analysis) data, which are influenced by linear flow. They pointed out that constant-rate solutions are different from the constant-pressure solution and the use of wrong equations in the analysis of tight gas wells may result in errors as high as 60%. They also showed the application of techniques in analyzing field production data.

Helmy[40, 41] developed different methods for analyzing the performance of wells producing at constant flowing bottomhole pressure from tight gas reservoirs exhibiting linear flow and subjected to periodic shut-ins.

Hale and Evers[42] used numerical simulation to achieve type curves for vertically fractured wells producing at constant rate or constant flowing bottomhole pressure. The fracture was considered elliptical in shape. They used elliptical flow equations to study the production data. They concluded that a single group of elliptical equations properly models tight-gas wells when flow is linear, radial, or transitional between those two systems. They also showed that the group of constant-pressure equations is different from the group of constant-rate equations. The authors also showed two field cases where linear flow occurred for 3 and 5 years respectively; commenting that several tight gas wells in Wyoming exhibited linear flow for years.

Kohlhaas and Abbott[24] explained that linear flow conditions develop early in the life of a well that has been hydraulically fractured. This early linear-flow regime is followed by early radial flow. Then, late-linear flow may develop depending upon configurations of reservoir geometry. They developed techniques for analyzing spherical and linear flow and suggested that the pressure data should be graphed in different plots to help identify and recognize the different flow regimes.

Stright and Gordon[25] described long-term linear performance on tight gas wells in the Picenace basin, which did not have particularly large fracture treatments. They observed that this linear flow behavior for many years indicates that fracture lengths are much longer than would be expected from hydraulic fracturing treatments. They determined that if a log-log diagnostic plot of gas production, q_g versus t for the first one or two years of production has a half slope, then an $\sqrt{t}$ extrapolating technique would be used for q_g forecasting. They suggested that boundary-dominated effects can be represented by an exponential decline curve.

Hale[30] used different decline equations to analyze the production data of more than 6,000 gas wells in tight formations. The wells studied are in the Rocky Mountains, ranging from the Green River Basin of Wyoming to the San Juan Basin of New Mexico. Most of these wells are in tight gas reservoirs that have been hydraulically fractured and many exhibited long-term linear flow. He concluded that linear flow decline analysis is the best technique for reserves forecasting before the reservoir boundary is detected, which would normally be detected after 4 years of production. Exponential decline forecasts would be used after this time.

Ammer *et al.*[31] used log-log plots of cumulative gas produced versus time to analyze the production mechanisms of 284 producing wells in the Clinton formation of eastern Ohio. The production characteristics signified that the sandstone exhibits linear flow (1/2 slope) in 48% of the wells, intermediate slopes (0.5 to 0.9) in 45% of the wells, and radial flow slope (0.9) in 7% of the wells. Nearly all of the intermediate slopes were close to linear slopes. The authors established a correlation of slope with the environment of deposition. They mentioned that intermediate flow is may indicate of a well draining multiple layers with different flow characteristics.

Nott and Hara[43] analyzed production data from 17 oil wells in a low-permeability, high-porosity, and hydraulically fractured reservoir. They explained that refracturing treatments in these wells successfully extended the existent fractures and the productivity increased 17% for 18 months after treatment. They used Miller's linear flow

model to analyze these wells using the half-slope straight line detected on plots of cumulative oil produced, N_p, versus t to determine the fracture half-length, x_f.

Bagnall and Ryan[44] described cases that present linear flow behavior in Devonian shale filed production data. They concluded that the gas rate from such wells is a function of the density and width of natural fractures largely controlling Devonian shale gas production.

Stuart *et al.*[45] presented reserves estimation techniques for tight gas reservoirs. Both decline curves and material balance methods were found to have serious drawbacks when applied to tight gas reservoirs that had not established a constant drainage area. Gas production analysis (GPA) using a combination of decline curves and material balance in conjunction with classical pressure-transient analysis was more accurate in determining reserves.

Rahman *et al*[46] presented an analytical method that analysis flow conditions and accounts for the effect of hydraulic fractures and non-Darcy components resulting in computationally efficient estimation of production from tight gas reservoirs. Their algorithm couples these two different models by matching production rate, establishing a hybridized transient-pseudo-steady-state (TPSS) model to predict the production profile during the whole production life.

Ibrahim *et al*[47] presented a simple and accurate method to determine all the reservoir parameters for transient constant-pressure drawdown data of gas wells influenced by wellbore storage, formation damage, and high-velocity flow effects. This work systematically illustrates the applicability of the derived equations using several simulated examples. The final working equations are written in various forms, which allow the well-test analyst to select the form that is most convenient for his application.

Superposition Time Function

Superposition (or convolution) is a method whereby constant-rate solutions can be combined to create a variable-rate pressure profile. Van Everdingen and Hurst[48]

introduced the use of Duhamel's principle to model a variable rate history with the summation of simpler constant rate solutions.

Helmy and Wattenbarger[41] presented a novel application of the principle of superposition to filter out the scatter in production rate data and establish the production trend for cases with shut-ins established an analytical reservoir model that matches the production and pressure history of the well.

In 1965, Odeh and Jones[49] presented a second-order approximation to the exact solution of the diffusivity equation. Corresponding to the pressure buildup of a well producing at a variable rate, this approximation is applicable when the well's shut-in time is larger than the total time elapsed since the well was first produced. The resulting equations are compact and easy to use.

Odeh and Jones[50] also provided a theoretical method of handling drawdown analysis for both oil and gas wells flowing at variable rates. This method is still used in well test analysis.

Cinco-Ley and Samaniego[51] analyzed use and misuse of the superposition time function. This function usually assumed that radial flow equations are valid, although in practice reservoirs may exhibit several flow regimes, especially near fractured or partially penetrating wells.

Samaniego and Cinco-Ley[52] also considered the effect of damage and high-velocity flow in analysis of variable-rate tests in gas wells. Their direct method allows an estimation of the turbulent term coefficient D and the skin factor without using a trial and error procedure. The method which is applicable to infinite-acting radial flow, considers a step-function approximation of the flow rate. It can be applied to continuously varying rate flow tests

Craven[53] used superposition to define transient-rate behavior from the constant terminal pressure. The standard methods available to determine reservoir pressure from pressure buildup observations rely on the assumption of flow geometry in the reservoir. Craven method of calculating reservoir pressure does not require a specified reservoir flow pattern; instead, it uses the principle of superposition to develop a single pressure-

drawdown curve for each well. The method has the advantage of requiring only a short shut-in period.

Zheng and Stewart[54] presented a method for analyzing buildup tests by the principal of superposition. This method uses the constant-rate drawdown solution of an "infinite" reservoir with uniform properties.

Tiab *at el*[55] presented a technique based on the pressure derivative for interpreting a multi-rate flow test. A Cartesian plot of the pressure-derivative data versus a time group is a straight line from which the reservoir permeability can be estimated. The technique includes a step-by-step procedure for interpreting a multirate test using pressure and pressure-derivative data.

Whitson and Sognesand[56] applied superposition to pressure-transient analysis when rate varies significantly before and during pressure measurements. To apply rigorous superposition, they recommended use of conventional pressure-transient and rate-time methods to estimate permeability, skin, and in some cases, drainage area. They address problems in choosing the dimensionless pressure solution, estimating initial pressure by extrapolation of the superposition plot, and analyzing rate-dependent effects

This work presents a new method of using superposition time to analyze long-term production data for tight-gas wells. The work included derivation of the pressure-response function with the superposition time function for different flow types, derivation of the tangent slope for OGIP calculation with current properties, derivation of the pseudotime equation, combination of the pseudotime and superposition equation into one equation, and development of software to handle all these equations for the pressure-response function and pseudotime. The resulting method can determine the correct value of OGIP with any change of rate and reservoir properties. The method can determine the type of pressure response function, flow type, and initial oil or gas in place using only flow rate, with or without shut-in periods.

CHAPTER III

EFFECT OF VARIABLE RATES ON ANALYZING PRODUCTION DATA-LIQUID CASE

Introduction

Conventional well tests can be used to estimate reservoir properties if the test well produces at a constant flow rate or constant bottomhole flowing pressure (p_{wf}) during the test. But wells with long-term production data may have considerable variation in rates and pressures. For these wells, it may be possible to use a superposition time to estimate reservoir properties.

The main problem in analyzing long-term production data is the difficulty in determining the actual flow regime following extreme changes in flow rate, including possible shut-in periods. So, our approach to analyze these wells is to find the pressure-response function (radial, linear, bilinear, and *PSS*). Then, apply the superposition time function for all flow regimes until the pressure response function matches the observed flow rate. The slope and intercept of the final pressure response function can be used to determine the reservoir properties (permeability, skin, and reservoir size).

Superposition Time Plots

If both p_{wf} and flow rate are changing with time the superposition time can be used to plot production data. This technique assumes that production time in each term of the mathematical series behaves as a function of the flow regime analyzed. This technique has three disadvantages:

1) It assumes one flow regime (radial, linear, bilinear or *PSS*).

2) The points go backward and forward with the rate change.

3) The properties of the reservoir and fluid are functions of pressure.

This means for example, that in radial flow that all production times are $\log(t)$ and in linear flow all production times are $\sqrt{t}$. However, for practical uses this technique gives us acceptable results in analyzing production data for oil and gas wells when both p_{wf} and flow rate are varying slowly and smoothly with time. Appendix A develops the superposition equation for radial, linear, bilinear and PSS flow periods. The superposition equation for different flow regimes is given in **Table 3-1**.

TABLE 3-1—SUPERPOSITION EQUATION FOR DIFFERENT FLOW REGIMES	
Radial Flow Superposition	$\dfrac{p_i - p_{wn}}{q_n} = m \left[\sum\limits_{j=1}^{n} \dfrac{\Delta q_j}{q_n} \log(t_n - t_{j-1}) \right] + b$
Linear Flow Superposition	$\dfrac{p_i - p_{wn}}{q_n} = m \left[\sum\limits_{j=1}^{n} \dfrac{\Delta q_j}{q_n} \sqrt{(t_n - t_{j-1})} \right] + b$
Bilinear Flow Superposition	$\dfrac{p_i - p_{wn}}{q_n} = m \left[\sum\limits_{j=1}^{n} \dfrac{\Delta q_j}{q_n} (t_n - t_{j-1})^{0.25} \right] + b$
PSS Flow Superposition	$\dfrac{p_i - p_{wn}}{q_n} = m \left[\sum\limits_{j=1}^{n} \dfrac{\Delta q_j}{q_n} (t_n - t_{j-1}) \right] + b$

In these equations, *m* is the slope used to calculate the permeability for transient radial, linear, and bilinear flow and to determine OOIP for the PSS period. B is the intercept used to calculate the skin factor during transient or OOIP during PSS. **Table 3-2** gives the different parameters that can be calculated from each flow regime plot.

TABLE 3-2—PARAMETERS CALCULATED FROM SUPERPOSITION PLOT FOR OIL WELLS PRODUCTION	
Radial Flow	
Permeability	$m = \dfrac{162.6 B \mu}{kh}$
Skin	$s = 1.151[\dfrac{b}{m} - \log(\dfrac{k}{\phi \mu c_t\, r_w^2}) + 3.23]$
Linear Flow	
$\sqrt{k}\, A_c$ Pore Volume	$\sqrt{k}\, A_c = \dfrac{79.65\ B\mu}{\sqrt{(\phi\, \mu\, c_t)_i}}\left(\dfrac{1}{\tilde{m}_{CRL}}\right)$ $V_p = 8.962 \dfrac{B}{c_t} \dfrac{\sqrt{t_{ehs}}}{\tilde{m}_{CRL}}$
Bilinear Flow	
Slope Intercept	$wk_f = \left(\dfrac{44.1 q B \mu}{hm_B}\right)^2 \left(\dfrac{1}{\phi \mu c_t k}\right)^{0.5}$ $s_f = \dfrac{0.00708 kh}{qB\mu}(p_i - p_0)$
PSS Flow	
Pore Volume OOIP	$V_P = \dfrac{-0.234 B}{c_t \tilde{m}_{PSS}}$ $OOIP = V_P (1 - S_{wi}) / B_{oi}$

Pressure Response Function

The pressure response function, *F(t)*, is defined as the reservoir pressure response to a unit rate change.[57-65] For constant oil rate, the relationship between pressure, flow rate, and the pressure response function is given by

$$p_i - p_{wf}(t) = q_o F(t) \quad \text{..} \quad (3.1)$$

However, the flow rate is seldom constant. For this case, the convolution or superposition theorem is used. The continuous form of superposition time for the pressure response function is given by

$$p_i - p_{wf}(t) = \sum_{j=1}^{n} (q_j - q_{j-1}) F(t_n - t_{j-1}) \quad \text{...} \quad (3.2)$$

The pressure drop can be calculated as

$$\Delta p = \sum_{j=1}^{n} \Delta q_j F(t_n - t_{j-1}) \quad \text{...} \quad (3.3)$$

The superposition equation with pressure response function is given in **Table 3-3** for different flow regimes.

The plot of $\dfrac{\sum_{j=1}^{n} \Delta q_j F(t_n - t_{j-1})}{q_n}$ vs. Superposition time for each flow regime will give a straight line only for the correct flow regime that exists in this well.

TABLE 3-3—SUPERPOSITION EQUATION WITH PRESSURE RESPONSE FUNCTION FOR DIFFERENT FLOW REGIMES	
Radial Flow Superposition	$$\frac{\sum_{j=1}^{n} \Delta q_j\, F(t_n - t_{j-1})}{q_n} = m\left[\sum_{j=1}^{n} \frac{\Delta q_j}{q_n} log(t_n - t_{j-1})\right] + b$$
Linear Flow Superposition	$$\frac{\sum_{j=1}^{n} \Delta q_j\, F(t_n - t_{j-1})}{q_n} = m\left[\sum_{j=1}^{n} \frac{\Delta q_j}{q_n} \sqrt{(t_n - t_{j-1})}\right] + b$$
Bilinear Flow Superposition	$$\frac{\sum_{j=1}^{n} \Delta q_j\, F(t_n - t_{j-1})}{q_n} = m\left[\sum_{j=1}^{n} \frac{\Delta q_j}{q_n}(t_n - t_{j-1})^{0.25}\right] + b$$
PSS Flow Superposition	$$\frac{\sum_{j=1}^{n} \Delta q_j\, F(t_n - t_{j-1})}{q_n} = m\left[\sum_{j=1}^{n} \frac{\Delta q_j}{q_n}(t_n - t_{j-1})\right] + b$$

Procedures for New Superposition Time Plots

To apply the pressure-response function for long-term production in oil wells we use Visual Basic to calculate the superposition time for each flow regime with the following procedures

a) Plot flow rate vs. time.

b) Assume pressure response function (radial, linear, bilinear, and PSS).

c) Plot the pressure response function F*(t)* vs. time.

d) Calculate the left-hand side for the equations in **Table 3-3** for each flow regime that represents the y-axis value.

e) Calculate the superposition time for each flow regime for the equations from **Table 3-3** that represents the x-axis value.

f) Construct plots for each flow regime (radial, linear, bilinear, and PSS).

g) Determine which flow regime best match the flow schedule.

h) Determine the slope and intercept of the final pressure-response function.

i) Determine permeability from slope and skin from intercept.

j) Determine the OOIP from the PSS period.

Results and Discussion

Simulation cases for constant and variable rates with different pressure-response functions illustrate the benefits of this method.

Simulation Case 1: Variable Rate with Linear Flow

In Case 1, we use simulation results for linear flow. The simulation data are given in **Table 3-4**. The production schedule given in **Fig. 3-1** shows constant-rate production for most times except for one period of low rate. Eq. 3.4 gives the linear-flow pressure-response function; the actual pressure-response function is shown in **Fig. 3-2**.

$$p_{wD} = \sqrt{\pi t_{Dx_e}} \quad\quad\quad\quad\quad\quad\quad\quad\quad\quad\quad\quad\quad\quad\quad\quad\quad\quad\quad\quad (3.4)$$

Where

$$p_{wD} = \frac{kh(p_i - p_{wf})}{141.2 q_o B_o \mu_o} \quad\quad\quad\quad\quad\quad\quad\quad\quad\quad\quad\quad (3.5)$$

$$t_{Dx_e} = \frac{0.00633 kt}{\phi \mu_o c_t x_e^2} \quad\quad\quad\quad\quad\quad\quad\quad\quad\quad\quad\quad\quad (3.6)$$

The results from the superposition calculation for different flow regimes are shown in **Figs. 3-3** to **3-6**. The low rate period affects the superposition time of all flow regimes except linear flow. The superposition time for linear flow still gives a straight line even with the low rate period as shown in **Fig. 3-4**. This mean that the well remained in linear flow even the flow rate was not constant. The other flow regimes do not give straight lines because the well never left linear flow. The slope from the linear flow superposition plot, Fig. 3.4, is 1.96. The product of $\sqrt{k} A_c$ is 53,555.73 $\sqrt{md}$ -ft^2, which is the same as the simulation value.

We can conclude that the right flow regimes will give a straight line under any flow schedule if the well remains in this regime.

TABLE 3-4—SIMULATION DATA FOR CASE 1		
Initial pressure, p_i	3000	psia
Formation porosity	0.15	fraction
Reservoir half-length	1070	ft
Reservoir Width	467	ft
Formation net pay thickness, h	361.99	ft
Formation volume factor, Bo	1.472	Bbl/STB
Viscosity, μ_o	0.72	cp
Formation permeability, k	0.1	md
Total compressibility, c_t	6.01×10^{-6}	$psia^{-1}$
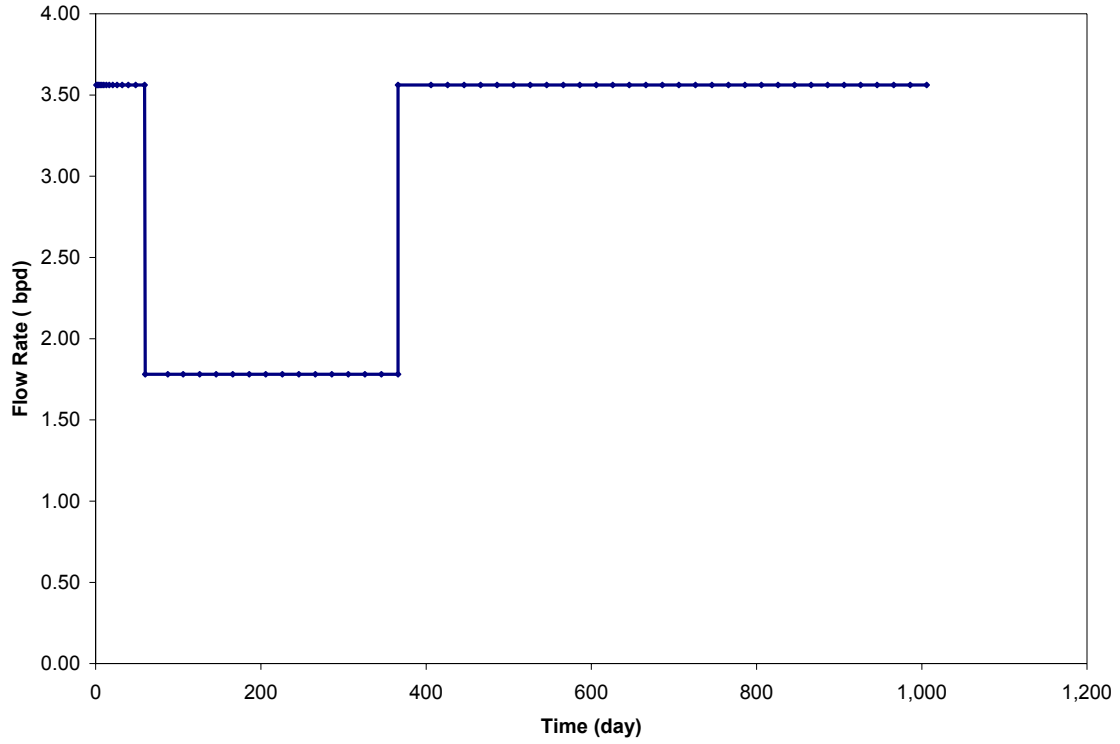
Fig. 3-1—Rate schedule for Simulation Case 1 shows period of low flow rate.
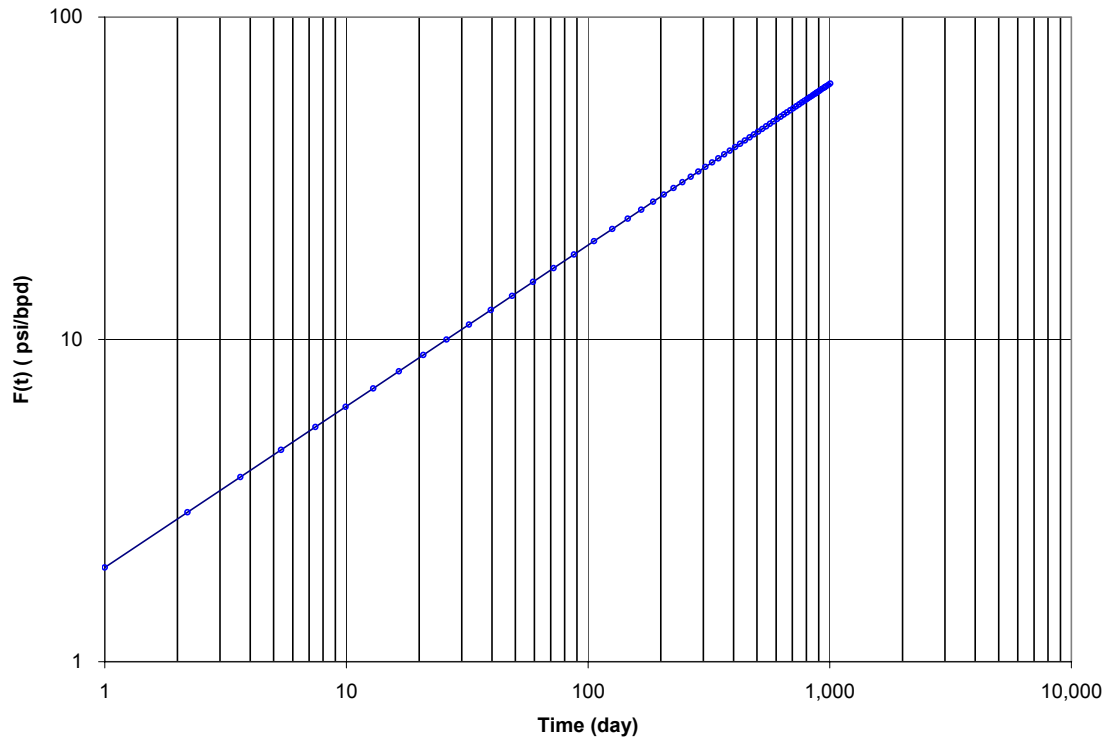
Fig. 3-2—Linear flow pressure response function for Simulation Case 1.

Fig. 3-3—Plot of $\Delta p/q$ vs. radial superposition time for Simulation Case 1.

Fig. 3-4—Plot of Δp/q vs. linear superposition time for Simulation Case 1.

Fig. 3-5—Plot of Δp/q vs. bilinear superposition time for Simulation Case 1.
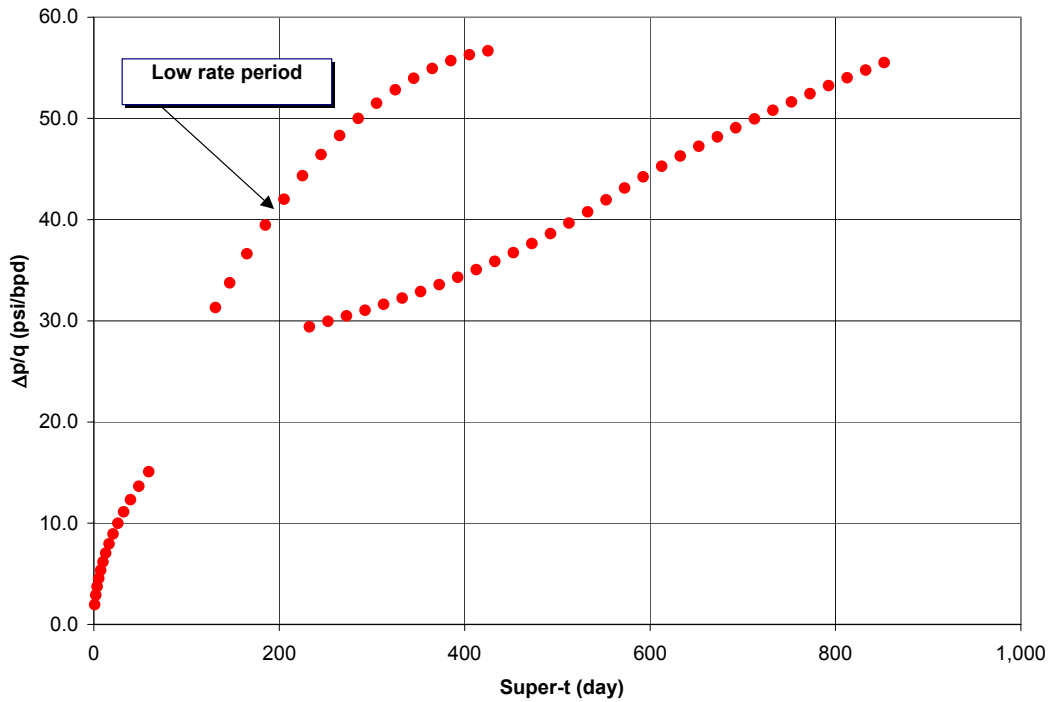
Fig. 3-6—Plot of Δp/q vs. Super-t of PSS flow for Simulation Case 1.

Simulation Case 2: Constant-Rate, Linear and PSS Flow

In Case 2, we used the same simulation data for Case 1 but produced the well until PSS. The well produced at constant rate during all times so in this case there is no effect of rate change on the pressure-drop calculation. The pressure-response function for this well is linear flow in the transient period(1/2 slope) and PSS (unit slope) in later time as shown in **Fig. 3-7**. The pressure-response function representing a finite, closed reservoir is

$$p_D = t_{DL} + \frac{1}{3} - \frac{2}{\pi^2} \sum_{n=1}^{\infty} (\frac{1}{n^2})e^{(-n^2\pi^2 t_D)}$$ .... (3.7)
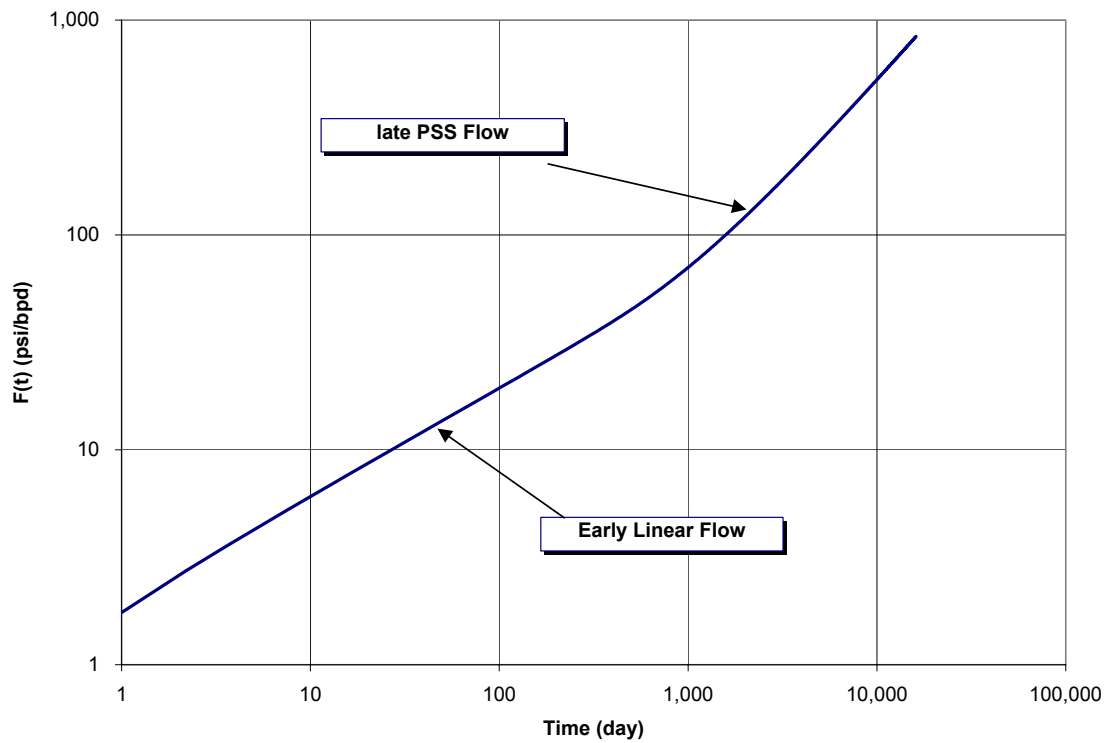
Fig. 3-7—Simulation Case 2 exhibits linear flow at early time and PSS flow at later time.

The results from superposition time for linear flow give a straight line for in the pressure response function as shown in **Fig. 3-8**. Also, the PSS period matches the later part as shown in **Fig. 3-9**. The radial and bilinear superposition does not give a straight line because the actual flow regime is linear and PSS as shown in **Figs. 3-10** and **3-11**.
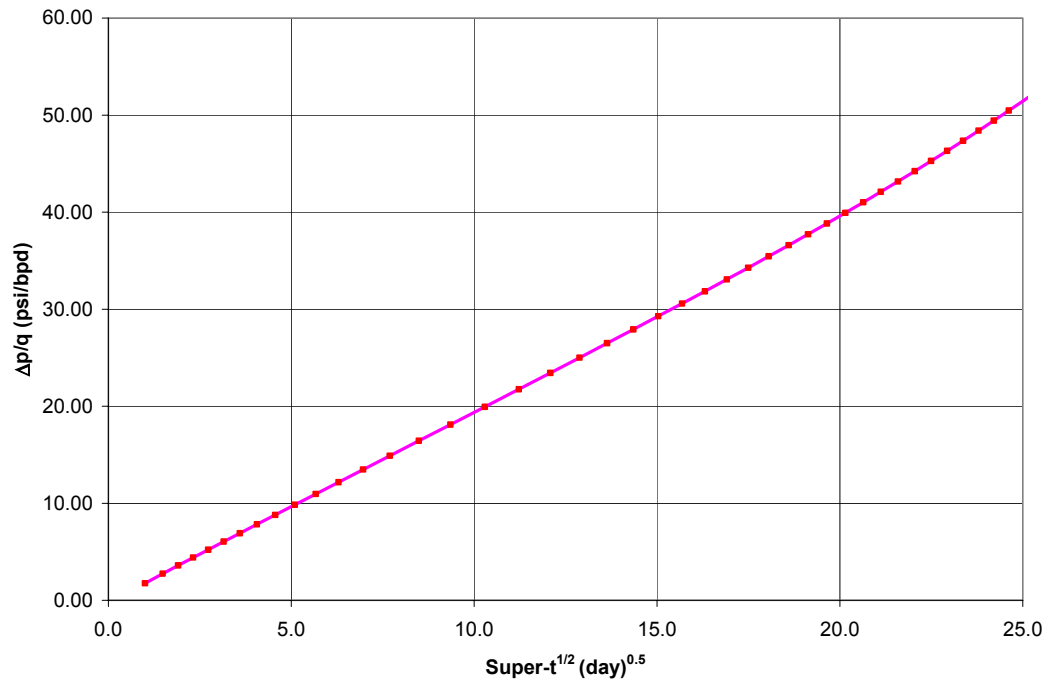
Fig. 3-8—Plot of Δp/q vs. linear superposition time for Simulation Case 2 shows a straight line for early linear flow.
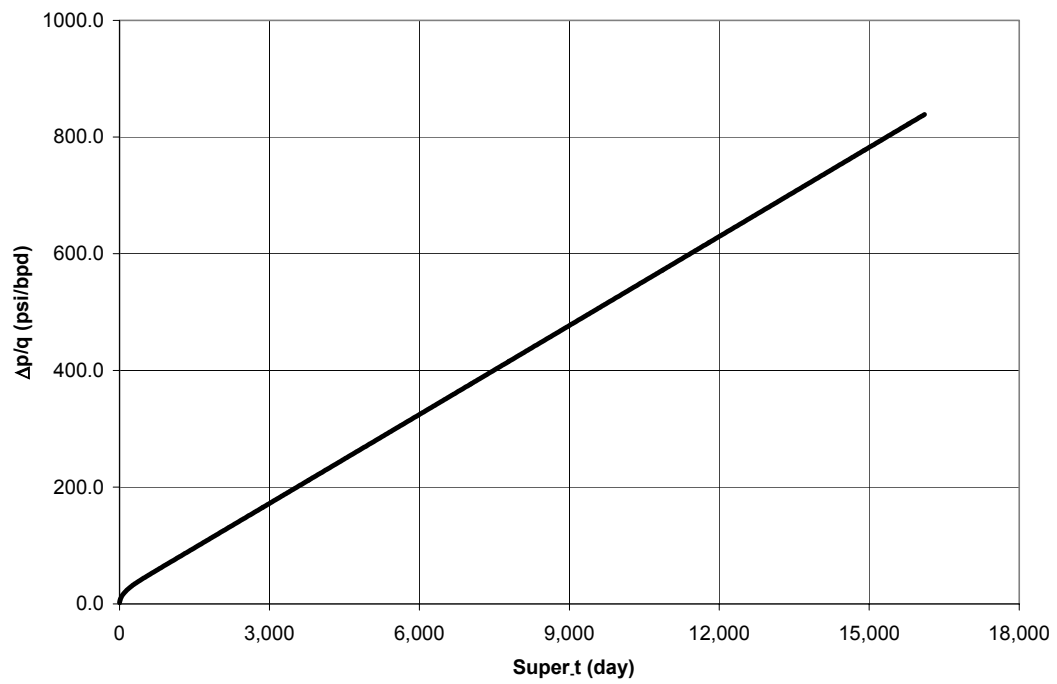
Fig. 3-9—Plot of Δp/q vs**.** Super‗t for Simulation Case 2.

Fig. 3-10—Plot of Δp/q vs. radial superposition time for Simulation Case 2.

Fig. 3-11—Plot of Δp/q vs. bilinear superposition time for Simulation Case 2.

Simulation Case 3: Variable-Rate, Linear and PSS Flow

In Case 3, we used the same simulation data for Case 1, expect that the well produced at variable rates as shown in **Fig. 3-12**. The actual pressure response function is the same as in simulation Case 2 with linear and *PSS* flow in the late period. The linear superposition still gives a straight line even with different periods as shown in **Fig. 3-13,** which proves that the rate schedule does not change the flow regime if the well is still in this period. The *PSS* superposition gives a straight line because the pressure response function has PSS flow in the later period as shown in **Fig. 3-14**. The radial and bilinear superposition time do not give straight lines as shown in **Figs. 3-15** and **3-16**, because the actual function does not have a radial or bilinear period.

We can conclude that the actual flow regime will fit the right superposition function regardless the flow schedule. So if the well produces in linear flow only, the linear superposition time will give a straight line.
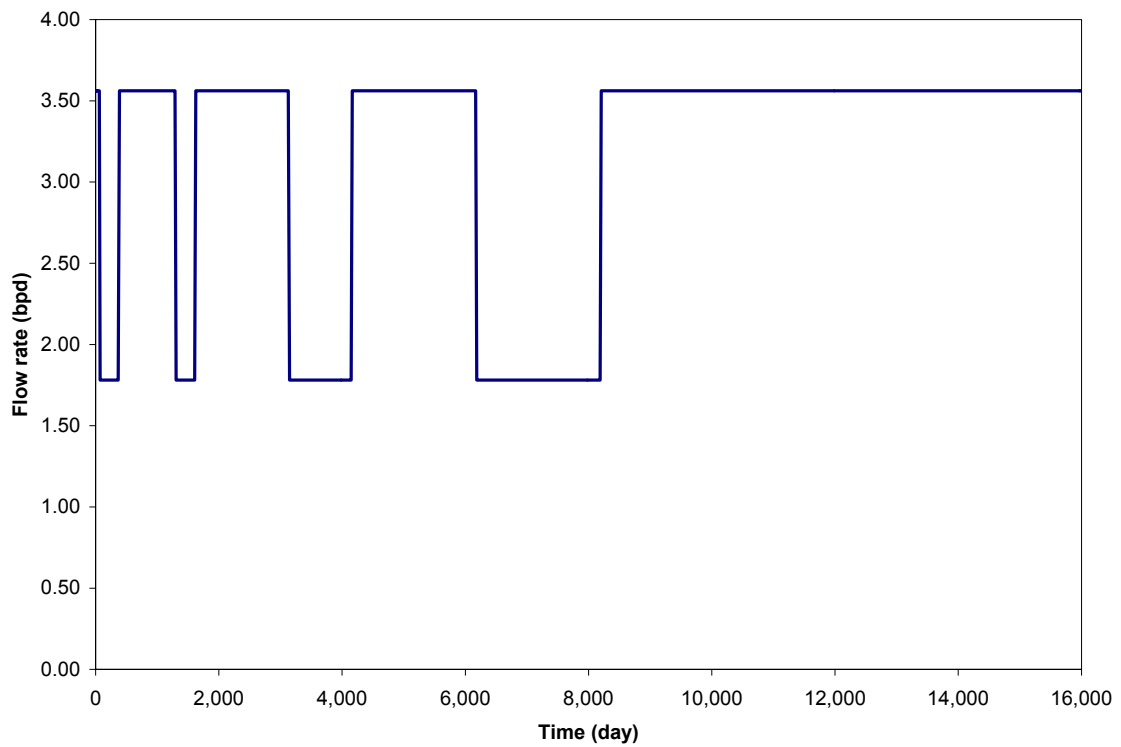
Fig. 3-12—Rate schedule for simulation Case 3.
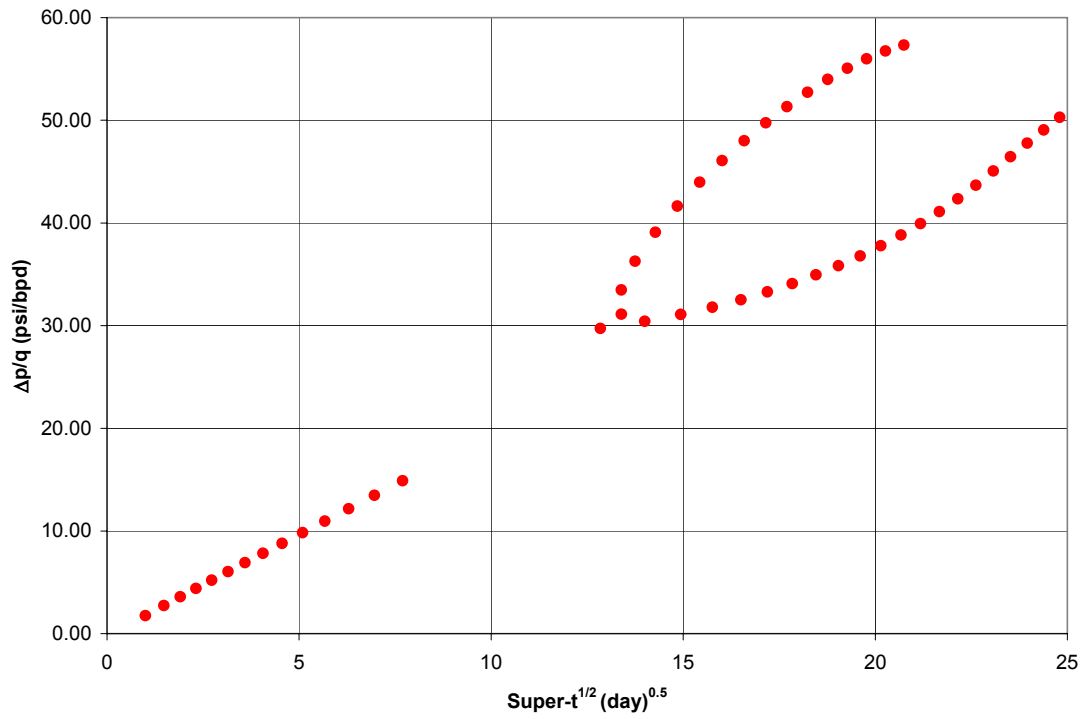
Fig. 3-13—Plot of Δp/q vs. linear superposition time for Simulation Case 3.
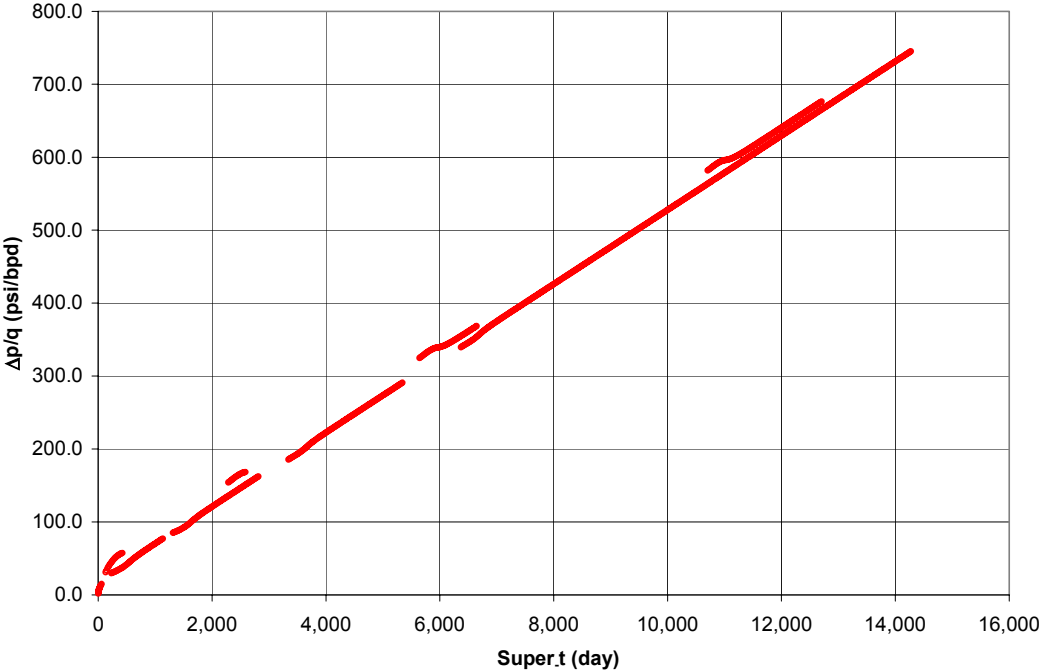
Fig. 3-14—Plot of Δp/q vs. PSS superposition time for Simulation Case 3.
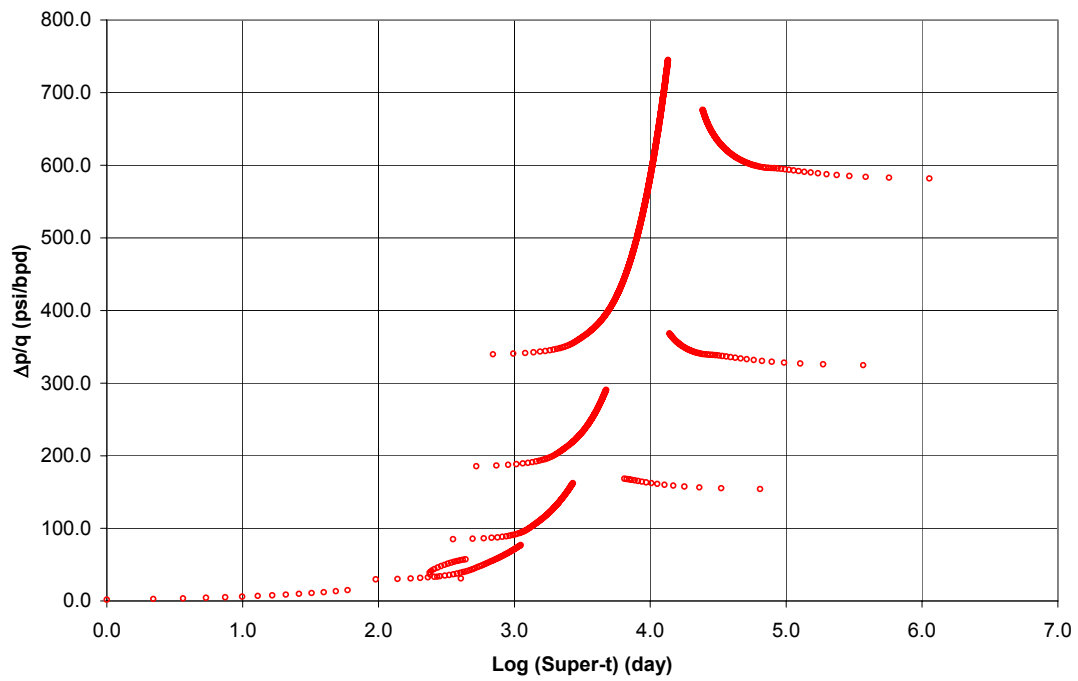
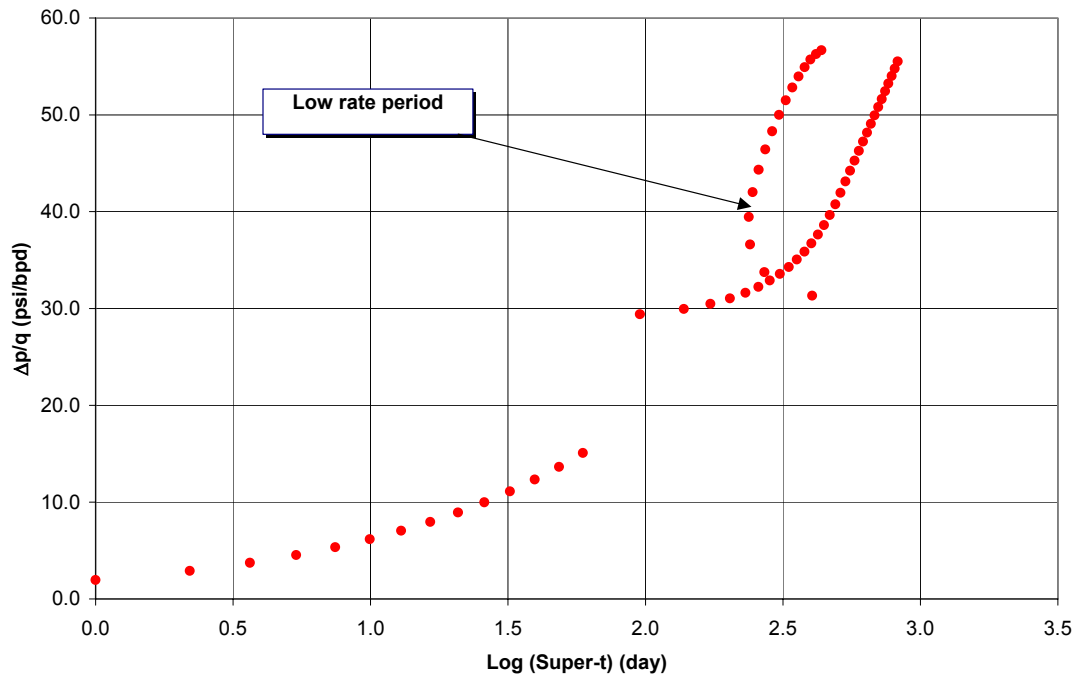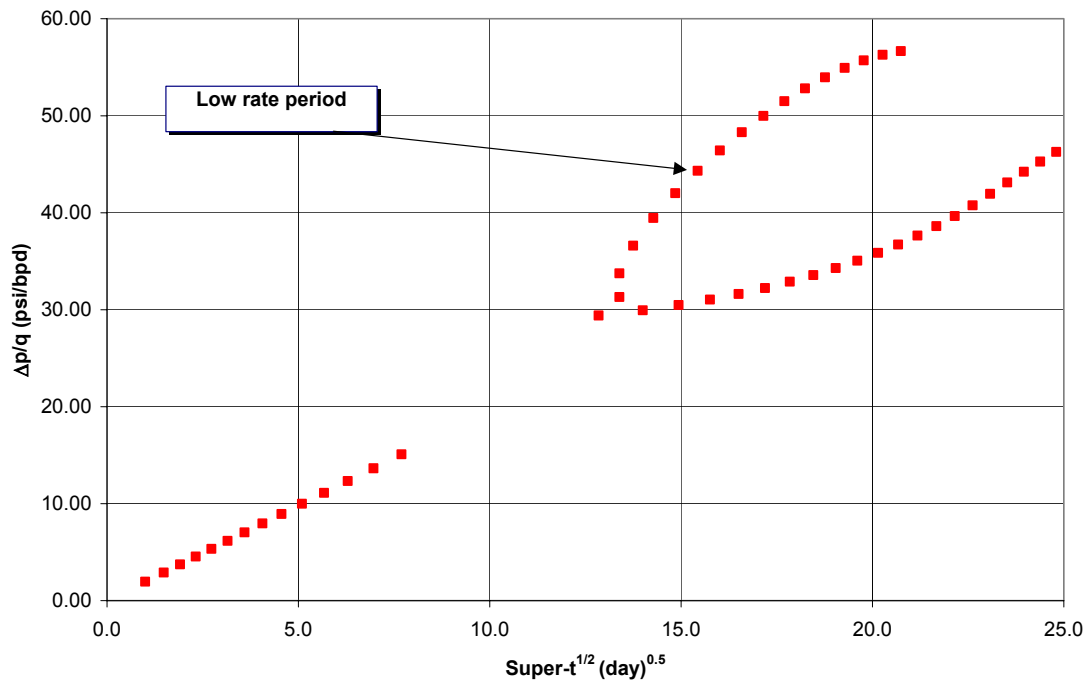**Fig. 3-15**—Plot of Δp/q vs. radial superposition time for Simulation Case 3.
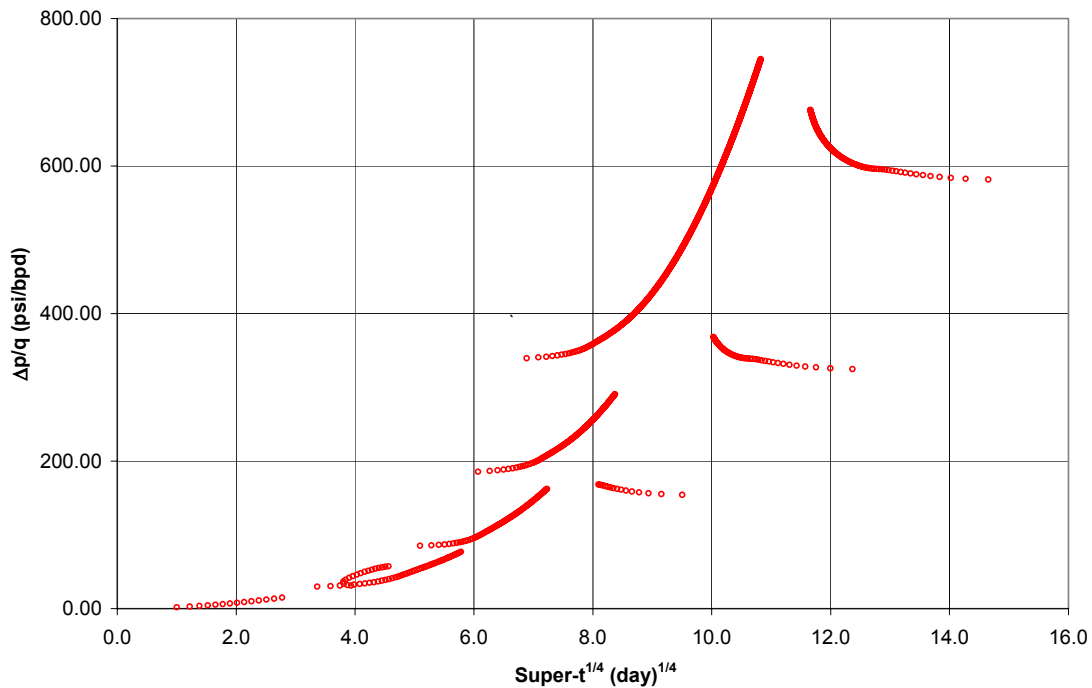
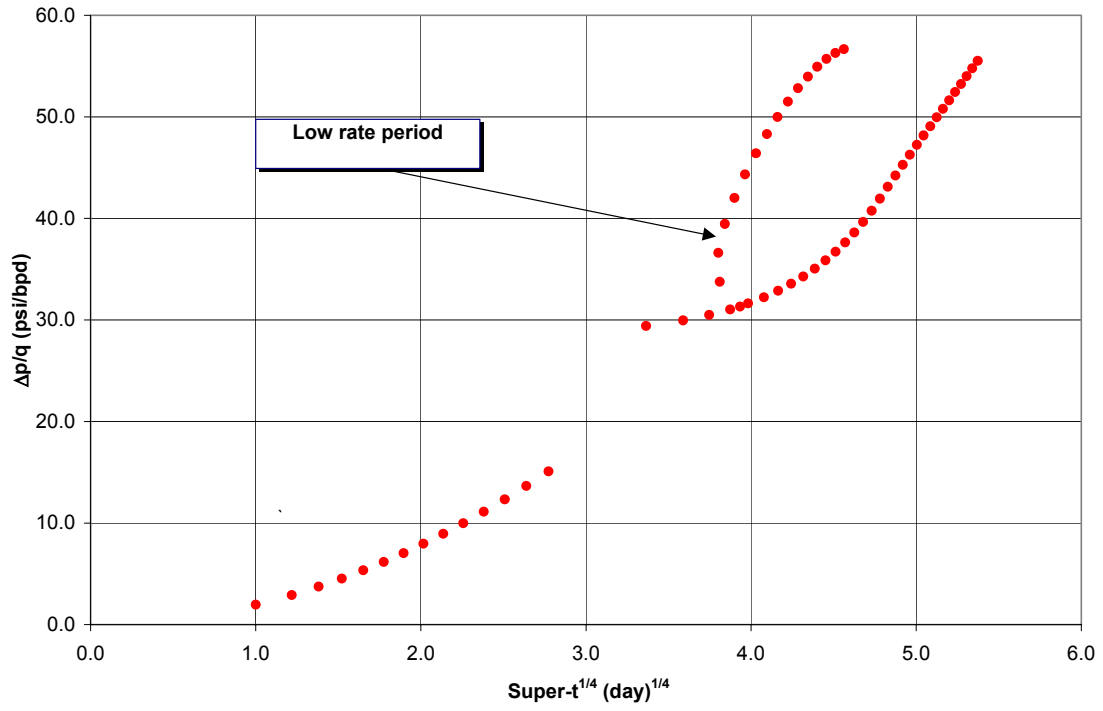**Fig. 3-16**—Plot of $\Delta p/q$ vs. bilinear superposition time for Simulation Case 3.

Variable Rate and p_{wf} Production

Superposition time accounts for the effects of rate and p_{wf} changes as given in **Table 3-1**. We illustrate the effect of using the Super-t with variable rate and p_{wf} to calculate the OOIP for the liquid case.

Simulation Case 4: Variable Rate

The production data for Case 4 with variable rate production is shown in **Fig. 3-17**. The cumulative production is equal to 1.55 billion bbl. **Fig. 3-18** is a plot of $\dfrac{[p_i - p_{wf}]}{q_o}$ vs. Super-t, which shows the following:

1) All production periods have a transient flow period.
2) All production periods fall along a straight line.

3) There is a unique straight line from Super₋t because properties do not change

We can conclude that the Super₋t takes into account the rate changes. Also, the value of OOIP from the slope of the Super₋t plot is correct.
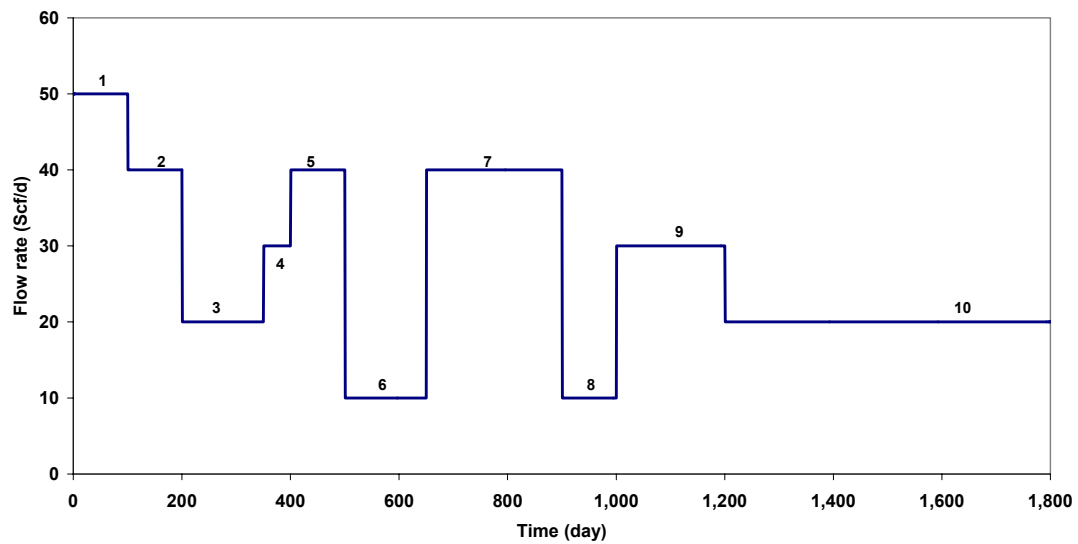
Fig. 3-17—Production rate for Simulation Case 4.
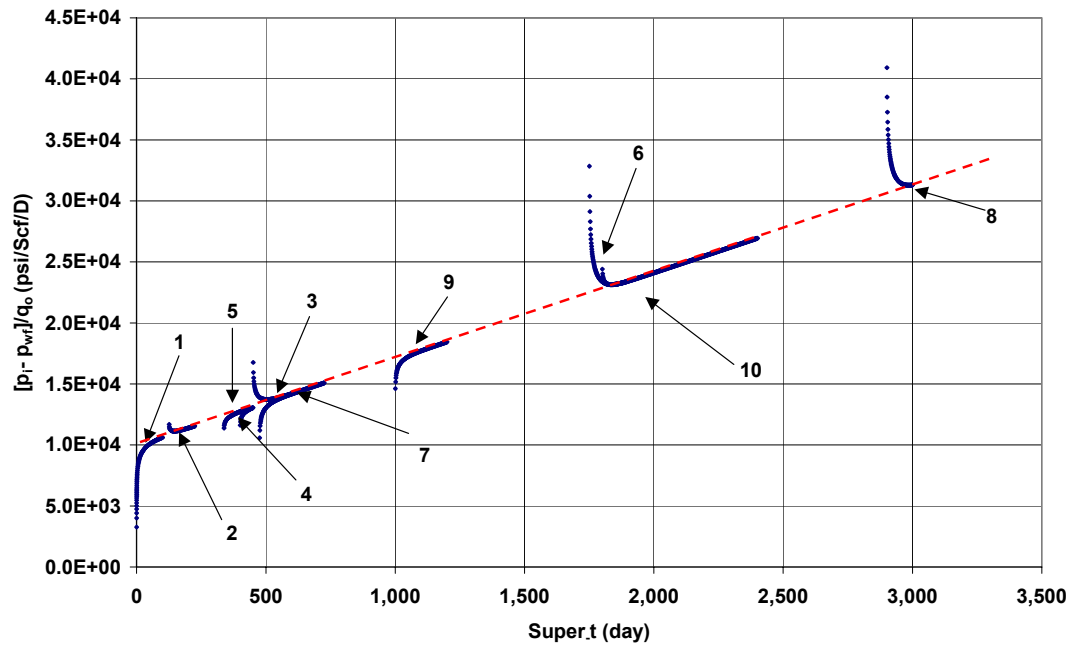
Fig. 3-18—Plot of $\Delta p/q$ vs. Super.t, gives a straight line for the PSS period in Simulation Case 4.

Summary

The following specific conclusions can be drawn from our findings in this project:

1. This method is effective in analyzing the performance of oil wells producing with variable rates.
2. This method gives good results compared with previous methods for analyzing variable-rate wells.
3. The pressure response-function helps in determining the actual flow regimes.
4. The value of initial oil in place from this method is accurate
5. Superposition takes into account the effect of rate and p_{wf} change.

CHAPTER IV

DETERMINING OGIP FOR WELLS IN PSEUDOSTEADY-STATE FLOW

Tangent Slope Using Initial Properties

The superposition time (Super_t) function has been used as a tool to analyze the variable flow rate without knowing the average reservoir pressure. The Super_t given is by Eq. 4.1:

$$\frac{[m(p_i) - m(p_{wf})]}{q_{gn}} = \tilde{m}_{PSS} [\sum_{i=1}^{n} \frac{\Delta q_{gi}}{q_{gn}} (t_n - t_{i-1})] + b \ \text{.. (4.1)}$$

The slope ($\tilde{m}_{PSS}$) from plotting $\dfrac{[m(p_i) - m(p_{wf})]}{q_g}$ vs. Super_t is used to determine the

OGIP for constant rate from Eq. 4.2:

$$OGIP = \frac{2 p_i S_{gi}}{z_i (\mu_g c_t)_i} \left(\frac{1}{\tilde{m}_{PSS}} \right) \ \text{.. ....(4.2)}$$

For constant pressure, the equation is

$$OGIP = \frac{56 \, T \, S_{gi}}{(\mu_g c_t B_{gi})_i} \left(\frac{1}{\tilde{m}_{\exp d}} \right) \ \text{... (4.3)}$$

Note that initial properties are used in Eqs. 4.2 and 4.3.

This chapter addresses the shortcomings in using Super_t with initial properties to calculate the OGIP from Eqs. 4.2 and 4.3. It appears that, regardless of the flow regimes exhibited by the well reservoir system the reservoir properties change with pressure. If the depletion increases more than 10%, the Super_t plot become non linear, and estimated OGIP can have errors greater than 300%. The Super_t must be corrected for these changing reservoir and fluid properties.

Tangent Slope Using Current Properties

The tangent slope method with current reservoir properties for determining OGIP in the PSS period takes into account the effect of pressure change on reservoir

properties. The complete derivation of tangent slope for constant rate and p_{wf} are given in Appendix B and C. The final equation used to calculate OGIP with current properties is given as

$$OGIP = (\frac{2p\,S_g\,\phi}{z})_i\,(\frac{1}{\phi(\overline{p})\mu(\overline{p})c_t(\overline{p})})(\frac{1}{\widetilde{m}_{PSS}})$$ .... (4.4)

For constant rate, and as

$$OGIP = J_{CP}\frac{2\,p_i\,S_{gi}\,\phi_i}{2.303z_i}\,(\frac{1}{\phi(\overline{p})\mu(\overline{p})c_t(\overline{p})})(\frac{1}{\widetilde{m}_{exp\,d}})$$ .... (4.5)

For constant p_{wf}

The constant rate and p_{wf} simulation cases illustrate the effect of using initial and current reservoir properties in determining OGIP.

Simulation Case 5, Constant Rate

In Case 5, we use simulation results to illustrate the shortcoming in using the initial properties in Eqs. 4.2. The reservoir properties for the simulation Case 5 are given in **Table 4-1**, which represents a tight-gas well at high pressure. The constant-rate production data for this well are shown in **Fig. 4-1**. **Fig. 4-2** shows a plot of $\Delta m(p)/q_g$ vs. time, which exhibits non linearity during the *PSS* period. This non linearity indicates the change in reservoir properties as you can see in **Fig. 4-3** which show ($\phi\mu c_t$) increases as the average reservoir pressure decreases during depletion.

The point-wise calculation of OGIP from using Eq. 4.2 with initial properties is shown in **Fig. 4-4**, which gives a high value of OGIP (20 Bcf) at later times compared to the simulated value of OGIP (8.70 Bcf). The error in OGIP value is 129%.

But when we use Eq. 4.4 to calculate the OGIP with current properties, we get the correct value of OGIP as shown in **Fig. 4-4** with error of only1.8%.

We can conclude that the tangent slope with current reservoir properties gives an accurate value of OGIP independent of changes of properties change or depletion values.

TABLE 4-1—RESERVOIR AND FLUID DATA FOR SIMULATION CASE 5		
Gas specific gravity (air = 1), γ_g	0.64	
Initial temperature, T	335	^{o}F
Initial pressure, p_i	12,300	psia
Formation porosity, ϕ	0.1	fraction
Average water saturation, S_w	0.376	fraction
Formation net pay thickness, h	394.5	ft
Water compressibility at p_i, c_w	3.6×10^{-6}	1/psia
Formation compressibility, c_f	4.00×10^{-6}	1/psia
Formation permeability, k	0.045	md
OGIP	8.7	Bcf
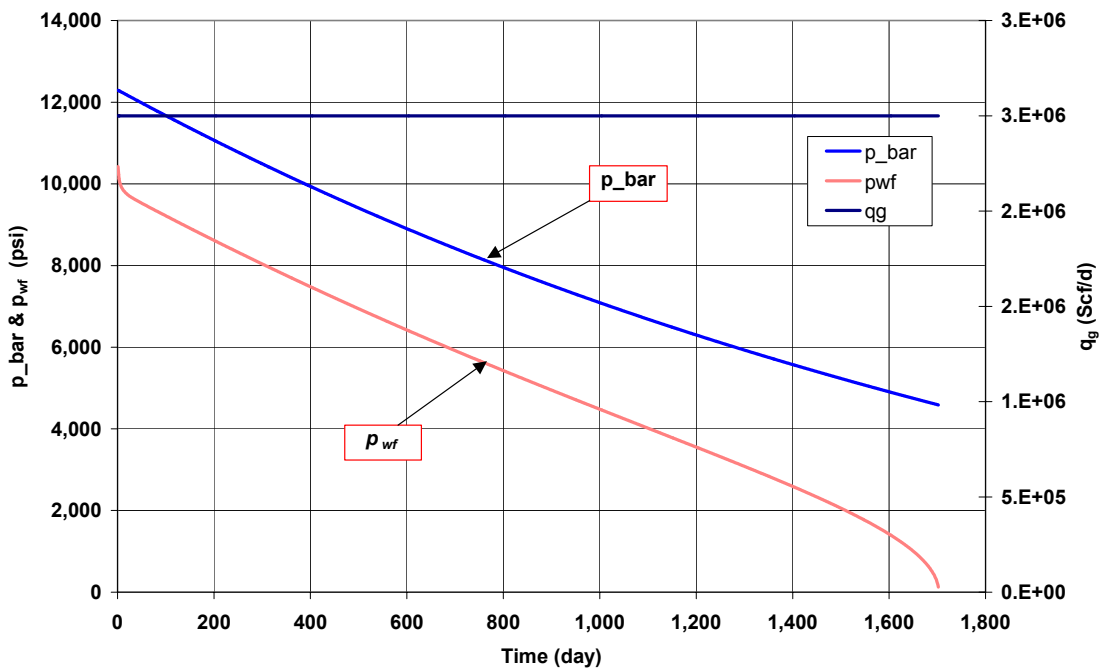
Fig. 4-1—Simulation result of Case 5.
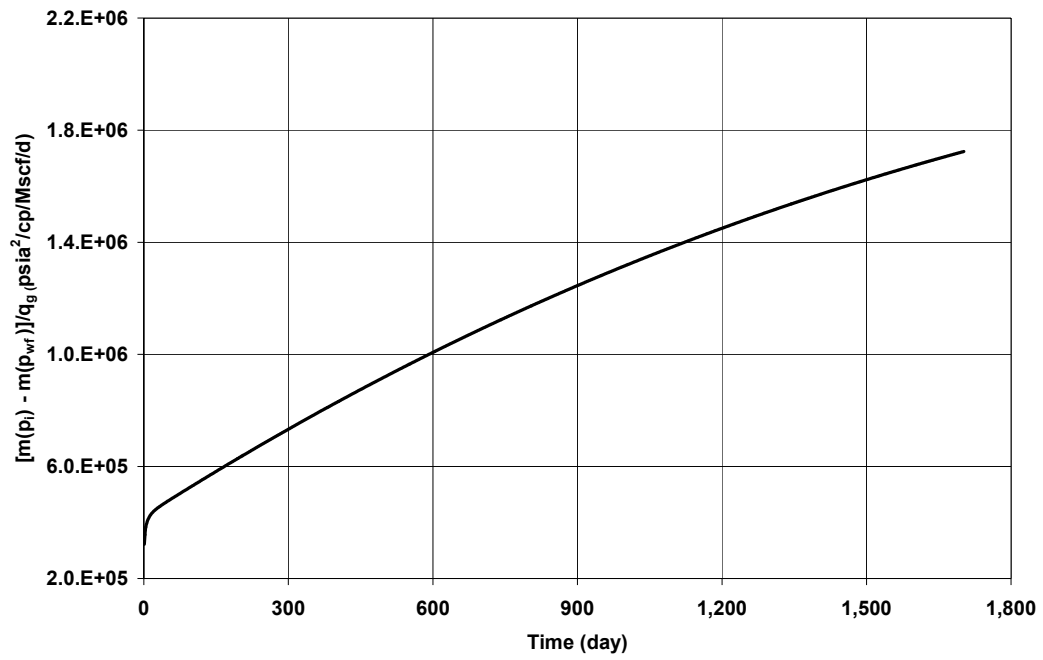
Fig. 4-2—Plot of $\Delta m(p)/q_g$ vs. time for constant rate. Note that this is not a straight line for *PSS* period (Simulation Case 5).
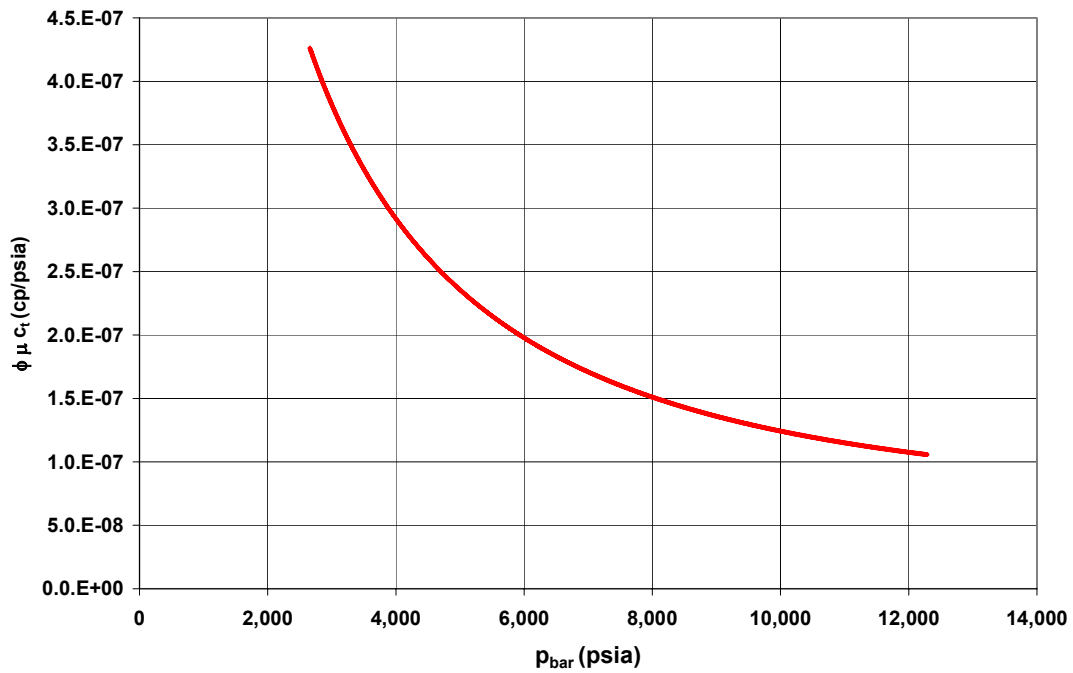
Fig. 4-3—Values of $(\phi \mu c_t)$ for Simulation Case 5 increase as reservoir pressure decreases during depletion.
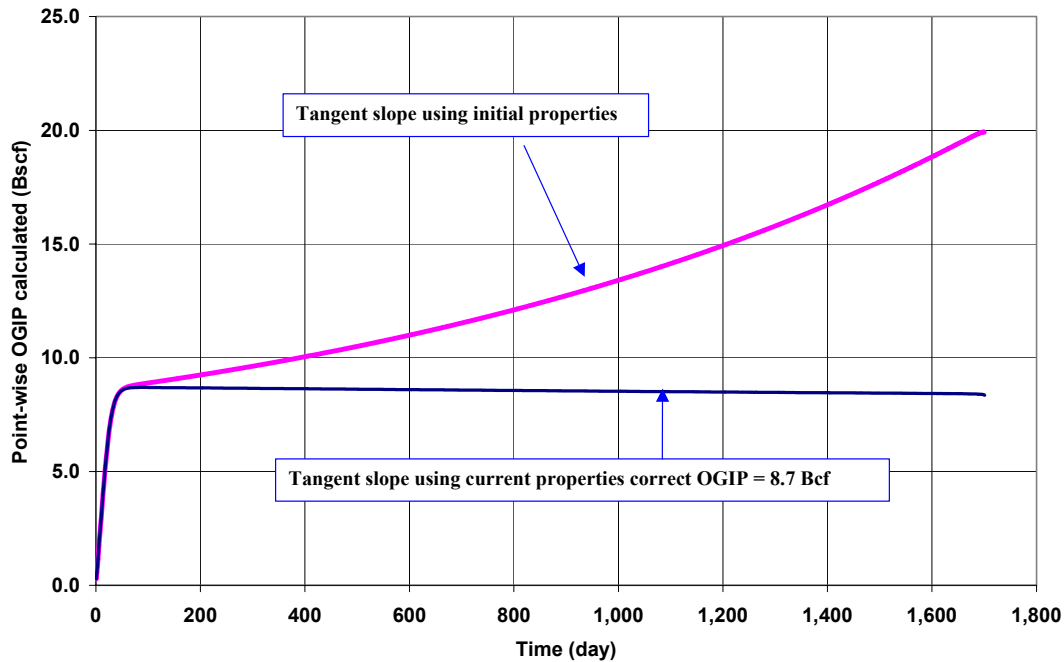
Fig. 4-4—Point-wise OGIP calculated vs. time with initial properties for simulation Case 5.

Simulation Case 6, Constant p_{wf}

In Case 6, we used simulation results from a tight gas formation, which produced at constant p_{wf}. The production schedule for Simulation Case 6 is given in **Fig. 4-5**. A plot of log $\dfrac{1}{q_g}$ vs. time **Fig. 4-6** does not give a straight line, but shows the property changes with average reservoir pressure. Eq. 4.3 with initial reservoir properties does not give the correct value of OGIP as shown in **Fig. 4-7**. The error in OGIP value reaches up to 839% at later times. When we use Eq. 4.4 to calculate the OGIP with current properties, it gives the correct value of OGIP with error of only 1.8% as shown in Fig. 4-7.

We can conclude that the tangent slope with current reservoir properties gives the more accurate value of OGIP as properties and depletion value change.
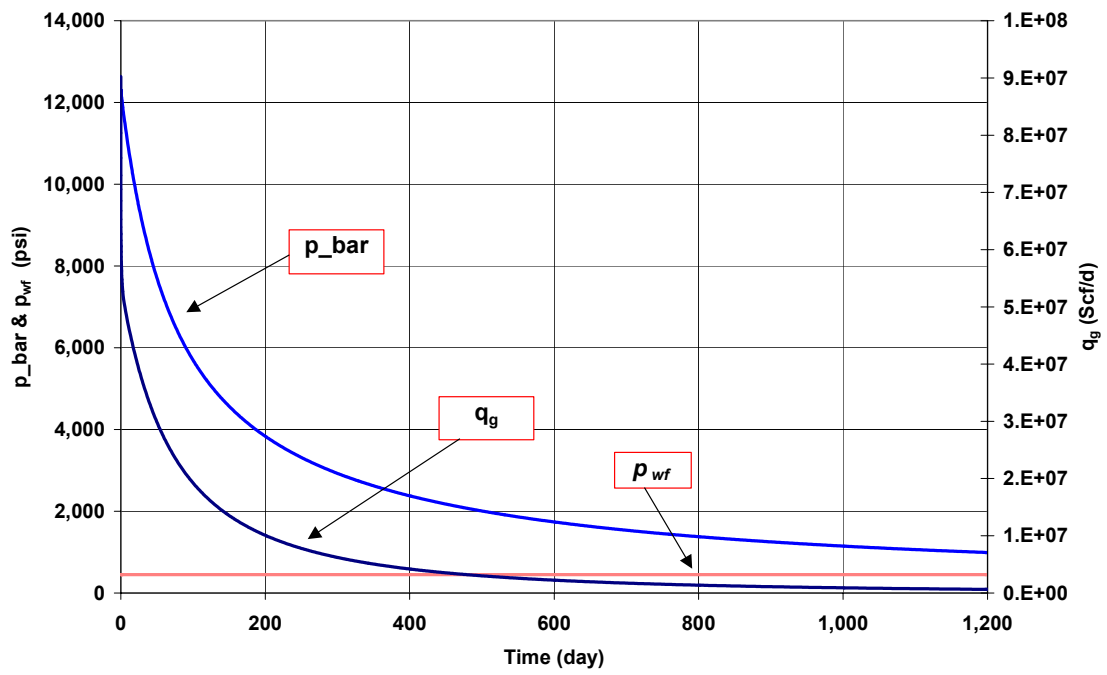
Fig. 4-5—Plot of production data for Simulation Case 6.
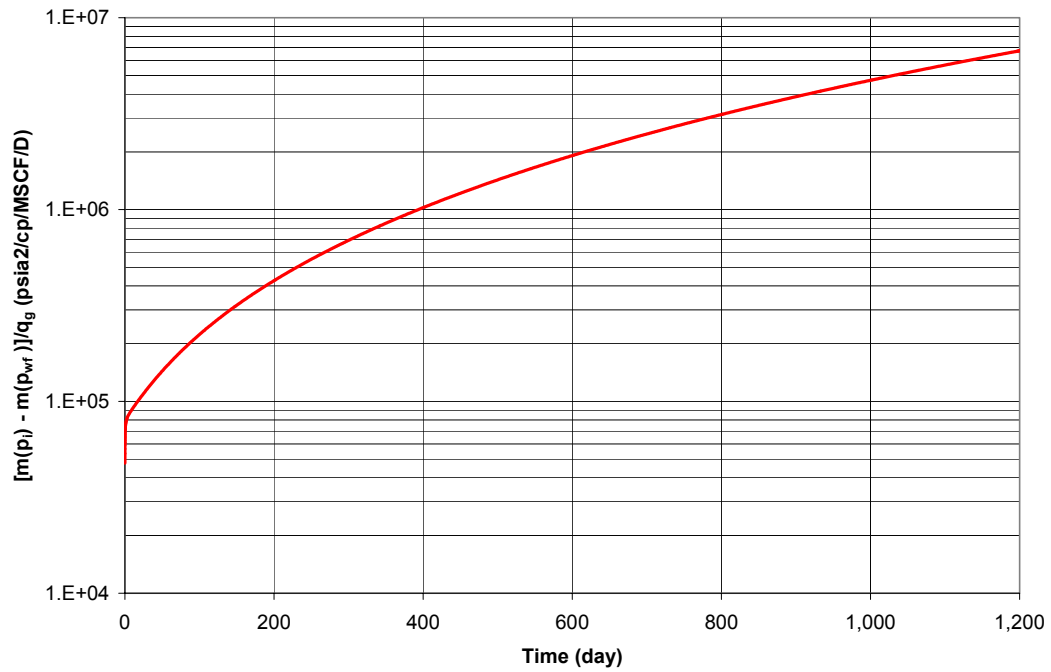
Fig. 4-6—Plot of 1/qg vs. time for Simulation Case 6, shows non-linearity due to change in properties.
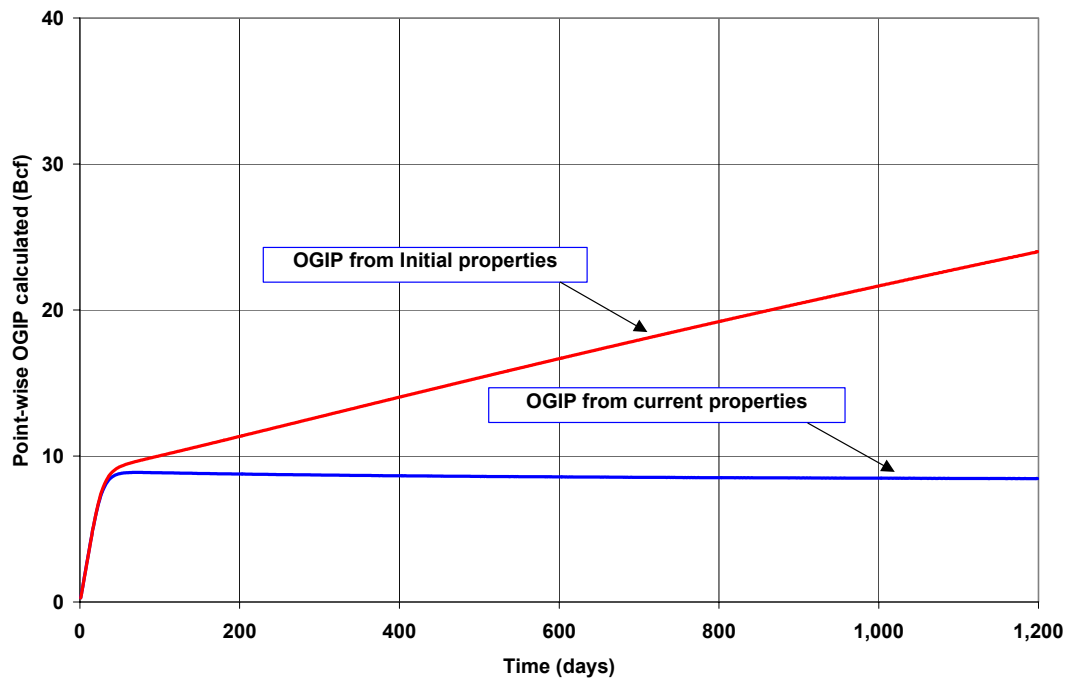
Fig. 4-7—Point-wise OGIP calculated from time plot with initial and current properties for Simulation Case 6.

Normalized Pseudotime

The new normalized pseudotime provides a plotting function for smoothing the production data by taking into account the effect of changes in reservoir properties and average pressure. The derivation of normalized pseudotime equation is given in Appendix B. The new normalized pseudotime is given by

$$t_n = (\phi \mu c_t)_i \int_0^t \frac{1}{\phi(\bar{p}) \mu(\bar{p}) c_t(\bar{p})} dt \quad \text{.. (4.6)}$$

This integration can be evaluated numerically using the trapezoidal rule.

A plot of $\Delta m(p)/q_g$ vs. normalized pseudotime for simulation result of Case 5 gives a straight line as shown in **Fig. 4-8**. The slope from the normalized pseudotime plot used to calculate OGIP from Eq. 4.3 which gives 8.54 Bcf with error of 1.8% from the simulation value of OGIP of 8.7 Bcf.

Also, a plot of $\dfrac{1}{q_g}$ vs. t_n for simulation result of Case 6 gives straight line as shown in **Fig. 4-9**. The slope from t_n plot used to calculated OGIP from Eq. 4.3, which the correct OGIP with error 1.80% from the simulation value of OGIP = 8.15 Bcf.

We can conclude that the normalized pseudotime gives the correct OGIP because it takes into account the effect of property changes with average reservoir pressure.
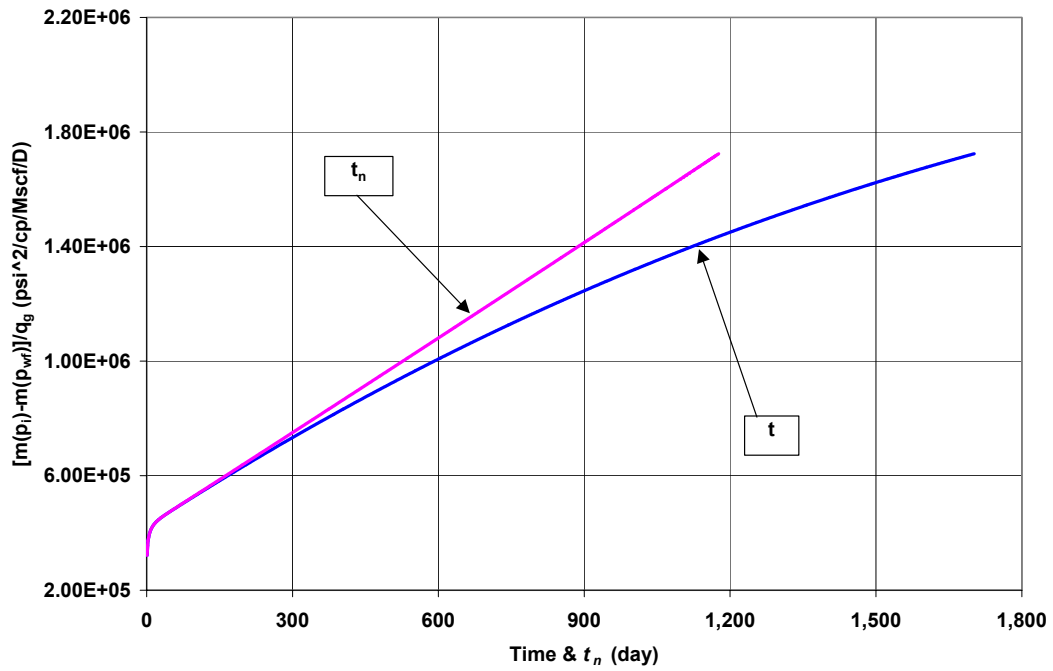
Fig. 4-8—Plot of $\Delta m(p)/q_g$ vs. t and t_n, showing that normalized pseudotime gives a straight line for the *PSS* period (Simulation Case 5).
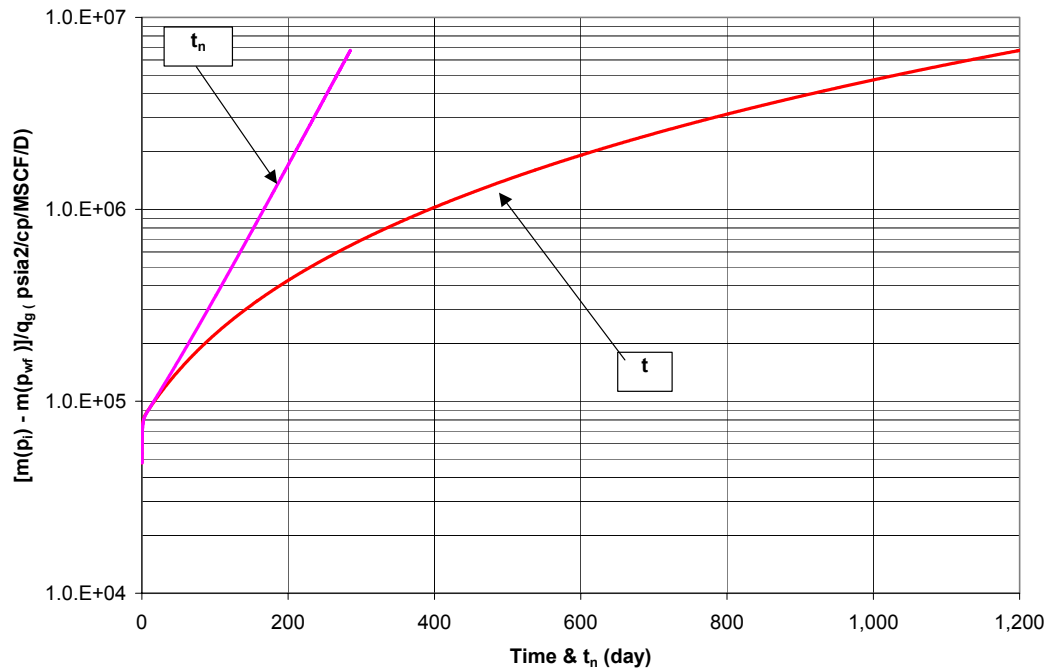
Fig. 4-9—Plot of $\dfrac{1}{q_g}$ vs. t and t_n, showing that normalized pseudotime gives a straight

line for the *PSS* period (Simulation Case 6).

Variable Rate and p_{wf}: Superposition Time

The Super_t takes into account the effect of rate and p_{wf} change as given in Eq. 4.1. To illustrate the shortcoming of using Eq. 4.1 with initial properties to calculate the OGIP, we used a simulation case with variable rate.

Simulation Case 7, Variable Rate

In this case, we use the same data for Case 5. The production data for Case 7 are with variable rate production shown in **Fig. 4-10**. The cumulative production is 4.73 Bcf with recovery factor of 54%. **Fig. 4-11** shows a plot of $\Delta m(p)/q_g$ vs. Super_t, which shows the following:

1) All periods have a transient period.
2) Periods 6 and 10 occur at same Super_t but do not fall in a straight line because of property changes.
3) Property changes prevent a unique straight line on Super_t plot.

We can conclude that Super_t takes into account the rate change but it does not correct for properties changes. Also, there is no unique value of OGIP from Super_t plot.

New Method: Normalized Pseudotime and Superposition

We combined the superposition effect with the effect of normalized pseudotime to cover the rate and properties change by replacing the real time with normalized pseudotime. By substituting Eq. 4.6 into Eq. 4.1, we have the new superposition
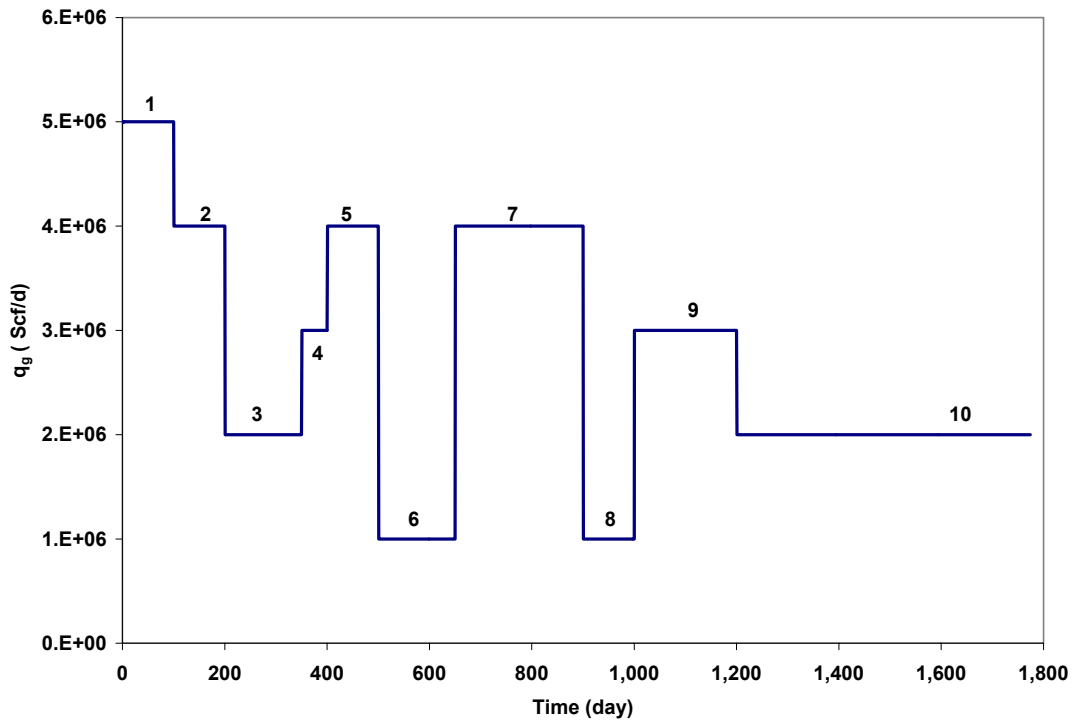
Fig. 4-10—Simulation Case 7 production rate.
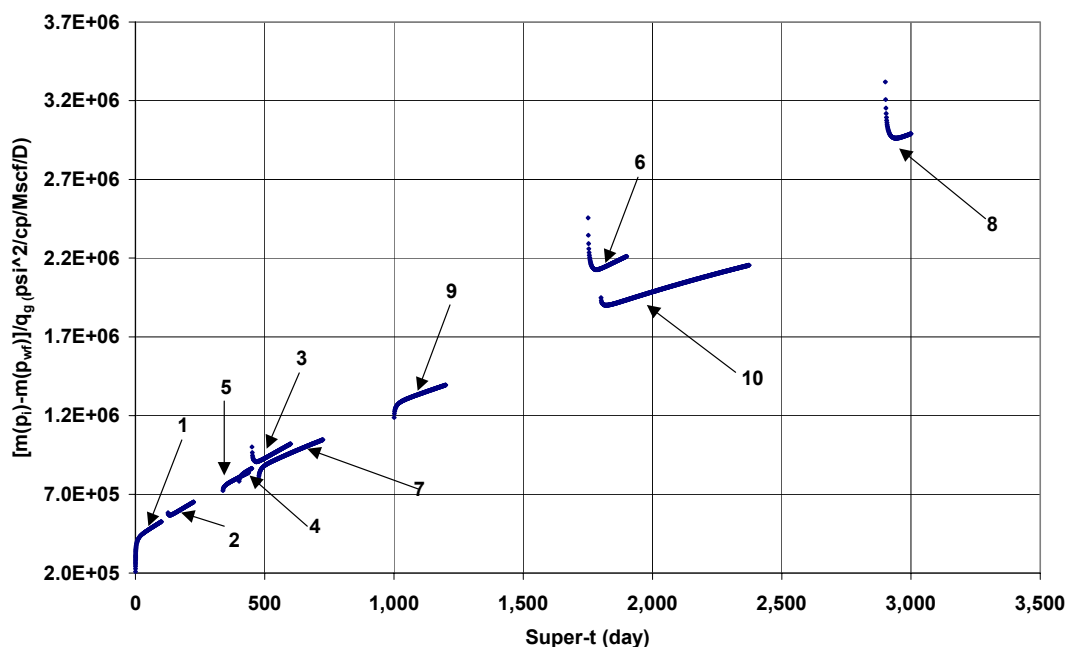
Fig. 4-11—Plot of $\Delta m(p)/q_g$ vs. Super-t, showing Super-t for Simulation Case 7.

normalized pseudotime equation,

$$\frac{[m(p_i) - m(p_{wfm})]}{q_{gm}} = \tilde{m}_{PSS} \left[\sum_{j=1}^{m} \frac{\Delta q_{gj}}{q_{gm}} (t_{nm} - t_{nj-1}) \right] + b \dots\dots\dots\dots\dots\dots\dots\dots (4.7)$$

The new superposition equation with normalized pseudotime corrects the error in Super-t and gives a straight line in the plot of $\Delta m(p)/q_g$ vs. normalized pseudotime and superposition (Super-t_n) instead of plotting Super-t. The slope $\tilde{m}_{PSS}$ of this plot can be used to calculate the OGIP from Eq. 4.2.

When we plot the simulation result of Case 7 by using Super-t_n all periods fall in straight line as shown in **Fig. 4-12.** The slope from **Fig. 4-12** gives OGIP equal to 8.54 Bcf, which is the same value from the tangent slope with current properties.

We can conclude that the normalized pseudotime gives unique value for OGIP for any rate schedule, property changes and depletion value.

Procedures for New Normalized Pseudotime and Superposition

The procedures to use the new normalized pseudotime and superposition follow.

1. Assume Value of OGIP.
2. Calculate average reservoir pressure from material balance at each time step.
3. Calculate the fluid properties at each $\bar{p}$.
4. Calculate normalized pseudotime from Eq. 4.5 at each time step.
5. Calculate the normalized pseudotime and superposition from Eq. 4.7 at each time step.
6. Calculate the OGIP from Eq. 4.2.
7. Repeat steps 1-6 until the value of OGIP converges within (2%).

We also include the change in porosity and water saturation with average reservoir pressure in calculating the total compressibility. The change in porosity as the pressure changes may be great especially in high-pressure gas reservoirs.

In calculating the normalized pseudotime, we update the initial water saturation and total compressibility at current average pressure by using Eqs. 4.8 and 4.9:

$$S_w(\bar{p}) = S_{wi} \, e^{(c_f + c_w)(p_i - \bar{p})} \quad\text{.. (4.8)}$$

$$c_t(\bar{p}) = c_f + c_w \, S_w(\bar{p}) + c_g \, (1 - S_w(\bar{p})) \quad\text{.. (4.9)}$$

The change in water in all cases is higher than 10% from the original value. To use the normalized pseudotime and superposition, we follow the iteration procedures as discussed in the next section.

57
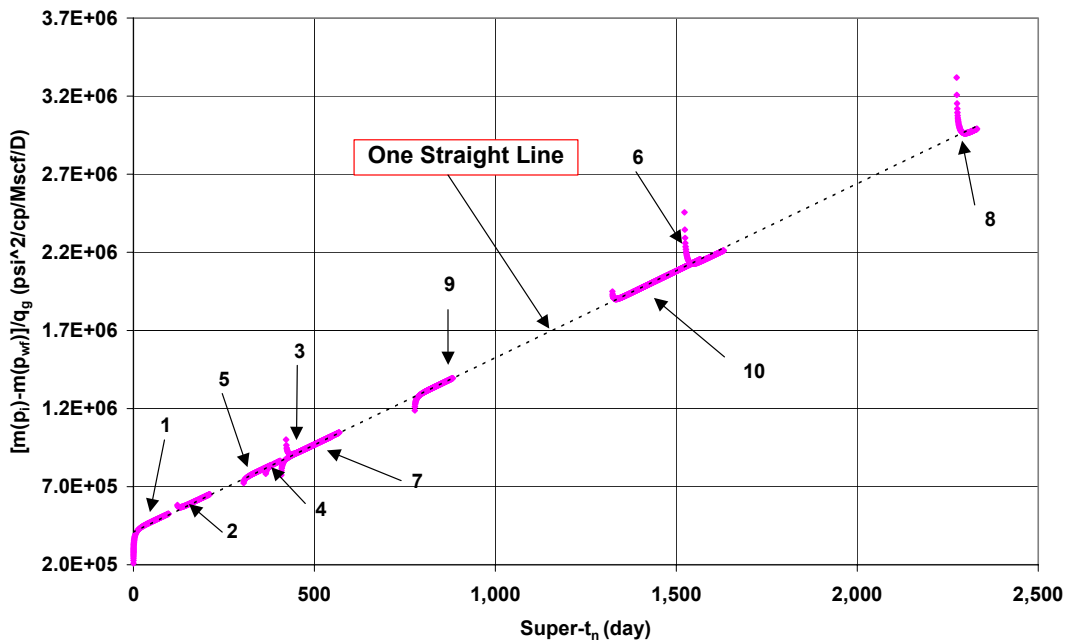
Fig. 4-12—Plot of Δm(p)/q$_g$ vs. Super.t$_n$ for Simulation Case 7.

Production Forecast with Initial Properties

Once OGIP has been evaluated gas-rate forecasting is not difficult. We can use the minimum OGIP from the forecast if no reservoir boundaries were reached during production. If the reservoir boundary was detected, we should correct our forecast with a normalized time function. We can use a method that is based on solving the material balance equation for volumetric gas reservoirs with the productivity index equation. The average reservoir pressure, $\bar{p}$, is estimated from material balance equation by using actual G_p:

$$R_F\left(\frac{\bar{p}}{\bar{z}}\right) = \left(\frac{p_i}{z_i}\right)\left(1 - \frac{G_p}{\text{OGIP}}\right) \quad\dots\dots\dots\text{(4.10)}$$

We should to use the most updated data, which uses stabilized q_g and p_{wf} to estimate a productivity index:

$$J_g = \frac{q_g}{[m(\bar{p}) - m(p_{wf})]} \quad \text{..(4.11)}$$

Then, we select future time steps and update the cumulative gas at each time step. Later, we use the material-balance equation to determine a new $\bar{p}$ to be used in the productivity-index equation to calculate q_g. Forecasting calculations will be conservative, if boundary effects have not yet been observed.

Production Forecast with Current Properties

The production forecast can be calculated by solving Eq. 4.1 as

$$\tilde{m}_{expd} = J_{CP} \frac{2 p_i S_{gi} \phi_i}{2.303 z_i\, OGIP} \left(\frac{1}{\bar{\phi}\bar{\mu}\,\bar{c}_t} \right) \quad \text{..................................} (4.12)$$

By solving Eq. 4.12 for q_{g2}, we have

$$q_{g2} = \frac{q_{g1}}{10^{[J_{CP} \frac{2 p_i S_{gi} \phi_i}{2.303 z_i\, OGIP} (\frac{t_2 - t_1}{\bar{\phi}\bar{\mu}\,\bar{c}_t})]}} \quad \text{...............................} (4.13)$$

Eq. 4.13 can be written as

$$q_{g2} = q_{g1}\, 10^{-[J_{CP} \frac{2 p_i S_{gi} \phi_i}{2.303 z_i\, OGIP} (\frac{t_2 - t_1}{\bar{\phi}\bar{\mu}\,\bar{c}_t})]} \quad \text{.................................} (4.14)$$

We can replace log (base 10) by natural log in Eq. 4.14 and write the final equation in general form:

$$q_{gi} = q_{gi-1}\, e^{-[J_{CP} \frac{2 p_i S_{gi} \phi_i}{z_i\, OGIP} (\frac{t_i - t_{i-1}}{\bar{\phi}\bar{\mu}\,\bar{c}_t})]} \quad \text{.................................} (4.15)$$

Eq. 4.15 is the similar to the exponential decline equation[13] but Eq. 4.15 uses of current reservoir properties instead of initial properties.

Summary

We have provided three new methods to calculate the correct value of OGIP for any change in pressure dependent properties and amount of depletion. The validity of these methods is confirmed by simulation cases for a single-layer reservoir; our future

work should extend these methods for commingled or multi layer reservoirs. The method does not include liquid load-up in calculating the bottomhole flowing pressure because we consider only single-phase gas flow.

From this work, we reached the following conclusions:

1. The use of pseudotime and pseudopressure transformation is essential in analyzing gas-well performance.

2. A new pseudotime presented here improves the accuracy of calculating OGIP.

3. If the recovery factor is high, reservoir pressure will decrease and reservoir properties will change, so that all methods for calculating OGIP using initial properties will have error.

4. The tangent slope method with current properties gives accurate OGIP under any change in reservoir pressure for constant-rate and constant pressure production.

5. The new method combing pseudotime with superposition gives accurate OGIP for any change in average pressure.

CHAPTER V

DETERMINING OGIP FOR WELLS IN PSEUDOSTEADY STATE WITH PERMEABILITY-DEPENDENT PRESSURE

In this chapter, we add the change of permeability with pressure to the calculation of OGIP in PSS for production at constant and variable rate and pressure.

Tangent Slope Using Current Properties

The tangent slope for determining OGIP in the *PSS* period with current reservoir properties takes into account the effect of reservoir property changes with pressure. Eq. 5.1 gives the modified equation for tangent slope for constant rate:

$$\text{OGIP} = \left(\frac{2p\,S_g\,\phi}{z}\right)_i \left(\frac{k(\bar{p})}{\phi(\bar{p})\mu(\bar{p})c_t(\bar{p})}\right)\left(\frac{1}{\tilde{m}_{PSS}}\right) \quad\text{.. (5.1)}$$

For constant pressure,

$$\text{OGIP} = J_{CP}\frac{2\,p_i\,S_{gi}\,\phi_i}{2.303z_i} \left(\frac{k(\bar{p})}{\phi(\bar{p})\,\mu(\bar{p})c_t(\bar{p})}\right)\left(\frac{1}{\tilde{m}_{\exp d}}\right) \quad\text{.. (5.2)}$$

The permeability variation is calculated by using the relationship defined by Petro *et al*[66]:

$$k = k_i\,e^{-\gamma(p_i-p)} \quad\text{.. (5.3)}$$

Eq. 5.3 shows the exponential relationship that is used in this work for all simulation cases. The γ value in Eq. 5.3 is calculated from experimental data. Without data to provide the correct value of γ a value of 0.0001 was used in our simulations to test Eqs. 5.2 and 5.3 in calculating OGIP.

Simulation Case 8, Constant Rate

The reservoir properties for Simulation Case 8 are given in **Table 4-1**, which represents a tight-gas well with high pressure. The production data for this well is shown in **Fig. 5-1** with constant rate production. **Fig. 5-2** shows a plot of $\Delta m(p)/q_g$ vs. *t*, which

shows non linearity during the *PSS* period which indicates changes in reservoir properties.

The point-wise calculation of OGIP from Eq. 4.2 with initial properties (**Fig. 5-3)** gives a high value of OGIP compared to the simulation value (OGIP = 8.7 Bcf). The error in OGIP value is as large as 129%.

But when we use Eq. 5.1 to calculate the OGIP with current properties, it gives the correct value of OGIP as shown in **Fig. 5-3** with error of only 1.8%.

We can conclude that the tangent slope with current reservoir properties gives the accurate value of OGIP for any properties change and depletion value.
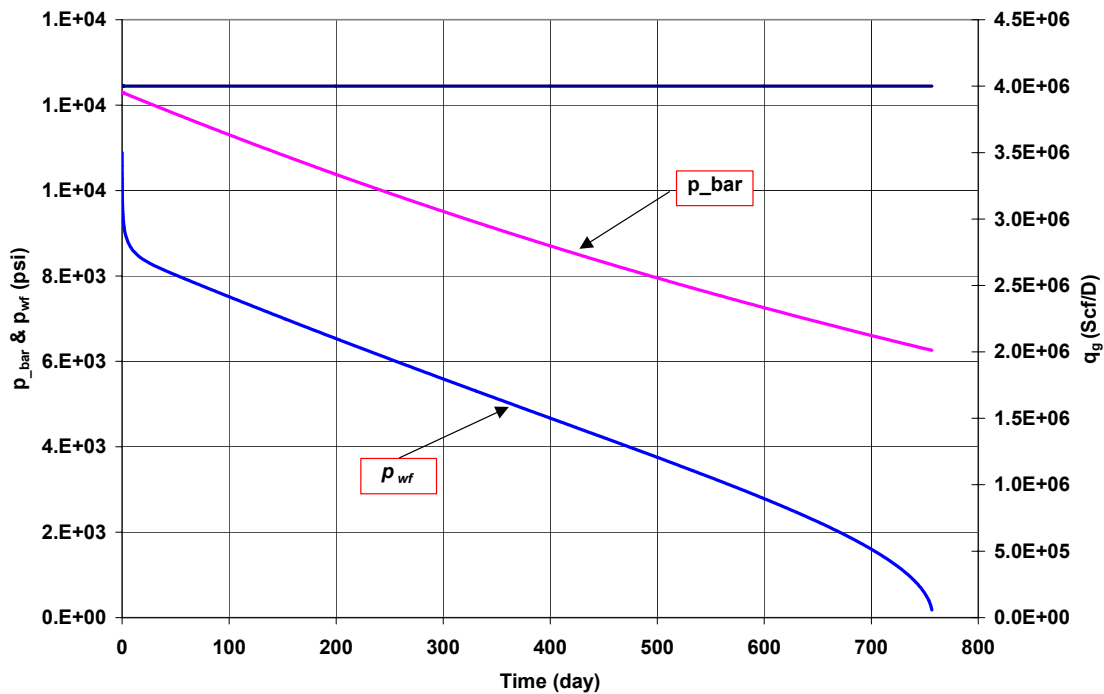
Fig. 5-1—Simulation Case 8 production data.
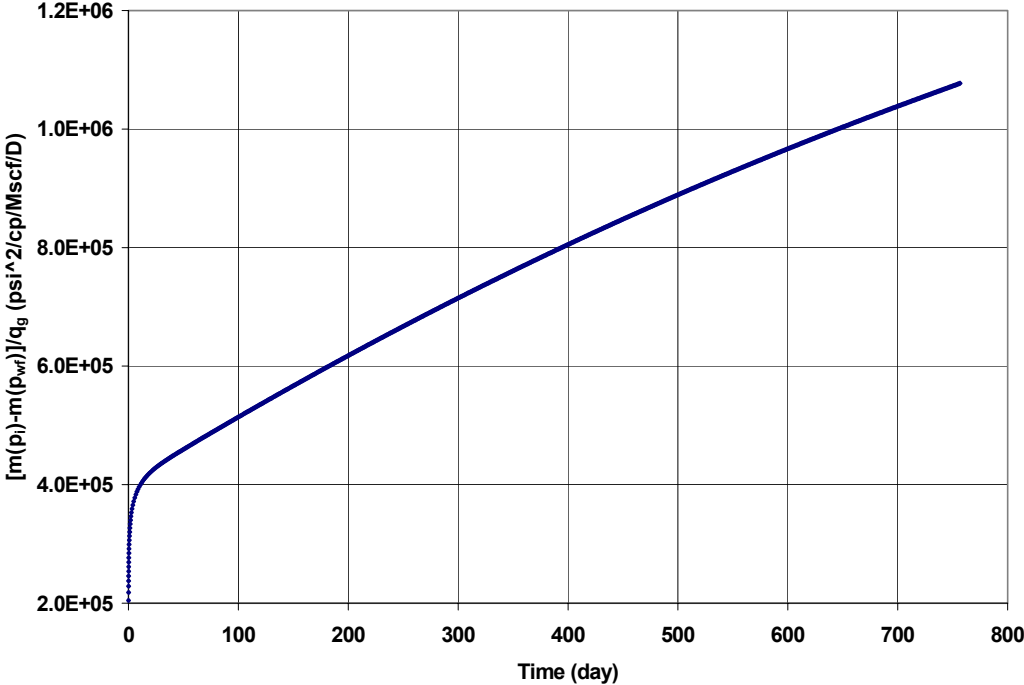
Fig. 5-2—Plot of $\Delta m(p)/q_g$ vs. time for Simulation Case 8.
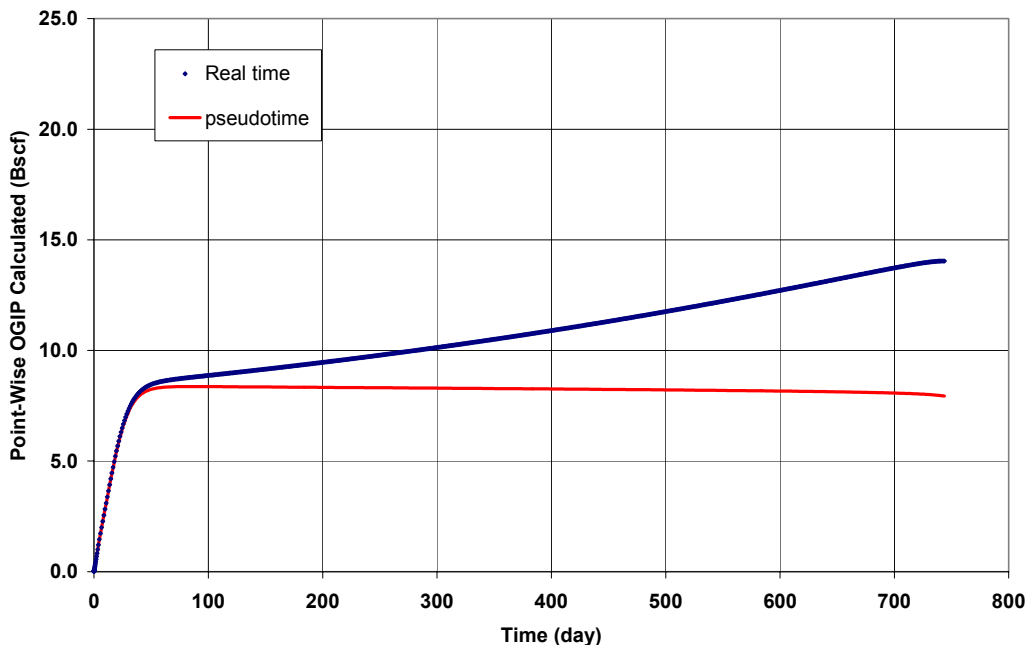
Fig. 5-3—Point-wise OGIP calculated vs. time with initial properties for Simulation Case 8.

Updated Normalized Pseudotime

The new normalized pseudotime provides a plotting function for analyzing the production data by taking into account the effect of reservoir property changes with average pressure. The derivation of the normalized pseudotime equation is given in Appendix B. The new normalized pseudotime with including permeability-dependent pressure is given by

$$\tilde{t}_n = (\frac{\phi\mu c_t}{k})_i \int_0^t \frac{k(\bar{p})}{\phi(\bar{p})\mu(\bar{p})c_t(\bar{p})} dt \quad\text{.. (5.4)}$$

This integration can be calculated using the trapezoidal rule.
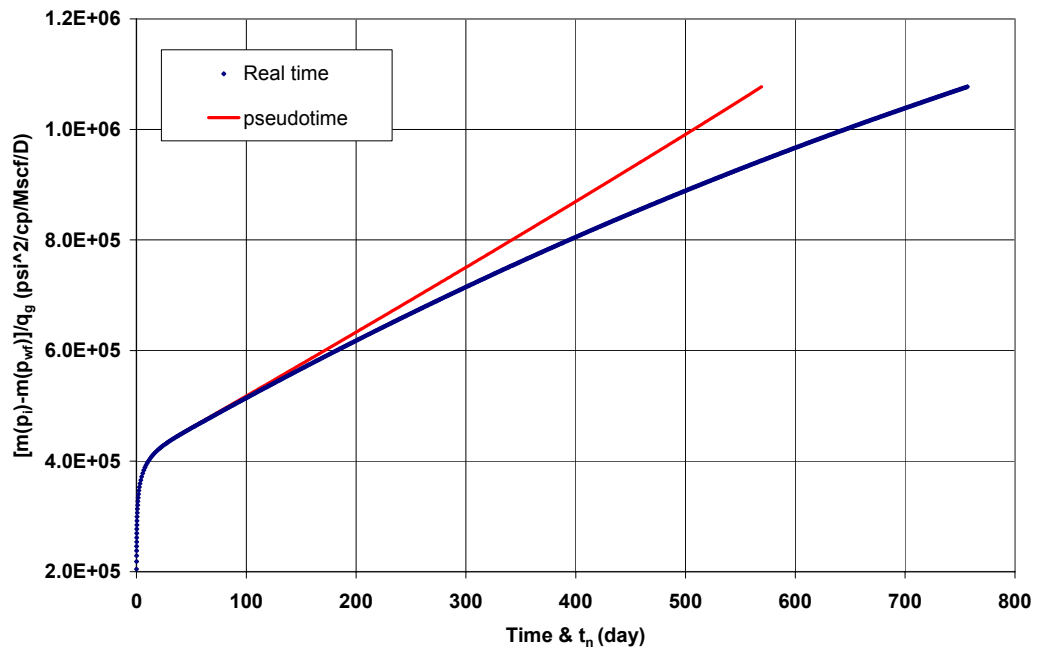
Fig. 5-4—Plot of $\Delta m(p)/q_g$ vs. time and $\widetilde{t}_n$ for Simulation Case 8.

A plot of $\Delta m(p)/q_g$ vs. $\tilde{t}_n$ for simulation result of Case 8 gives a straight line, (**Fig. 5-4)**. The slope from the $\tilde{t}_n$ plot used to calculate OGIP from Eq. 4.3 gives 8.54 Bcf with error of 1.8 % from the simulation value of OGIP = 8.7 Bcf.

We can conclude that the normalized pseudotime gives the correct OGIP because it takes into account the effect of property changes with average reservoir pressure.

Variable Rate and p_{wf}: Superposition Time

Superposition time takes into account the effect of rate and p_{wf} change as given in Eq. 4.1. To illustrate the shortcoming of using Eq. 4.1 with initial properties to calculate OGIP, we used a simulation case with variable rate.

Simulation Case 9, Variable Rate

In Case 9, we use the same data for Case 5 except permeability is function on pressure. The production data for Case 9 with variable rate production are shown in **Fig. 5-5**. The cumulative production is equal to 4.73 Bcf with recovery factor of 54%. **Fig. 5-6** shows a plot of $\Delta m(p)/q_g$ vs. Super-t, which shows the following:

4) All production periods have transient flow period.
5) Periods 6 and 9 occur at same Super-t but do not fall in a straight line because of property changes.
6) Property changes prevent a unique straight line from Super-t.

We can conclude that the Super-t takes into account the rate change but it does not correct for property changes. Also, Super-t does not give a unique value of OGIP due to property changes.
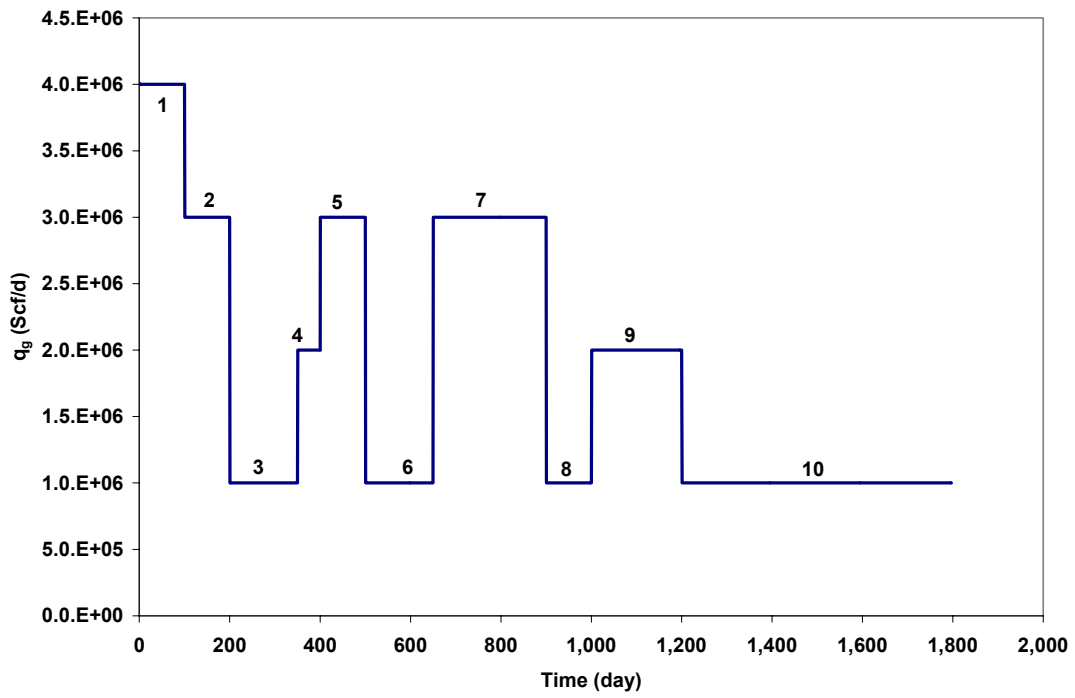
Fig. 5-5—Simulation Case 9 production rate.
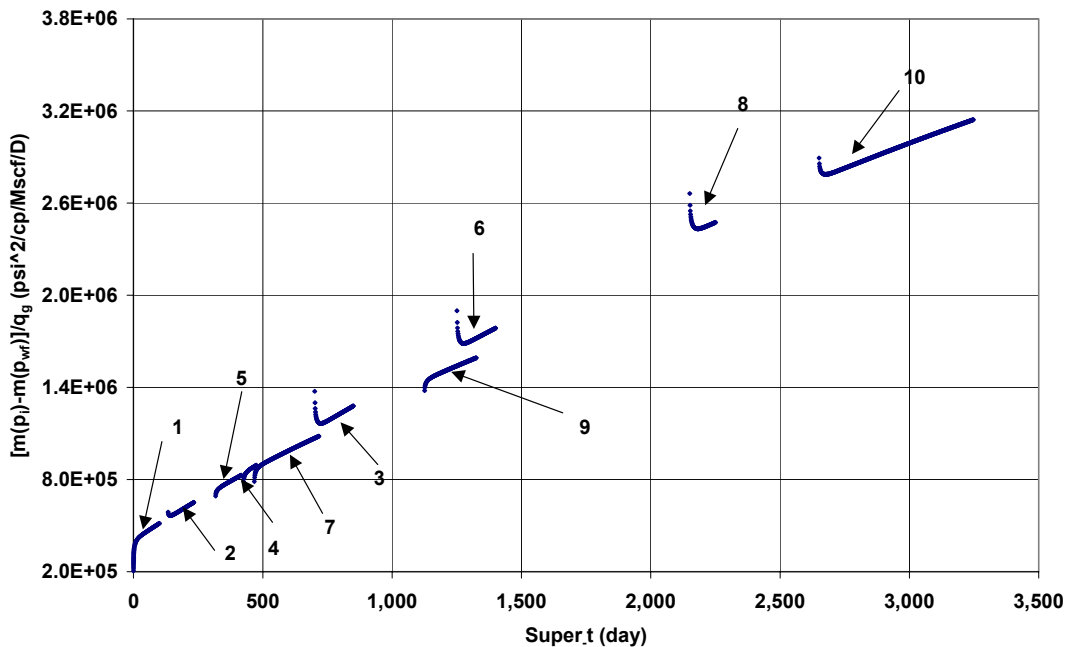
Fig. 5-6—Plot of $\Delta m(p)/q_g$ vs. Super.t for Simulation Case 9.

Updated Normalized Pseudotime and Superposition

We combined the superposition effect with the effect of normalized pseudotime to cover the rate and property changes by replacing the real time with normalized pseudotime. By substituting Eq. 5.4 into Eq. 4.1, we have the new superposition normalized pseudotime equation:

$$\frac{[\,m(\,p_i\,) - m(\,p_{wfm}\,)\,]}{q_{gm}} = \widetilde{m}_{PSS}\,[\sum_{j=1}^{m} \frac{\Delta q_{gj}}{q_{gm}}(\,t_{nm} - t_{nj-1}\,)\,] + b \,\dots\dots\dots\dots\dots\dots\dots (5.5)$$

The new Super.t$_n$ corrects the error in Super.t and gives a straight line plot of $\Delta m(p)/q_g$ vs. Super.t$_n$. The slope $\widetilde{m}_{PSS}$ of this plot can be used to calculate the OGIP from Eq. 4.2.

When we plot the simulation result of Case 9 by using Super.t$_n$, all periods fall in a straight line as shown in **Fig. 5-7.** The slope from **Fig. 5-7** gives OGIP equal to 8.16

Bcf, which is the same value of the tangent slope method with current properties. The average error percent is equal 9%, which is higher than the error without including pressure dependent permeability.

We can conclude that the Super_t_n gives a unique value for OGIP under any rate schedule, property change, and depletion value including the effect of pressure dependent permeability.
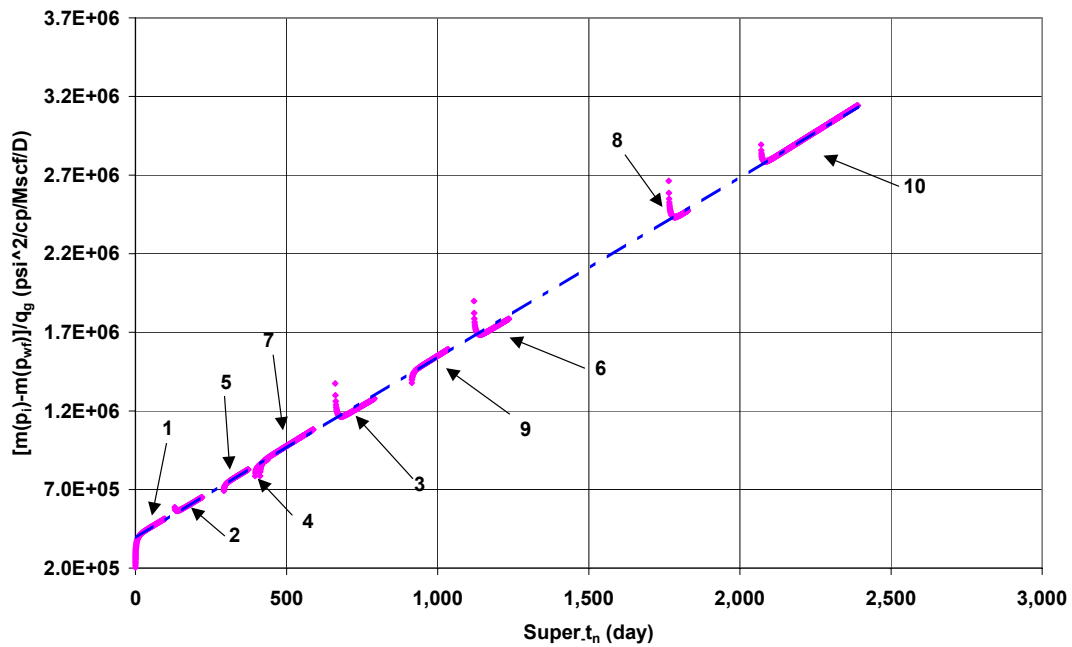
Fig. 5-7—Plot of $\Delta m(p)/q_g$ vs. Super_t_n, for Simulation Case 9.

Summary

From this work, we conclude that ignoring the pressure dependence of permeability will result in erroneous values of OGIP. We suspect that ignoring this pressure dependence is probably common and that accurate laboratory data are rare.

CHAPTER VI

ANALYSIS OF RATE DEPENDENCE IN TRANSIENT PERIOD

OF LINEAR FLOW IN TIGHT GAS WELLS

Reservoir Properties for Constant Rate and p_{wf} Production

The reservoir properties for constant-rate and constant-pressure production in the transient period can be calculated from analytical solutions. The interpretation expressions described in **Table 6-1** can be used to calculate the permeability-thickness product; the drainage area, A; the pore volume, V_p; and the OGIP for either constant-rate production or constant-pressure production. Additionally, for the case of linear flow with intercept at the origin, we can evaluate formation damage or the earlier-flow-regime effect, b. We need to know the slope, the intercept to the origin, if it exists, and values for other reservoir parameters. The calculations of A_c and b are very difficult, unless k is known independently. We do not need to know the value of k and A_c to estimate A.

We can estimate a precise value of V_p without actually having good knowledge of permeability of the formation, k; porosity, ϕ; thickness, h; or drainage area, A. Similarly, the evaluation of OGIP is insensitive to the value of initial water saturation, S_{wi}, used, if initial gas compressibility, c_{gi}, dominates the initial total compressibility, c_{ti} (or $c_{ti} \approx S_{gi}c_{gi}$). We can estimate a precise value of *OGIP* without actually having good knowledge of k, h, A, S_{wi} and ϕ.

The direct determination of V_p and OGIP without known ϕ, k, h and A is an advantage, since these properties are often not known in tight gas reservoirs.

The estimates of A, V_p, and OGIP evaluated with the expressions in **Table 6-1** for either constant-rate production or constant-pressure production would be considered minimum values, if all the history data are still on the straight line trend on the $\sqrt{t}$ plot (i.e. infinite-acting linear flow: no outer boundaries are reached). In this case, the latest production time is used instead of the end time of the straight line on the $\sqrt{t}$ plot, t_{esr}.

The boundary distance, y_e, evaluated with the expressions for y_e in **Table 6-1** would be considered the minimum value if all the history data are still on the straight-line trend on the $\sqrt{t}$ plot. In this case, instead of t_{esr} the latest production time gives the distance of investigation. These formulas require that k be known, K be known from an independent source because uncertainty in k results in uncertainty in the calculated value of y_e.

Modified Equations for Calculating Reservoir Properties

Arévalo[2-3] modified the constant-rate and pressure equations to match the actual value of OGIP in simulation models but did not mention the reason for the error in these equations. We investigated parameters that prevent simulation results from matching the analytical results. The modified equation for both constant rate and pressure is given in **Table 6-2** with 22% error. In the next section we going present the effect of drawdown on the accuracy of the solution.

TABLE 6-1—CALCULATION OF RESERVOIR PROPERTIES FOR LINEAR FLOW REGIME FOR BOTH CONSTANT p_{wf} PRODUCTION AND CONSTANT q_g PRODUCTION

Constant p_{wf} production	Constant q_g production
$$\sqrt{k}\,A_c = \frac{1261.73\,T}{\sqrt{(\phi\mu_g c_t)_i}}\left(\frac{1}{\tilde{m}_{CPL}}\right)$$	$$\sqrt{k}\,A_c = \frac{803.24\,T}{\sqrt{(\phi\mu_g c_t)_i}}\left(\frac{1}{\tilde{m}_{CRL}}\right)$$
$$A = \frac{200.769\,T}{(\phi\mu_g c_t)_i}\left(\frac{\sqrt{t_{esr}}}{\tilde{m}_{CPL}h}\right)$$	$$A = \frac{90.36\,T}{(\phi\mu_g c_t)_i}\left(\frac{\sqrt{t_{esr}}}{\tilde{m}_{CRL}h}\right)$$
$$V_p = \frac{200.769\,T}{(\mu_g c_t)_i}\left(\frac{\sqrt{t_{esr}}}{\tilde{m}_{CPL}}\right)$$	$$V_p = \frac{90.36\,T}{(\mu_g c_t)_i}\left(\frac{\sqrt{t_{esr}}}{\tilde{m}_{CRL}}\right)$$
$$OGIP = \frac{200.769\,T\,S_{gi}}{(\mu_g c_t B_g)_i}\left(\frac{\sqrt{t_{esr}}}{\tilde{m}_{CPL}}\right)$$	$$OGIP = \frac{90.36\,T\,S_{gi}}{(\mu_g c_t B_g)_i}\left(\frac{\sqrt{t_{esr}}}{\tilde{m}_{CRL}}\right)$$
$$b = \frac{b_{CPL}k\sqrt{A_c}}{1422\,T}$$	$$b = \frac{b_{CRL}k\sqrt{A_c}}{1422\,T}$$
$$y_e = 0.1125\sqrt{\frac{kt_{esr}}{(\phi\mu_g c_t)_i}}$$	$$y_e = 0.1591\sqrt{\frac{kt_{esr}}{(\phi\mu_g c_t)_i}}$$

TABLE 6-2—MODIFIED EQUATIONS FOR LINEAR FLOW REGIME IN HOMOGENEOUS MODEL FOR BOTH CONSTANT p_wf PRODUCTION AND CONSTANT q_g PRODUCTION

Constant p_{wf} production	Constant q_g production
$$\sqrt{k}\,A_c = \frac{1262\,T}{\sqrt{(\phi\mu_g c_t)_i}}\left(\frac{1}{\tilde{m}_{CPL}}\right)$$	$$\sqrt{k}\,A_c = \frac{803\,T}{\sqrt{(\phi\mu_g c_t)_i}}\left(\frac{1}{\tilde{m}_{CRL}}\right)$$
$$A = \frac{225\,T}{(\phi\mu_g c_t)_i}\left(\frac{\sqrt{t_{esr}}}{\tilde{m}_{CPL}\,h}\right)$$	$$A = \frac{128\,T}{(\phi\mu_g c_t)_i}\left(\frac{\sqrt{t_{esr}}}{\tilde{m}_{CRL}\,h}\right)$$
$$V_p = \frac{225\,T}{(\mu_g c_t)_i}\left(\frac{\sqrt{t_{esr}}}{\tilde{m}_{CPL}}\right)$$	$$V_p = \frac{128\,T}{(\mu_g c_t)_i}\left(\frac{\sqrt{t_{esr}}}{\tilde{m}_{CRL}}\right)$$
$$OGIP = \frac{225\,T\,S_{gi}}{(\mu_g c_t B_g)_i}\left(\frac{\sqrt{t_{esr}}}{\tilde{m}_{CPL}}\right)$$	$$OGIP = \frac{128\,T\,S_{gi}}{(\mu_g c_t B_g)_i}\left(\frac{\sqrt{t_{esr}}}{\tilde{m}_{CRL}}\right)$$
$$b = \frac{b_{CPL}\,k\sqrt{A_c}}{1424\,T}$$	$$b = \frac{b_{CRL}\,k\sqrt{A_c}}{1424\,T}$$
$$y_e = 0.1779\sqrt{\frac{k t_{esr}}{(\phi\mu_g c_t)_i}}$$	$$y_e = 0.1591\sqrt{\frac{k t_{esr}}{(\phi\mu_g c_t)_i}}$$

Effect of Drawdown on Constant p_{wf}

We studied the effect of drawdown on the constant-p_{wf} production in linear flow. We compared analytical solution with simulation results for different values of drawdown and found that the drawdown value affects the slope in all equations in **Table 6-1**. The drawdown parameter is given by

$$m_{DR} = \frac{[m(p_i) - m(p_{wf})]}{m(p_i)} \quad \text{..} \quad (6.1)$$

A plot of $\Delta m(p)/q_g$ vs. $\sqrt{t}$ gives a straight line with slope ($\tilde{m}_{CPL}$). The slope gives the value of $\sqrt{k} A_C$. We simulated the effect of drawdown on the accuracy of slope and we found that the difference between the analytical slope and simulated slope increases as the drawdown increases.

Simulation Case 10, Constant p_{wf}

The effect of drawdown (m_{DR}) on slope is verified by using reservoir simulation. The simulation data appear in **Table 6-3**. **Fig. 6-1** compares the analytical solution and different drawdown values. As the drawdown value increased, the non linearity increased, which gave the wrong slope, which is used to calculate the product of $\sqrt{k} A_C$ and OGIP. The error in OGIP from the slope can reach up to 22% compared to the actual value for the highest drawdown. The non linearity effect is the same for different initial reservoir pressures as shown in **Fig. 6-2** and **Fig. 6-3** for the same simulation data except for the initial pressure.

We conclude that the initial pressure does not affect the non linearity, but the main factor is drawdown, thus proving that the linear model is rate dependent. The drawdown effect on the real-gas pseudopressure and p/z is shown in **Fig. 6-4,** which represents the non linearity problem with the higher drawdown value. The relation becomes increasingly non linear as the drawdown value increases which affect the slope of the plot of rate vs. $\sqrt{t}$.

Correction for Non-Linearity Problem

We used the simulation results to correct the error in the slope. First, we calculated the ratio between the actual value for each drawdown and the ideal value from the simulation model. The correct equations can be written as

$$\sqrt{k}\,A_C = f_{\sqrt{t}}\,\frac{1261.7308}{\sqrt{(\phi\mu c_t)_i}}\left\{\frac{T}{m_{CP}}\right\} \quad\text{...} (6.2)$$

and

$$OGIP = f_{\sqrt{t}}\,\frac{200.76\,T\,S_{gi}}{(\mu_g c_t B_g)_i}\left(\frac{\sqrt{t_{esr}}}{\tilde{m}_{CPL}}\right) \quad\text{...} (6.3)$$

Where $f_{\sqrt{t}}$ is the correction factor that corrects the slope value without the production rate.

Fig. 6-5 shows the simulation result of the correction factor for different drawdown value using the least square method to find the best correlation between correction factor $f_{\sqrt{t}}$ and drawdown (m_{DR}). This correlation is given by,

$$f_{\sqrt{t}} = 0.9895 - 0.0857\,m^2_{DR} - 0.0852\,m_{DR} \quad\text{...} (6.4)$$

The correction factor corrects the slope value for the rate-dependent problem and gives the correct value for $\sqrt{k}\,A_C$ and *OGIP*.

TABLE 6-3—SIMULATION DATA		
gas specific gravity (air = 1), γ_g	0.717	
Initial temperature, T	290	°F
Initial pressure, pi	8,800	psia
Formation porosity, ϕ	0.15	fraction
Average water saturation, S_w	0.47	fraction
Formation net pay thickness, h	361.99	ft
Water compressibility at p_i, c_w	4.1x10^{-6}	1/psia
Formation compressibility, c_f	4.08x10^{-6}	1/psia
Reservoir Width	1070	ft
Reservoir Length	467	ft
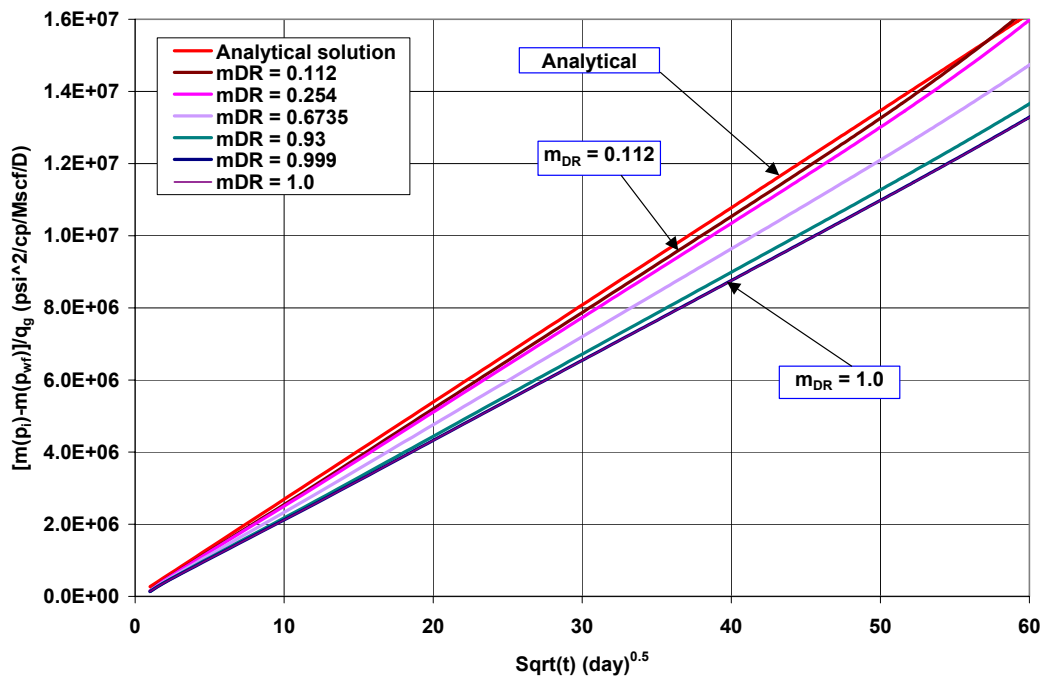
Fig. 6-1—Linear flow is "rate dependent" for extreme variations of constant p_{wf} cases at $p_i = 8{,}800$ psi.
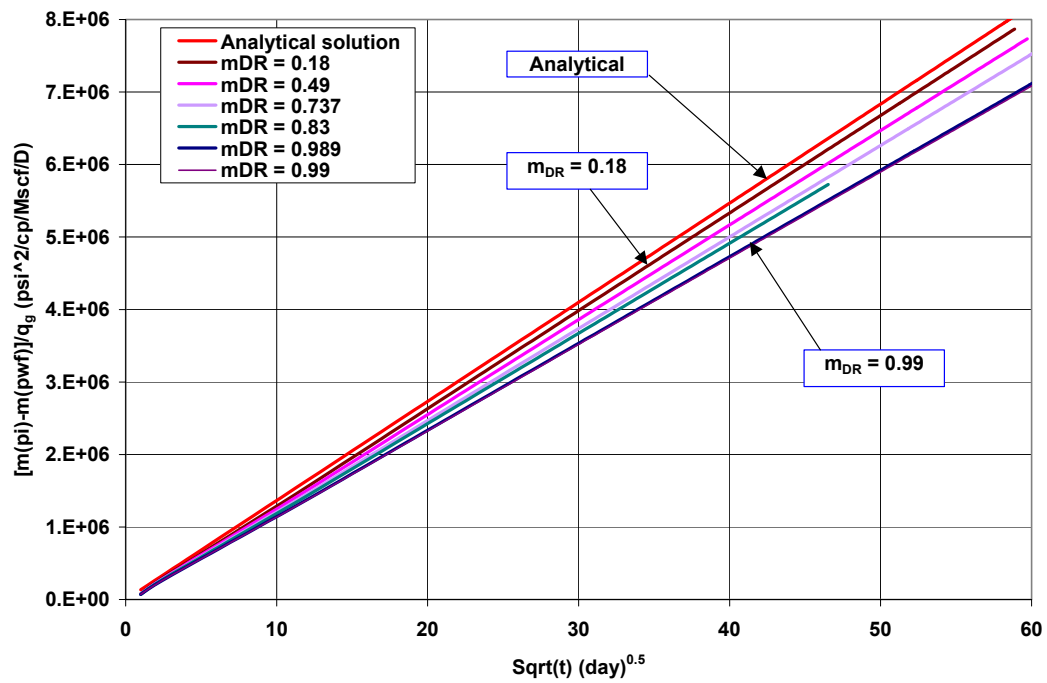
Fig. 6-2—Linear flow is "rate dependent" for extreme variations of constant p_{wf} cases at $p_i = 2,000$ psi.
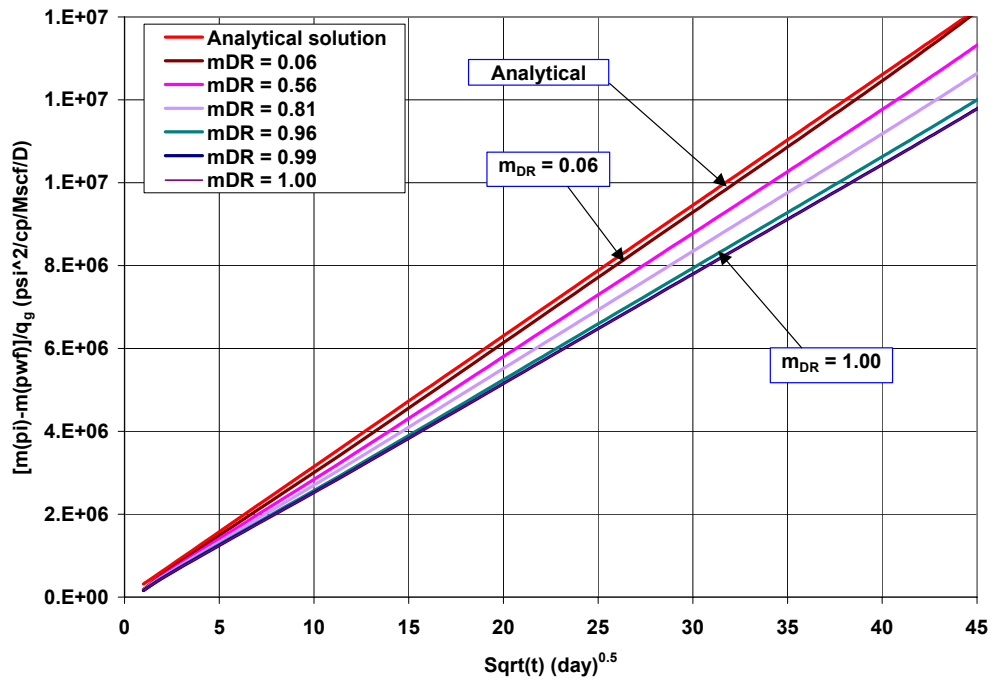
Fig. 6-3—Linear flow is "rate dependent" for extreme variations of constant p_{wf} cases at $p_i = 13,800$ psi.
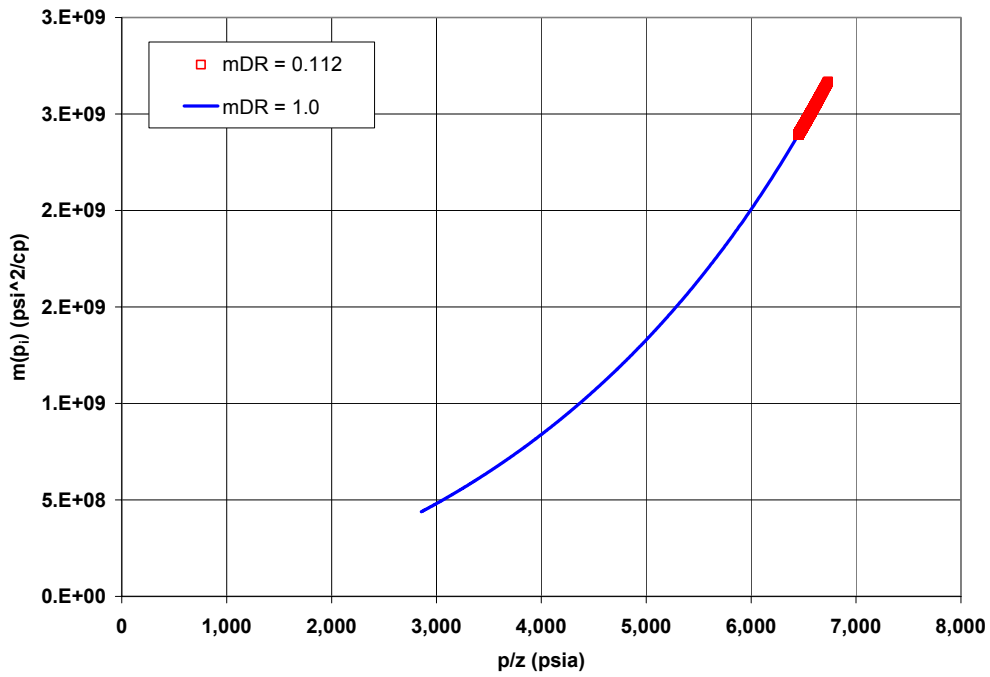
Fig. 6-4—Plot of real gas pseudopressure m(p) vs. p/z becomes non-linear for extreme variation of drawdown value (m_{DR}) cases at $p_i = 8,800$ psi.
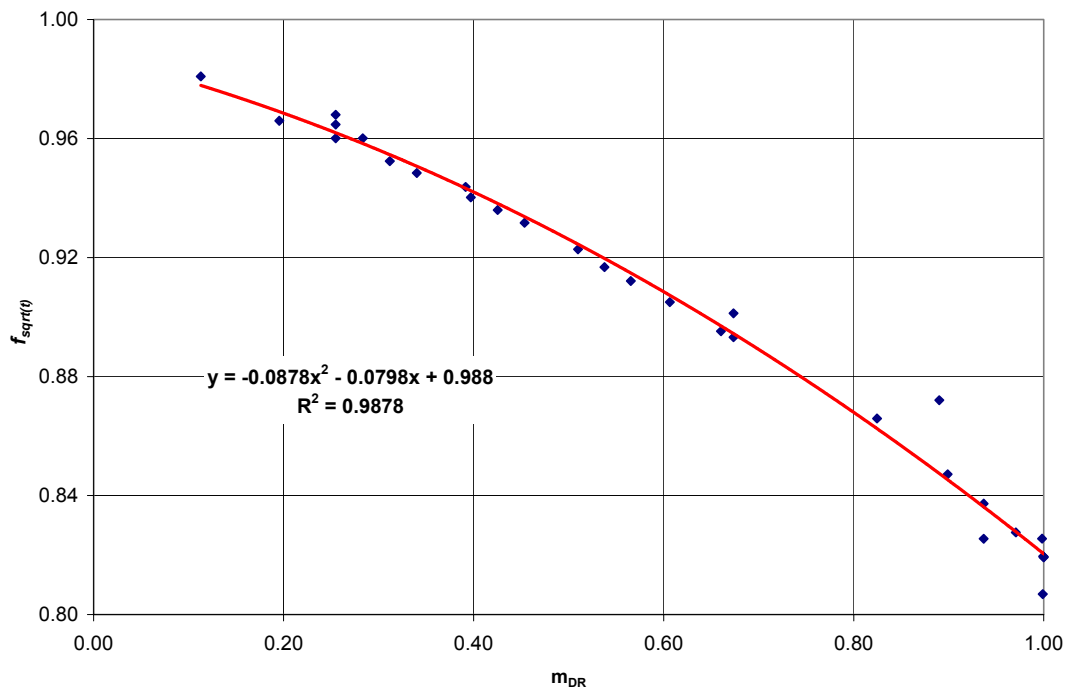
Fig. 6-5—The correction factor matches drawdown values for different reservoir conditions.

Effect of Drawdown on Superposition Time Plot

The superposition time accounts for variable rate production case. The superposition transfers the constant p_{wf} to constant rate production, so the constant rate

solution used to analyze the linear flow plot. Eq. 6.5 represents the infinite-acting linear flow for variable rate production.

$$\frac{[m(p_i) - m(p_{wf})]}{q_g} = \frac{803.243\,T}{\sqrt{k}\,A_c\,\sqrt{(\phi\mu_g c_t)_i}}\frac{1}{q_{g,n}}\sum_{j=1}^{n}(q_{g,j} - q_{g,j-1})\sqrt{t_n - t_j} \quad \text{..........} \quad (6.5)$$

The slope value m_{CR} used to calculate OGIP by determining the end point of transient period (t_{esr}) on the plot as in Eq. 6.6.

$$OGIP = \frac{90.36\,T\,S_{gi}}{(\mu_g c_t B_g)_i}\left(\frac{\sqrt{t_{esr}}}{\tilde{m}_{CPL}}\right) \quad \text{...} \quad (6.6)$$

Simulation result were used to show the effect of non linearity on constant-rate plot. **Fig. 6-6** shows the effect of drawdown on superposition time. The error in the value of OGIP for each drawdown value can be up to 20% compared to the actual (simulation) value.

Correction Factor for Superposition Time Plot

Fig. 6-7 shows the simulation result of the correction factor for different drawdown value using the least square method to find the best correlation between correction factor f_{super} and drawdown (m_{DR}). This correlation is given by,

$$f_{super} = 0.9833 - 0.1512\,m^2{}_{DR} - 0.0258\,m_{DR} \quad \text{...} \quad (6.7)$$

The correction factor corrects the slope value for the rate-dependent problem and gives the correct value for $\sqrt{k}\,A_C$ and *OGIP*.
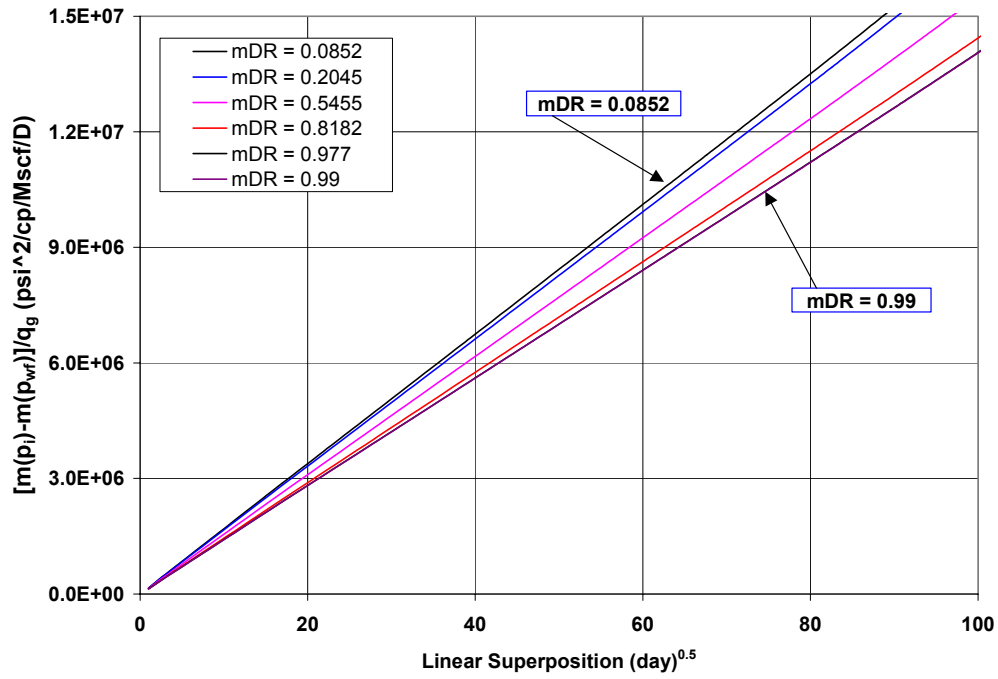
Fig. 6-6—Effect of drawdown value on the slope of superposition time plot.
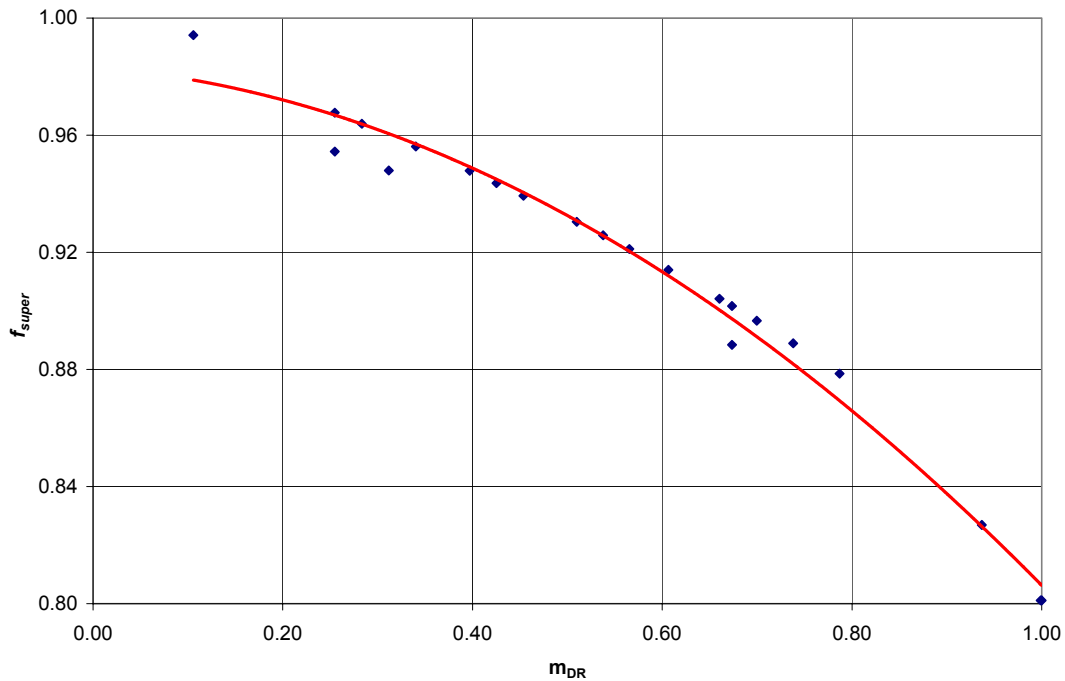
Fig. 6-7—The correction factor vs. drawdown values for different reservoir conditions.

Effect of Non-Linearity on Radial Model

In this section, we will discuss the effect of the non linearity problem on the radial model for both constant rate and pressure production. **Fig. 6-8** shows no effect of drawdown on the semi-log plot for different values of p_{wf} production. Also, **Fig. 6-9** show no effect of drawdown on the semi-log plot for different value of constant rate production. So, we can conclude that radial model is not rate dependent for both constant rate and pressure cases.
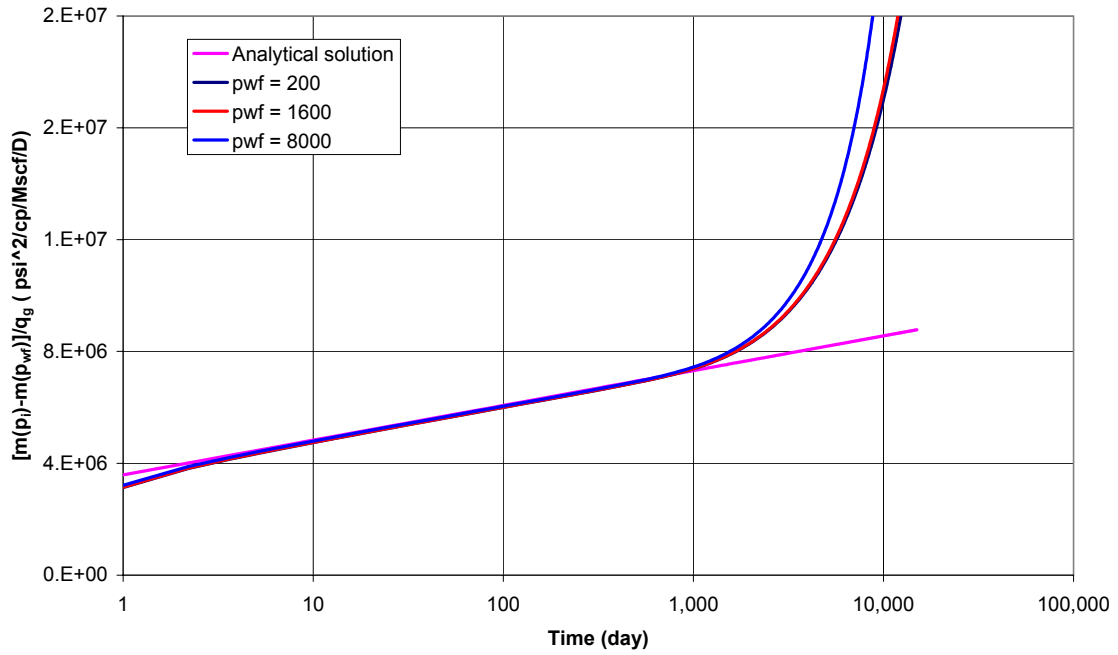
Fig. 6-8—Plot of Δm(p)/q_g vs. time for constant-pressure radial model.
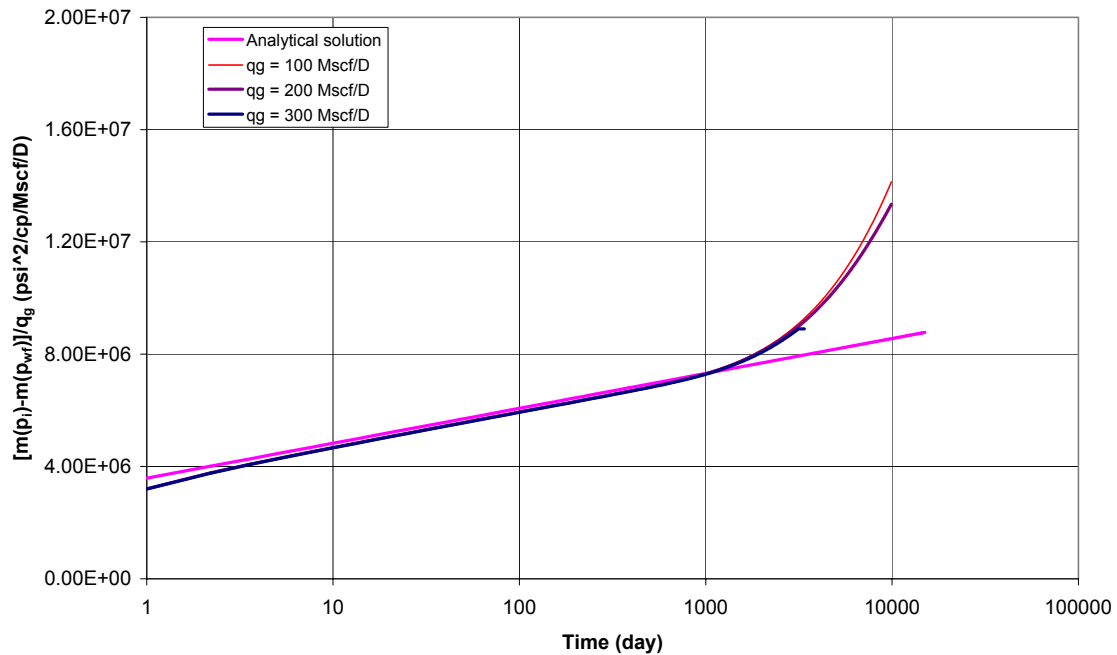
Fig. 6-9—Plot of $\Delta m(p)/q_g$ vs. time for constant-rate radial model.

Summary

From the work done in this study, the following conclusions can be reached.

1. The drawdown value is the major factor on the non linearity of $\sqrt{t}$ time plot.

2. The drawdown effect can cause error in OGIP up to 22%.

3. The drawdown value is the major factor on the non linearity of superposition time plot.

4. The radial model is not rate dependent.

CHAPTER VII

FIELD APPLICATIONS

Introduction

In the previous chapters, we introduced different methods to analyze the performance of wells producing with long-term production. In this chapter we introduce the application of those methods to several field cases for gas wells. We also present a computer program that incorporates some of the techniques presented in this dissertation. The procedure used different graphs and equations to identify flow regimes and estimate reservoir properties and OGIP.

Description of Computer Program

Our computer program is written in Visual Basic for Excel with a user-friendly menu structure. Different reservoir models are built into the program: Radial, Linear, and PSS. The program consists of six different modules:

Gas Properties and Pseudopressure Module

In gas properties and pressure module, we calculate the effect of gas impurities like (N_2, CO_2, and H_2S) by using Dranchuk and Abou-Kassem[67] correlation. The Sutton[68] correlations is used to calculate the z-factor. Gas viscosity is calculated with the Lee *et al* correlation[69]. Then, the pseudopressure is calculated with the Al-Hussainy and Ramey[7] integral.

Bottomhole Flowing Pressure Module

In the bottomhole flowing pressure module, p_{wf} is calculated from wellhead flowing pressure by using Cullender and Smith's method[70] for single phase gas flow.

Main Module

In the main module, we calculate the normalized pseudotime, normalized pseudotime and superposition, superposition, and time for radial, linear, and PSS flow.

Decline Curve Module

In the decline curve module, we calculate the decline-curve parameters by using new normalized pseudotime.

Export Data

In the export data module, can export the data file to text-file format.

Help Module

The help module provides the help for using the program.

Data Required for Analysis

The program for analysis of gas wells requires production and PVT data. The production data must include flow rates and wellhead flowing pressure. The PVT data must include a data table containing corresponding values of pressures, gas deviation factors, viscosities, and fluid properties.

Fig. 7-1 Shows a flow chart of the procedures used to calculate the correct value of OGIP from long-term production data.
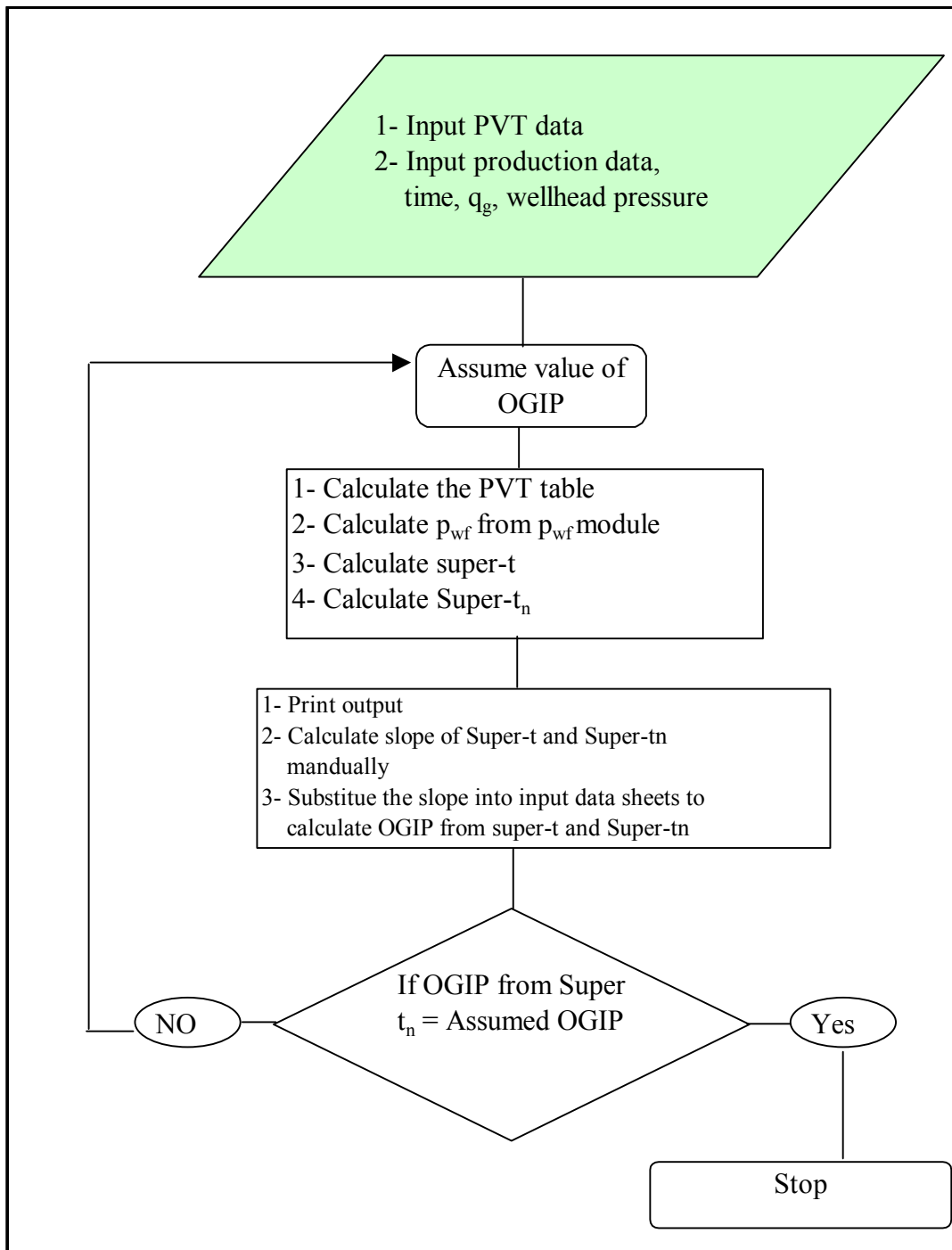
Fig. 7-1—Flow chart of OGIP program for gas well.

Analysis of Gas Well

In this section, we present analysis for 13 gas wells in the PSS and transient linear flow periods. **Table 7-1** shows the OGIP calculated from the Super.t method by using the initial properties. We will compare this value of OGIP with our new method. The complete analyses for 13 tight gas wells are presented in Appendix E.

TABLE 7-1—GENERAL INFORMATION OF CASE HISTORIES OF TIGHT GAS WELLS						
Number	**Well**	**Type of flow**	t_{prod}	p_i	G_p	**OGIP Super.t**
			(days)	psi	(Bcf)	(Bcf)
1	Boren 1	PSS	901	12,300	6.50	15.60
2	HR-58	PSS	532	14,000	6.29	16.21
3	HR-60	PSS	659	14,000	5.03	12.00
4	HR-61	PSS	218	13,000	3.38	9.00
5	HR-62	PSS	367	13,000	5.53	16.28
6	HR-64	PSS	298	14,000	0.13	0.24
7	HR-54	PSS	471	14,900	6.53	15.15
8	HR-56	PSS	470	14,100	5.39	12.21
9	CC-5	PSS	520	12,500	3.24	7.24
10	CC-6	PSS	488	14,068	2.82	6.71
11	CC-7	PSS	445	12,500	2.40	6.71
12	CC-2	PSS	671	13,500	4.65	10.53
13	WELL A	Linear	16,060	5,463	13.52	40.29

Analysis of Boren 1 Well

Boren 1 is from a tight gas reservoir with high pressure in south Texas. **Fig. 7-2** shows the production history of Boren 1. **Fig. 7-3** shows a log-log diagnostic plot of $\Delta(m)p/q_g$ vs. t for Boren 1. The diagnostic plots shows a half-slope for almost 100 days followed by a unit slope for more than 800 days. So this well shows boundary effects after 100 days due to small reservoir size.

Production data are plotted against the Super.t and Super.t_n on the same graph to illustrate the necessity of using normalized pseudotime as shown in **Fig. 7-4**. When

plotted against Super.t$_n$ the data exhibits a straight line with one slope. In this case the OGIP is calculated to be 8.14 Bcf, which is confirmed by the simulation model.

However, when real time is used, the production data do not show a straight line; instead, it shows a curve with decreasing slope. The OGIP calculated using the Super.t was as high as 32.0 Bcf based where the slope were taken.

The OGIP is calculated by using the slope from an early point in the PSS period. This value is used as the first trial to calculate the normalized pseudotime. This normalized pseudotime is then used in the superposition calculation to determine a new OGIP. The process is repeated until it converges as described in the above procedures to calculate the normalized pseudotime. **Fig. 7-5** shows the result of OGIP from iteration procedures that give 7.97 Bcf with error of 2.2% compared with the actual value (8.15 Bcf).
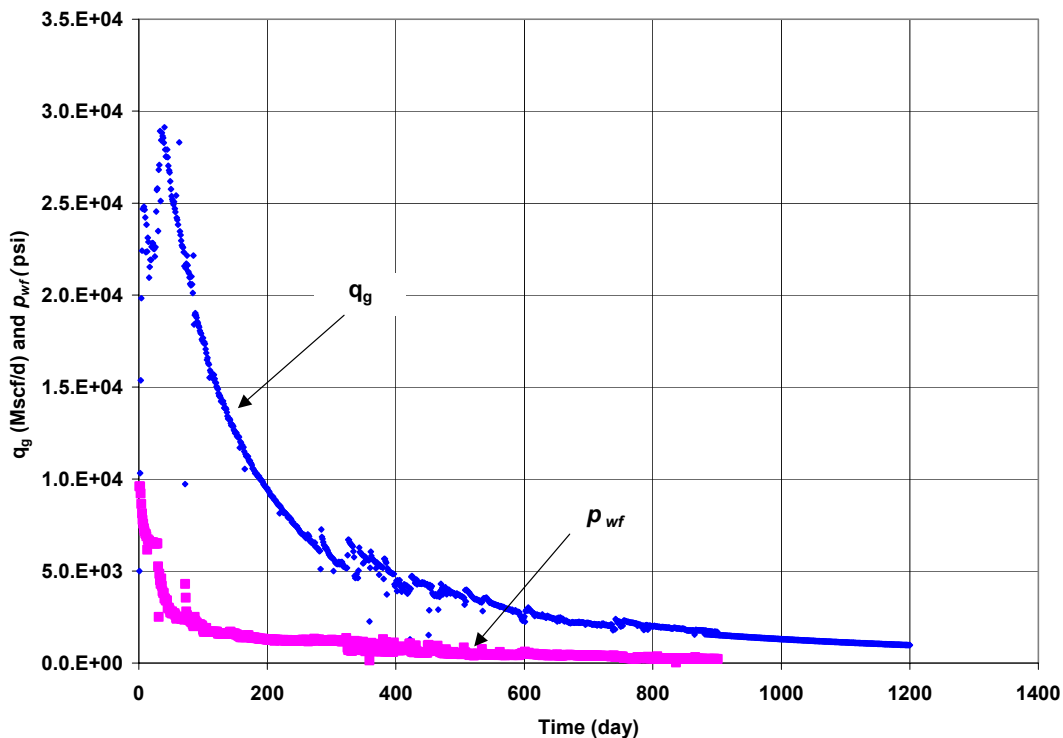
Fig. 7-2—Production history for Boren 1 well.
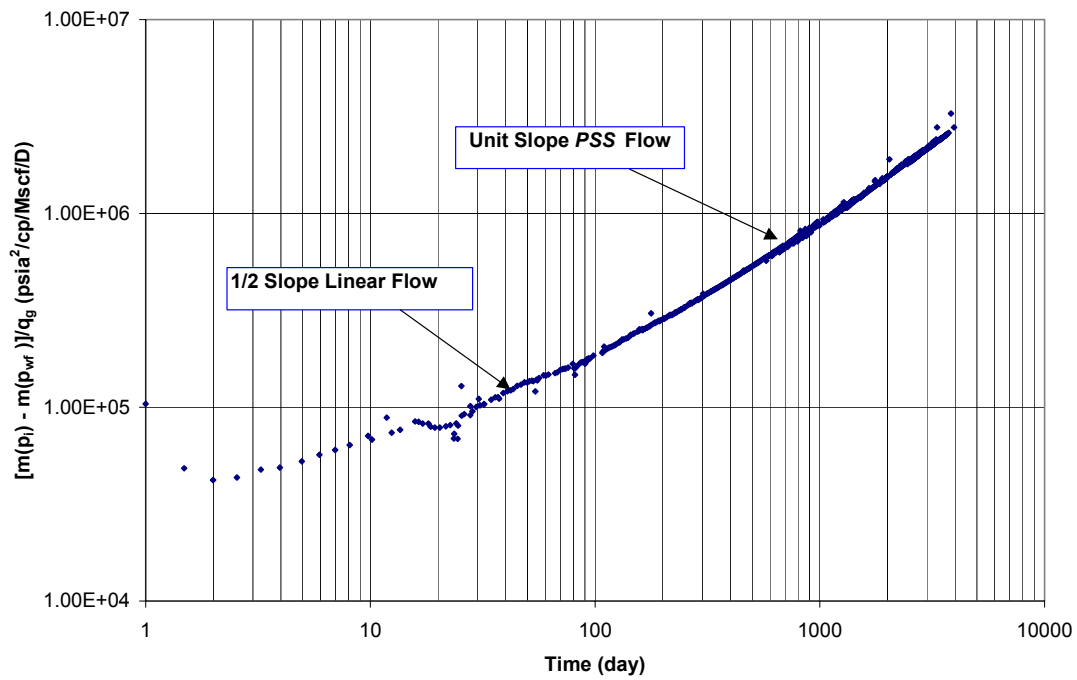
Fig. 7-3—Log-log diagnostic plot of $\Delta m(p)/q_g$ vs. *t* for Boren 1 well shows half slopes and unit slope.
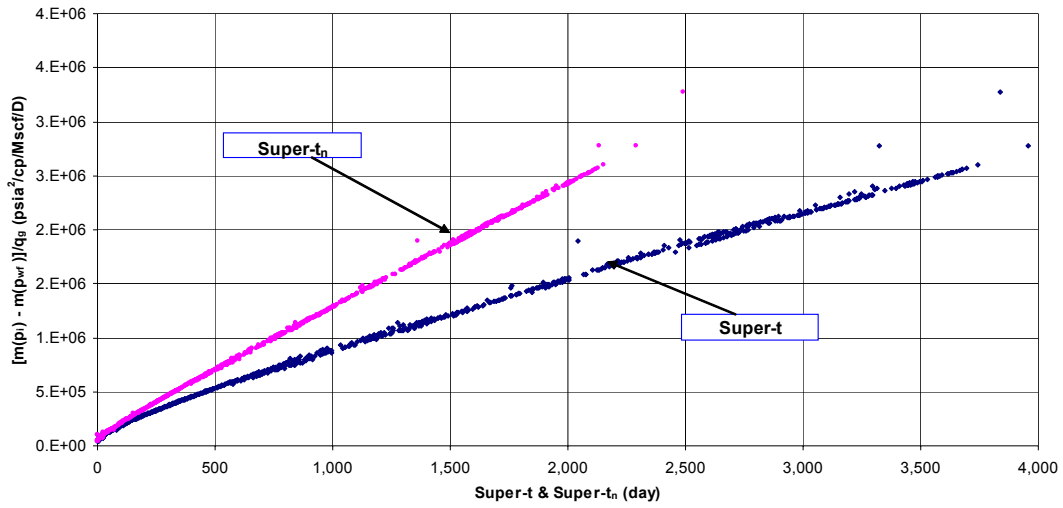
Fig. 7-4—Plot of $\Delta m(p)/q_g$ vs. Super.t and Super.t_n for Boren 1 well.
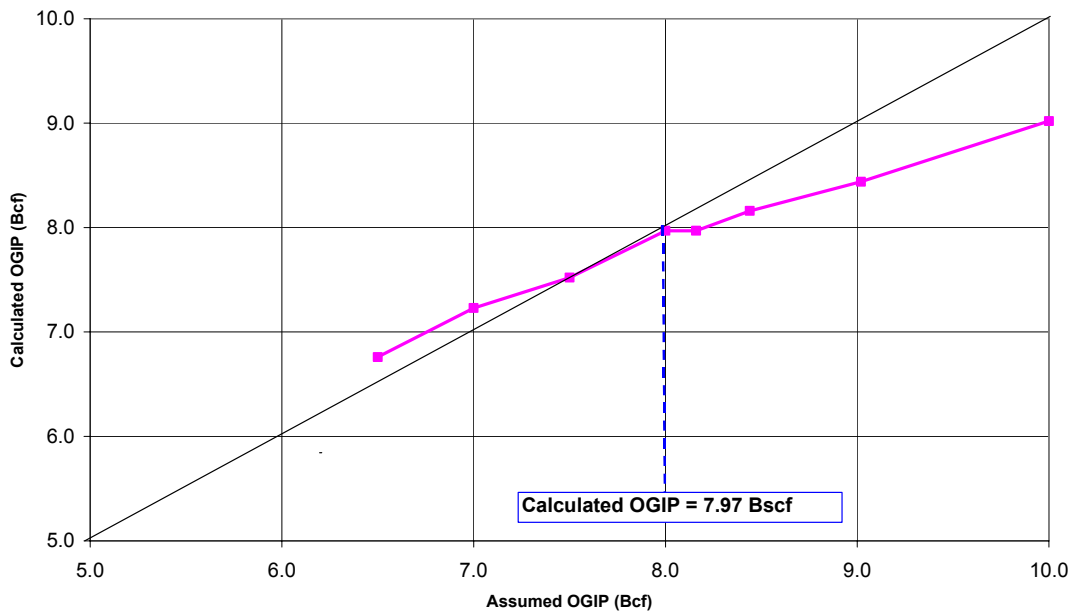
Fig. 7-5—Iteration procedure for calculating the correct OGIP by using normalized pseudotime method for Boren 1 well.

Analysis of Linear Flow Gas Wells

In this section, we provide the analysis of linear flow gas wells. These wells exhibit by linear flow for long time. Arévalo[1-3] provided the analysis of these wells, but we will apply the non linearity correction factor for the previous analysis.
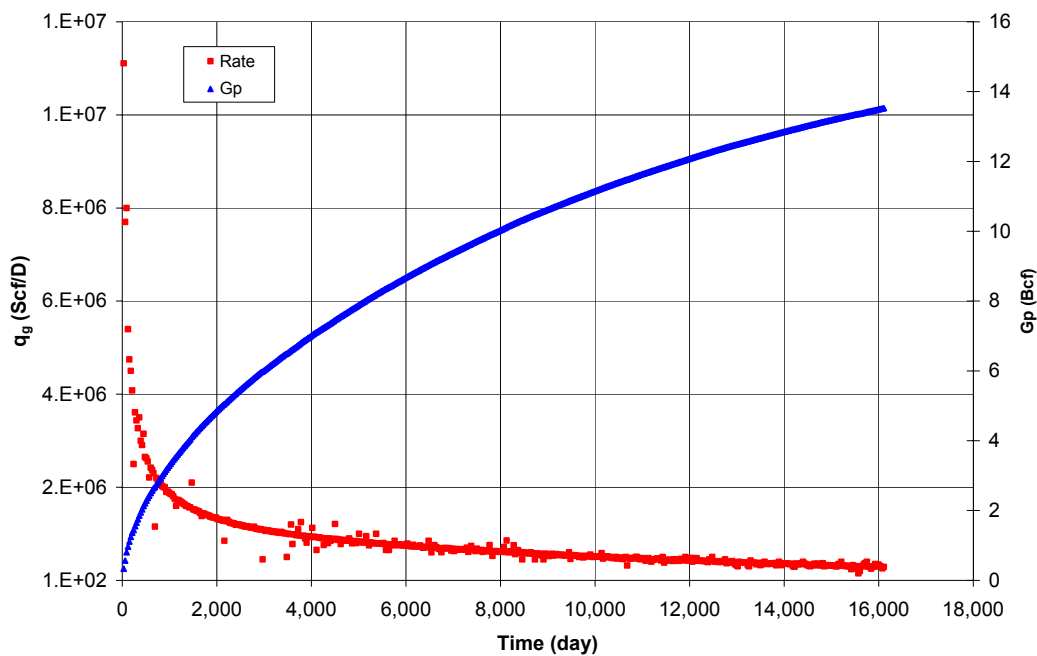
Fig. 7-6—Plot of q_g & G_p vs. t for well A. Total production is 13.52 Bcf.

Analysis of Well A

The well has produced for more than 44 years with no hydraulic fracture. It is the only well in this reservoir. **Fig. 7-6** shows the gas rates on a monthly basis, reservoir and fluid properties are the only available data. The cumulative production after 44.14 years is 13.52 Bcf and the recovery factor is 40%.

Diagnostic Plot for Well A

Fig. 7-7 shows a log-log diagnostic plot of $\Delta(m)p/q_g$ and q_g vs. t for Well A. Similarly, **Fig. 7-8** shows the log-log diagnostic plot of $\Delta(m)p/q_g$ and q_g vs. Super.t for this well. Both Figs. 7-7 and 7-8 Show linear flow for about 18.2 year and PSS flow period for the remaining production time. This is also confirmed by **Fig. 7-9** a plot of G_p vs. Super.t, which shows a "half-slope" followed by zero slope for PSS. We can conclude that Well A produced with linear flow for 18.2 years and then boundary effects begin.

Determining Reservoir Properties

In this section, we will use production data to determine reservoir properties, including the product of $\sqrt{k}\,A_c$ and OGIP. Two common methods are used to determine the reservoir properties from production data: superposition time and $\sqrt{t}$ plots.
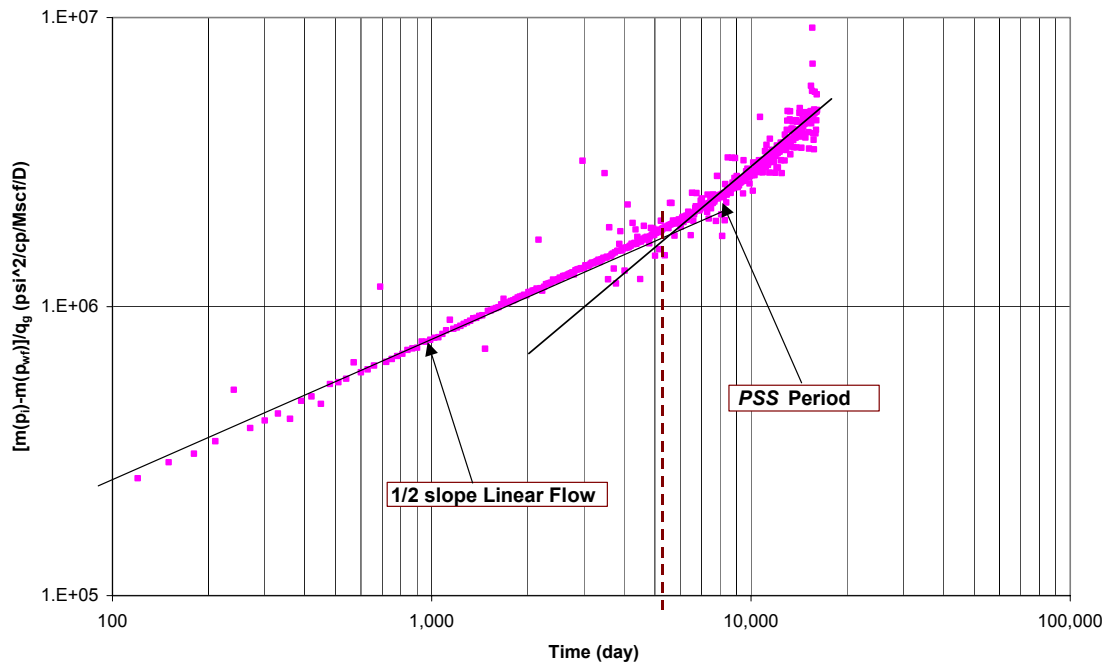
Fig. 7-7—Log-log diagnostic plot of $\Delta m(p)/q_g$ vs. t for Well A.
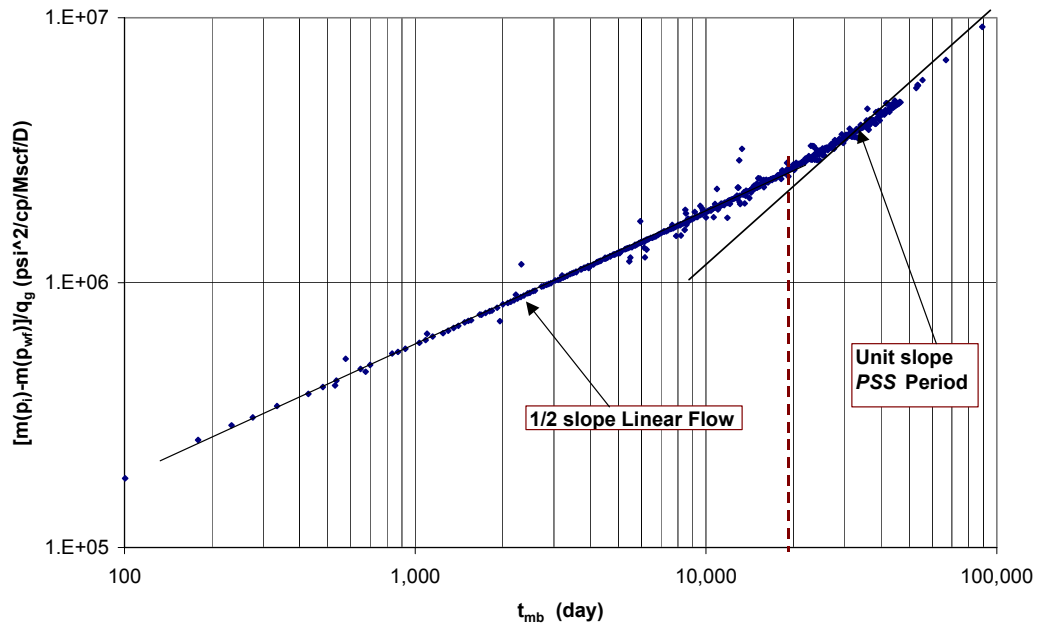
Fig. 7-8—Log-log diagnostic plot of $\Delta m(p)/q_g$ vs. t_{mb} for Well A.
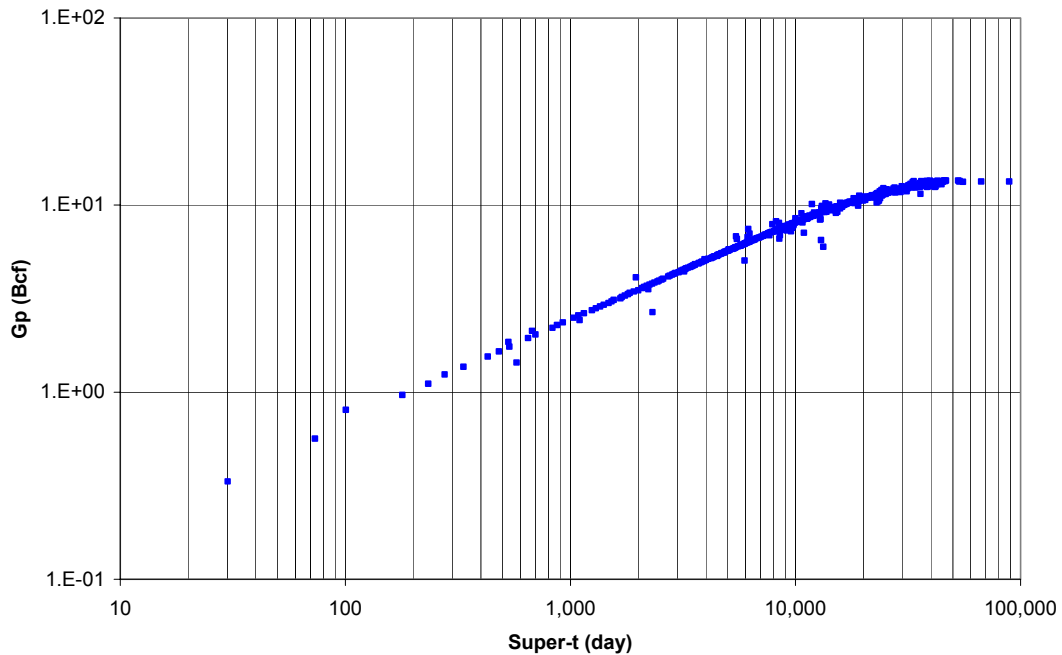
Fig. 7-9—Log-log diagnostic plot of G_p vs. Super.t for Well A.

Constant p_{wf}, $\sqrt{t}$ Plot

The first method we use to determine the product of $\sqrt{k}\, A_c$ and OGIP is the plot of $\Delta m(p)/q_g$ vs. $\sqrt{t}$. The slope of this plot is used to determine the product of $\sqrt{k}\, A_c$ and OGIP by using Eq. 7.5 for $\sqrt{k}\, A_c$ and Eq. 7.6 for OGIP.

Fig. 7-10 shows the plot of $\Delta m(p)/q_g$ vs. $\sqrt{t}$ for the actual data if also, and also, the analytical solution. The end of transient flow from **Fig. 7-10** is $t_{esr} = 6,630$ days, but the calculated time from analytical solution is $t_{esr} = 7,994.68$ days. The value of the slope in the $\Delta m(p)/q_g$ straight line was estimated to be 25×10^3 psia^2-D$^{1/2}$/Mscf-cp. The intercept to the origin was estimated as zero. The constant p_{wf} case is used even though pressure may have changed somewhat over the years. **Fig. 7-10** shows the difference between analytical and actual data, which called the non linearity problem because it shows the effect of the drawdown value. If we assume the $p_{wf} = 800$ psia for all production, the average drawdown value for this well is 0.963. Compared with the analytical solution the error in slope is 26%. The calculated value of product $\sqrt{k} A_c = 77,899$ md$^{1/2}$ ft^2 and OGIP = 40.29 Bcf. The correct value of $\sqrt{k} A_c = 57,717$ md$^{1/2}$ ft^2 and the correct OGIP = 33.9 Bcf. The correction factor calculated with Eq. 7.7 is 0.828. Then, we apply the correction factor to Eqs. 7.5 and 7.6 to get the correct value of $\sqrt{k} A_c = 64,499$ md$^{1/2}$ ft^2 and the correct OGIP = 33.36 Bcf. The slope value after applying the correction factor $\widetilde{m}_{CPL} = 30,194$. The difference in the value of $\sqrt{k} A_c$ compared with the analytical value arises because the p_{wf} is not constant for all times but varies from 500 to 1,500 psia; this means the correction factor is not 100% correct, but the OGIP is very close to the right answer.
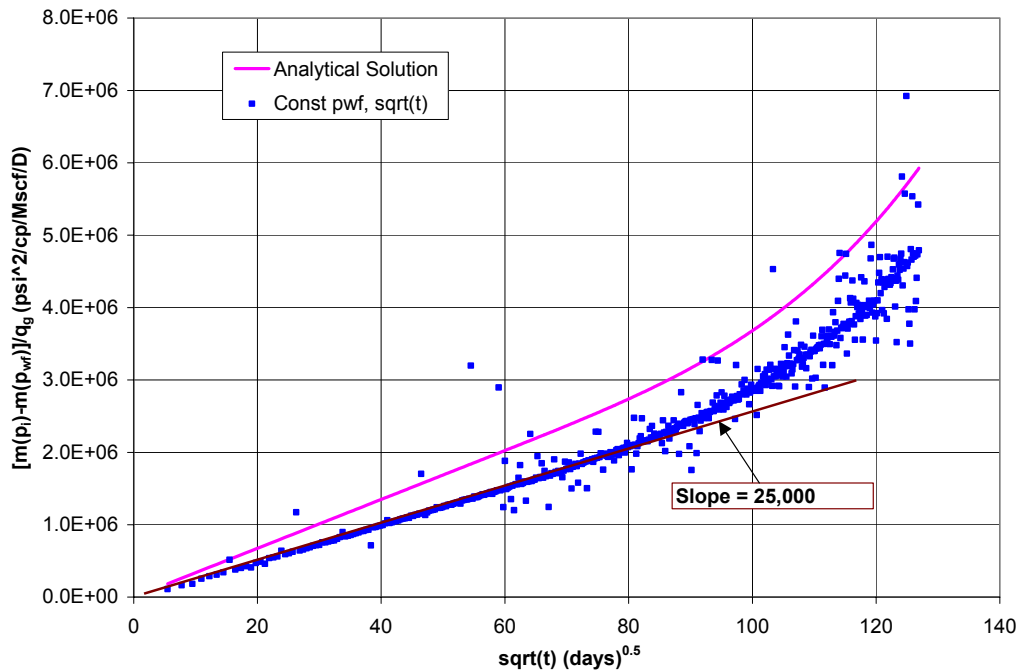
Fig. 7-10—Plot of $\Delta m(p)/q_g$ vs. $\sqrt{t}$ of actual data and analytical solution for Well A shows the slope and intercept to the origin of the straight line for the outer boundary.

Linear Flow, Superposition Time

In this section, we use superposition time because the flow rate and p_{wf} are not constant for all times. The assumed function for the superposition is linear flow. **Fig. 7-11** show the $\Delta m(p)/q_g$ vs. linear superposition for well A. The slope for the linear flow period is $\tilde{m}_{CPL} = 16,744$. The error in slope compared with the analytical slope is about 22%.

The calculated value of $\sqrt{k}A_c = 74,022.81$ md$^{1/2}$ ft^2 and the value of OGIP = 27.08 Bcf by using the constant-rate Eqs. 7.10 and 7.11. We apply the correction factor,

Eq. 7.12 for correcting the error in slope, which gives the $\tilde{m}_{CPL}$ = 20,463.52. The correct value of $\sqrt{k}\,A_c$ = 60,568 md$^{1/2}$ ft^2 by using the correct slope, but the OGIP does not give the right value even after we apply the correction.
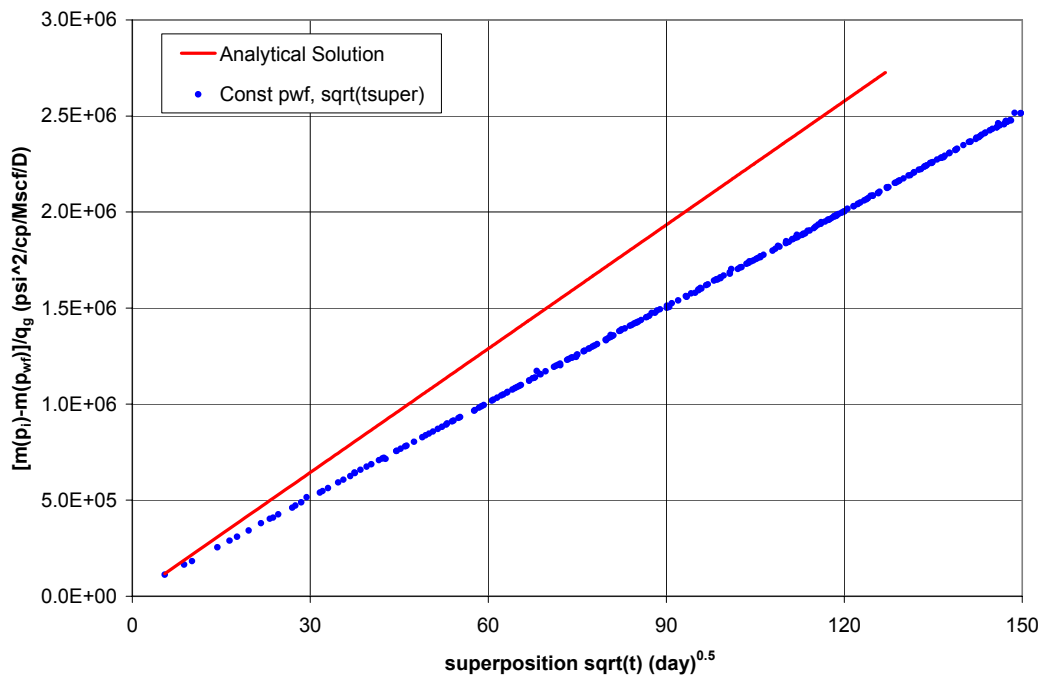
Fig. 7-11—Plot of $\Delta m(p)/q_g$ vs. Super-$t^{0.5}$ of actual data and analytical solution for Well A.

Comparison Between New Method and Decline Curve Method

In this section, we will present the comparison between our new method for calculating OGIP and the decline-curve method[19] for Jeffress field. The analysis for 13 wells from Jeffress field is shown in **Table 7-2**. The pseudotime method shows good agreement with the decline-curve method.

TABLE 7-2—COMPARISON BETWEEN PSEUDOTIME AND THE DECLINE CURVE FOR JEFFRESS FIELD					
Well Name	Cum as of 10/31/03 Bcf	Fetkovich EUR, Bcf	Fetkovich GIP	Fetkovich RF	Super-t_n GIP_x
Adame 1	3.59	3.87	5.39	72%	5.88
Adame 2	3.32	3.61	4.18	86%	4.67
Boren 1	6.38	7.13	9.91	72%	10.36
Boren 2 (W only)	9.16	10.50	14.93	70%	14.95
Boren 3	5.72	6.69	8.50	79%	10.43
Boyt 1	0.65	0.72	1.17	62%	1.13
Castillo Deep 2	1.53	1.92	2.88	67%	2.23
Coates B4	26.66	27.48	39.90	69%	54.30
Coates E1 (W only)	10.92	11.00	14.89	74%	16.66
Coates E2 (W only)	2.31	2.53	4.46	57%	4.11
Coates F1	23.01	25.02	43.90	57%	41.20
Coates F4	5.6	5.79	6.80	85%	10.20
Coates F6	4.56	4.83	7.75	62%	8.00
Sherwood 1	0	0.00	0.00	0%	0.00

Summary and Discussion

In this chapter, we provide an analysis for wells in *PSS* and transient period by applying the new method of calculating the reservoir parameters. The result confirms our new equation in calculating the OGIP and reservoir parameters. Liquid load-up is not included in our calculation for calculating p_{wf} value. The effect of multiple layers is not included in our calculation. The p_{wf} is calculated by using the Cullender and Smith[70] method for dry-gas well. The summary of well analysis is shown in **Table 7-3**.

TABLE 7-3—SUMMARY OF WELL ANALYSIS FOR *PSS* AND LINEAR FLOW					
Number	**Well**	**Type of**	**OGIP**	**OGIP**	**Error**
		flow	**Super.t**	**Super.t$_n$**	**%**
			(Bcf)	(Bcf)	
1	Boren 1	PSS	15.60	7.97	-95.7%
2	HR-58	PSS	16.21	9.80	-65.4%
3	HR-60	PSS	12.00	7.15	-67.8%
4	HR-61	PSS	9.00	4.91	-83.3%
5	HR-62	PSS	16.28	8.60	-89.3%
6	HR-64	PSS	0.24	0.18	-37.1%
7	HR-54	PSS	15.15	10.60	-42.9%
8	HR-56	PSS	12.21	8.00	-52.6%
9	CC-5	PSS	7.24	5.38	-34.6%
10	CC-6	PSS	6.71	5.50	-22.0%
11	CC-7	PSS	6.71	4.57	-46.8%
12	CC-2	PSS	10.53	7.00	-50.4%
13	WELL A	Linear	40.29	33.36	-20.8%

CHAPTER VIII

CONCLUSIONS AND RECOMMENDATIONS

Conclusions

This work presents the results of a systematic study with regard to production analysis in tight gas-wells. From this work, the following conclusions have been reached.

1 A new normalized pseudotime will improve the accuracy of calculating the OGIP.

2 Superposition with the new normalized pseudotime gives the accurate OGIP at any change in rate and properties.

3 We should take into account the change in porosity and initial water saturation with average pressure in calculating the OGIP.

4 Normalized pseudotime and superposition gives good agreement compared with the decline-curve method.

5 If pressure dependent permeability is ignored, erroneous values of permeability and skin factor will be calculated from well-test analysis of performance data.

6 The pressure response function helps in determining the actual flow regimes in variable rate well without knowing the actual pressure.

7 The drawdown value is the major factor on the non linearity of the transient period but radial model is not rate dependent.

8 Although each rate change cause a departure from the correct straight line during transient period, the data falls on the correct straight line following the transient time after the rate change, when super-t_n is used as the time variable.

Recommendations and Future Work

As result of the findings of this dissertation and the discussion in Chapter VII, the following recommendations and future research work are made to improve the methodologies developed in estimating the reservoir properties, OGIP, and production forecasting trends.

1. The inverse problem in the superposition pressure response function needs more research to determine the correct pressure function for actual production data.

2. The new pseudotime needs more research in determining OGIP in multi-layer reservoirs.

3. The absolute permeability changes dramatically in tight gas reservoirs with decreasing average reservoir pressure, so permeability should not be considered constant.

4. The rate-dependent problem for linear flow needs more research for multi layer reservoirs and also for different flow regimes.

5. Liquid load-up is not included in calculating bottomhole pressure for gas wells, so this needs to be included in the next calculation to correct the value of p_{wf}.

6. Pseudotime and superposition need more research on different flow regimes.

NOMENCLATURE

Variables

A = well drainage area, L^2, [ft^2, acres]

A_c = cross-sectional area to flow defined in Table 4-2 of Chapter IV, L^2 [ft^2] or cross-sectional in a rectangular medium (Appendix A), (= hL), [in^2, cm^2]

B_g = gas formation volume factor, L^3/L^3 [rcf/scf]

C_A = Dietz's shape factor, dimensionless

c_f = formation (rock) compressibility, Lt^2/m, [psia-1]

c_g = gas compressibility, Lt^2/m, [$psia^{-1}$]

c_{gi} = gas compressibility at initial reservoir pressure, Lt^2/m, [$psia^{-1}$]

CO_2 = carbon dioxide, mole fraction

c_t = total system compressibility, Lt^2/m, [$psia^{-1}$], [$= c_g S_g + c_o S_o + c_w S_{wi} + c_f$]

c_w = water compressibility, Lt^2/m [$psia^{-1}$]

F_R $= 1 - \dfrac{\Delta p (C_f + C_w S_{wi})}{(1 - S_{wi})}$, Ramagost factor

f_{super} = Superposition factor for superposition time plot

G_p = cumulative gas production, L^3, [Bcf]

h = net reservoir thickness, (h_{net}), L, [ft]

H_2S = sulfur, [mole fraction]

J_g = gas well productivity index, $L^4/t^2/m$, [Mscf-cp/D-psia]

H_2S = sulfur, [mole fraction]

k = permeability of the reservoir, L^2, [md]

L = distance to boundary for linear reservoirs, [ft]

$m(p)$ = real gas pseudo-pressure, m/Lt^3, [$psia^2/cp$]

$m(\bar{p})$ = real gas pseudo-pressure at average reservoir pressure, m/Lt^3, [$psia^2/cp$]

$m(p_i)$ = real gas pseudo-pressure at initial pressure, m/Lt^3, [psia^2/cp]

$m(p_{wf})$ = real gas pseudo-pressure at flowing bottomhole pressure, m/Lt^3, [psia^2/cp]

$m'(p)$ = modified gas pseudo pressure considering $k(p)$, md*psia^2/cp

$\widetilde{m}_{exp\,d}$ = intercept to origin for constant p_{wf} evaluated from the straight line on a plot of plot of $\log\left[\Delta m(p)/q_g\right]$ vs. t, [psia^2-D/Mscf-cp]

$\widetilde{m}_{CPL}$ = slope for constant p_{wf} evaluated from the straight line on a plot of $\Delta m(p)/q_g$ vs. $\sqrt{t}$ plot, [psia^2-D$^{1/2}$/Mscf-cp]

$\widetilde{m}_{CPL}$ = slope for constant p_{wf} evaluated from the straight line on a plot of $\Delta m(p)/q_g$ vs. $\sqrt{t}$ plot, [psia^2-D$^{1/2}$/Mscf-cp]

$\widetilde{m}_{CRL}$ = slope for constant rate evaluated from the straight line on a plot of $\Delta m(p)/q_g$ vs. $\sqrt{t}$ plot, [psia^2-D$^{1/2}$/Mscf-cp]

$m_{DR} = \dfrac{[m(p_i)-m(p_{wf})]}{m(p_i)}$ = Dimensionless drawdown parameters

$OGIP$ = original gas in place (G), L^3 [Bcf]

$\bar{p}$ = average reservoir pressure, m/Lt^2, [psia]

p_i = initial reservoir pressure, m/Lt^2, [psia]

PSS = pseudo-steady-state flow

p_{wf}= flowing bottomhole pressure, (BHFP), m/Lt^2, [psia]

p_{tf}= flowing surface tubing pressure, (WHFP), m/Lt^2, [psia]

q = volumetric flow rate, L^3/t, [cm^3/sec]

q_D= dimensionless pressure in radial flow for constant p_{wf}, $[=2/(\ln(t_D)+0.8097)]$

q_g = gas flow rate, L^3/t , [Mscf/D]

q_n = flow rate of well at time step n

r_e = reservoir drainage radius, L, [ft]

r_{eD} = dimensionless drainage radius, [$= r_e/r_{wa}$]

RV = volume of the reservoir, (FV), L^3, [MMrcf]

r_w = wellbore radius, L, [ft]

S_g = gas saturation, [fraction]

S_w = water saturation, [fraction]

T = reservoir temperature, T, [°R]

t = time, t, [days]

t_1 = end of the first straight line in a plot of $\Delta m(p)/q_g$ vs. function of time

t_2 = end of the second straight line in a plot of $\Delta m(p)/q_g$ vs. function of time

t_{DAc} = dimensionless time [$= 0.00633kt/\phi\mu_g c_t A_c$]

t_{Dd} = dimensionless decline time [$= 0.00633kt/\phi\mu_g c_t L^2$]

t_{DL} = dimensionless time [$= 0.00633kt/\phi\mu_g c_t L^2$]

t_{Dxe} = dimensionless time [$= 0.00633kt/\phi\mu_g c_t x_e^2$]

t_{esr} = end of the straight line on a square root of time plot

t_{prod} = production time, t, [days]

t_1-t_0 = time period for q_1

t_2-t_1 = time period for q_2

V = bulk volume, L^3, [rcf]

V_p = pore volume of the reservoir, L^3, [rcf]

x_e = distance from well to outer boundary, L, [ft]

x_f = fracture half-length, L, [ft]

y_D = dimensionless distance [$= y/\sqrt{A_c}$]

y_e = distance from hydraulic fracture to outer boundary, L [ft]

S_{gi} = initial gas saturation, fraction

S_{wi} = initial water saturation, fraction

$S_w(\bar{p})$ = water saturation at average pressure, fraction

Super.t = superposition time = $\sum_{i=1}^{m}\dfrac{\Delta q_{gi}}{q_{gm}}(t_m - t_{i-1})$, day

Super.t_n = superposition normalized pseudotime = $\sum_{i=1}^{m}\dfrac{\Delta q_{gi}}{q_{gm}}(t_{nm} - t_{ni-1})$, day

t = producing time, t, days

t_a = Agarwal's pseudotime, days

$\tilde{t}_a$ = Normalized Palacio pseudotime

t_{mb} = Material balance time

t_n = normalized pseudotime, days

$\tilde{t}_n$ = updated normalized pseudotime, days

T = reservoir temperature, T, ${}^{\circ}$R

z_i = initial gas deviation factor

$c_t(\bar{p})$ = total compressibility at average reservoir pressure

Subscripts

A = system A

CPL = constant flowing bottomhole pressure in linear flow

CP = constant flowing bottomhole pressure

CR = constant rate

CRL = constant gas rate in linear flow

esr = actual time of the end of the straight line on the square root of time plot

ehs = actual time of the end of the straight line in linear flow regime

f = fracture

g   = gas

i = initial condition (usually refer to initial pressure)

n = number of items

Greek Symbols

ϕ = porosity, [fraction]

γ_g = gas specific gravity (air = 1)

μ_g = gas viscosity, m/Lt, [cp]

ρ = fluid density, [lbm/ft^3, gm/cm^3] (water = 1)

$\phi(\bar{p})$ = porosity at average reservoir pressure

$\mu(\bar{p})$ = viscosity at average reservoir pressure

γ = "gamma" permeability modulus

REFERENCES

1- Arévalo-Villagrán, J.A., Wattenbarger, R.A., Samaniego-Verduzco, F., and Pham, T.T.: "Production Analysis of Long-Term Linear Flow in Tight Gas Reservoirs: Case Histories," paper SPE 71516 presented at the SPE 2001 Annual Technical Conference and Exhibition, New Orleans, 30 September-3 October.

2- Arévalo-Villagrán, J.A.: "Analysis of Long-Term Behavior in Tight Gas Reservoirs: Case Histories," PhD dissertation, Texas A&M U., College Station, Texas (2001).

3- Arévalo-Villagrán, Wattenbarger, R.A., García-Hernández, F. and Samaniego-Verduzco, F.: "Transient Analysis of Tight Gas Well Performance - More Case Histories," paper SPE 84476 presented at the 2003 SPE Annual Technical Conference and Exhibition, Denver, Colorado, 5-8 October.

4- Craft, B. C. and Hawkins, M. F.: *Applied Petroleum Reservoir Engineering*, Prentice-Hall, Inc., Englewood Cliffs, New Jersey, (1959) 40-43, 129-136.

5- Ramagost, B.P. and Farshad, F.F.: "P/Z Abnormally Pressured Gas Reservoirs," paper SPE 10125 presented at the 1981 SPE Annual Technical Conference and Exhibition, San Antonio, Texas, 5-7 October.

6- Arévalo, J.A., Wattenbarger, R.A., Samaniego, F., and Pham, Tai T.: "Some History Cases of Long-Term Linear Flow in Tight Gas Wells", paper 2001-15 presented at Canadian International Petroleum Conference 2001, Calgary, 12-14 June.

7- Al-Hussainy, R., and Ramey, H.J.: "Application of Real Gas Flow Theory to Well Testing and Deliverability Forecasting," *Trans* AIME (1966) **9**, 637.

8- Blasingame, T.A. and Lee, W.J.: "Variable-Rate Reservoir Limit Testing," paper SPE 15028 presented at the 1986 SPE Permian Basin Oil & Gas Recovery Conference, Midland, Texas, 13-14 March.

9- Agarwal, R.G.: "Real Gas Pseudo-Time - A New Function for Pressure Buildup Analysis of MHF Gas Wells," paper 8279 presented at the 1979 SPE Annual Technical Conference and Exhibition, Las Vegas, Nevada, 23-26 September.

10- Lee, W.J. and Holditch, S.A.: "Application of Normalized Pseudotime to Buildup Test Analysis of Low-Permeability Gas Wells with Long-Duration Wellbore Storage Distortion," *JPT* (December 1982) 2877-2887.

11- Fraim, M.L. and Wattenbarger, R.A.: "Gas Reservoir Decline-Curve Analysis Using Type Curves With Real Gas Pseudo-Pressures and Normalized Time," *SPEFE* (December 1987) 671-682.

12- Palacio, J.C. and Blasingame, T.A.: "Decline Curve Analysis Using Type Curves: Analysis of Gas Well Production Data," paper SPE 25909 presented at the 1993 SPE Rocky Mountain Regional/Low Permeability Reservoirs Symposium, Denver, 12-14 April.

13- Arps, J.J.: "Analysis of Decline Curves," Trans. AIME (1945) **160**, 228-247.

14- Fetkovich, M.J.: "Decline Curve Analysis Using Type Curves," *JPT* (June 1980) 1065-1077.

15- Slider, H.C.: "A Simplified Method of Hyperbolic Decline Curve Analysis," *JPT* (March 1968) 235-236.

16- Gentry, R.W.: "Decline-Curve Analysis," *JPT* (January 1972) 38-41.

17- Nind, T.W.: *Principles of Oil Well Production*, Second edition, McGraw-Hill, New York (1981).

18- Maley, S.: "The Use of Conventional Decline Curve Analysis in Tight Gas Well Applications," paper SPE/DOE 13898 presented at the 1985 SPE/DOE Symposium on Low Permeability Gas Reservoirs, Denver, 19-22 May.

19- Fetkovich, M.J., Vienot, M.E., Bradley, M.D., and Kiesow, U.G: "Decline Curve Analysis Using Type Curves – Case Histories," *SPEFE* (December 1987) 637-656.

20- Blasingame, T.A. and Lee, W.J.: "Variable-Rate Reservoir Limit Testing," paper SPE 15028 presented at the 1986 SPE Permian Basin Oil & Gas Recovery Conference, Midland, Texas, 13-14 March.

21- Blasingame, T.A. and Lee, W.J.: "Variable-Rate Reservoir Limit Testing of Gas Wells," paper SPE 17708 presented at the 1988 SPE Gas Technology Symposium, Dallas, 13 -15 June.

22- Blasingame, T.A., McCray, T.L., and Lee, W.J.: "Decline Curve Analysis for Variable Pressure Drop/Variable Flowrate Systems," paper SPE 21513 presented at the 1991 SPE Gas Technology Symposium, Houston, 23-24 January.

23- El-Banbi, A.H.: "Analysis of Tight Gas Well Performance," PhD dissertation, Texas A&M U., College Station, Texas, (1998).

24- Kohlhaas, C.A. and Abbot, W.A.: "Application of Linear and Spherical Flow Analysis Techniques to Field Problems–Case Studies," paper SPE 11088 presented at the 1982 SPE Annual Technical Conference and Exhibition, New Orleans, 26-29 September.

25- Stright, D.H. and Gordon, J.I.: "Decline Curve Analysis in Fractured Low Permeability Gas Wells in the Piceance Basin," paper SPE/DOE 11640 presented at the 1983 SPE/DOE Low Permeability Symposium, Denver, 14-16 March.

26- El-Banbi, A.H. and Wattenbarger, R.A.: "Analysis of Linear Flow in Gas Well Production," paper SPE 39972 presented at the 1998 SPE Gas Technology Symposium, Calgary, 15-18 March.

27- Arévalo-Villagrán, J.A. and et al: "Analysis of Long-Term Performance in Tight Gas Wells: Field Examples," paper SPE 74360 presented at the 2002 Annual Technical Conference and Exhibition, Villahermosa, Mexico, 10-12 February.

28- Bagnall, W.D. and Ryan, W.M.: "The Geology, Reserves, and Production Characteristics of the Devonian Shale in Southwestern West Virginia," paper presented at the 1975 Appalachian Petroleum Geology Symposium, Morgantown, West Virginia, 1-4 March.

29- Boardman, C.R. and Knutson, C.F.: "Unita Basin Lenticular Sandstone Reservoir Characteristics," paper SPE/DOE 9849 presented at the 1981 SPE/DOE Low Permeability Symposium, Denver, 27-29 May.

30- Hale, B.W.: "Analysis of Tight Gas Well Production Histories," paper SPE/DOE 11639 presented at the 1983 SPE/DOE Symposium on Low Permeability Gas Reservoirs, Denver, 14-16 March.

31- Ammer, J.R., Sawyer, W.K., and Drophin, M.J.: "Practical Methods for Detecting Production Mechanisms in Tight Gas Reservoirs," paper SPE/DOE/GRI 12864 presented at the 1984 SPE/DOE/GRI Unconventional Gas Recovery Symposium, Pittsburgh, Pennsylvania, 13-15 May.

32- Maley, S.: "The Use of Conventional Decline Curve Analysis in Tight Gas Well Applications," paper SPE/DOE 13898 presented at the 1985 SPE/DOE Symposium on Low Permeability Gas Reservoirs, Denver, 19-22 May.

33- Nott, D.C. and Hara, S.K.: "Fracture Half-Length and Linear Flow in the South Belridge Diatomite," paper SPE 21778 presented at the 1991 Western Regional Meeting, Long Beach, California, 20-22 March.

34- Wattenbarger, R.A. and Villegas M.E.: "Trends in U.S. Natural Gas Production," In *Advances in the Economics of Energy and Resources*, J.R. Moroney, (ed.), JAI Press, Greenwich, Connecticut (1995), 169-196.

35- Wattenbarger, R.A., El-Banbi, A.H., Villegas, M.E., and Maggard, J.B.: "Production Analysis of Linear Flow into Fractured Tight Gas Wells," paper SPE 39931 presented at the 1998 SPE Rocky Mountain Regional/Low Permeability Reservoirs Symposium and Exhibition, Denver, 5-8 April.

36- Muskat, M.: *Physical Principles of Oil Production*, McGraw-Hill Book Co., New York, (1949).

37- Miller, F.G.: "Theory of Unsteady-State Influx of Water in Linear Reservoirs," *Journal of the Institute of Petroleum*, (November 1956), **48**, No. 467, 365.

38- Nabor, G.W. and Barham, R.H.: "Linear Aquifer Behavior," *JPT* (May 1964) 561-563.

39- Carslaw, H.S. and Jaeger, J.C.: *Conduction of Heat in Solids*, Second edition, Oxford University Press, London (1959).

40- Helmy, M.W.: Analysis of Well Performance with Multiple Shut-In Periods", PhD dissertation, Texas A&M U., College Station, Texas, December 1999.

41- Helmy, M. W. and Wattenbarger, R. A.: "A New Approach to the Analysis of Gas-Well Performance with Periodic Interruptions", paper SPE 56695 presented at the 2000 SPE/CERI Gas Technology Symposium, Calgary, Alberta, 3-5 April.

42- Hale, B.W. and Evers, J.F.: "Elliptical Flow Equations for Vertically Fractured Gas Wells," *JPT* (December 1981) 2489.

43- Nott, D.C. and Hara, S.K.: "Fracture Half-Length and Linear Flow in the South Belridge Diatomite," paper SPE 21778 presented at the 1991 Western Regional Meeting, Long Beach, California, 20-22 March.

44- Bagnall, W.D. and Ryan, W.M.: "The Geology, Reserves, and Production Characteristics of the Devonian Shale in Southwestern West Virginia," paper presented at the 1975 Appalachian Petroleum Geology Symposium, Morgantown, West Virginia, 1-4 March, 41.

45- Stuart, A., John, V., Robert, P., and Ronald, P.: "Reserve Analysis for Tight Gas," paper SPE 78695 presented at the 2002 SPE Eastern Regional Meeting, Lexington, Kentucky, 23-25 October.

46- Rahman, M.M., Rahman, M.K., and Rahman, S.S.:" An Analytical Model for Production Estimation from Hydraulically Fractured Tight-Gas Reservoirs," paper SPE 77901 presented at the 2002 SPE Asia Pacific Oil and Gas Conference and Exhibition, Melbourne, Australia, 8-10 October.

47- Ibrahim, N., Fuad Q., Ridha, G., and Mohammad, M.: "Gas Well Decline Analysis Under Constant-Pressure Conditions, Wellbore Storage, Damage, and Non-Darcy Flow Effects," paper SPE 75526 presented at the SPE Gas Technology Symposium, Calgary, 30 April-2 May 2002.

48- Van Everdingen, A.F. and Hurst, W.: "The Application of the Laplace Transformation to Flow Problems in Reservoirs," *Trans*., AIME (1949) **186**, 305-325.

49- Odeh, A.S. and Jones, I.Q.: "Pressure Build-Up Analysis, Variable-Rate Case," paper SPE 546 presented at the 1965 SPE Production Research Symposium, Tulsa, Oklahoma, 29-30 April.

50- Odeh, A.S. and Jones, I.Q.: "Pressure Drawdown Analysis, Variable-Rate Case," *JPT* (August 1965) 960-964; *Trans*., AIME **234**.

51- Cinco-Ley, H. and Samaniego, F.V.: "Use and Misuse of the Superposition Time Function in Well Test Analysis," paper SPE 19817 presented at the 1989 SPE Annual Technical Conference and Exhibition, San Antonio, Texas, 8-11 October.

52- Samaniego, F.V. and Cinco-Ley, H.: "Transient Pressure Analysis for Variable Rate Testing of Gas Wells," paper SPE 21831 presented at the 1991 SPE Rocky Mountain Regional Meeting and Low-Permeability Reservoirs Symposium, Denver, 15-17 April.

53- Craven, A.: "Estimating Reservoir Pressure Using the Principle of Superposition," paper SPE 2324 presented at the 1968 SPE Second Regional Technical Symposium Saudi Arabia Section, Dhahran.

54- Zheng, S. and Stewart, G.: "Analyzing Pressure Transient Test in Semi-Infinite and Finite Reservoirs Using De-superposition Method," paper SPE 64753 presented at the 2000 SPE International Oil and Gas Conference and Exhibition, Beijing, 7-10 November.

55- Tiab, D., Ispas, N., Mongi, A., and Berkat, A.: "Interpretation of Multirate Tests by the Pressure Derivative-1. Oil Reservoirs," paper SPE 53935 presented at the 1999 SPE Latin American and Caribbean Petroleum Engineering Conference, Caracas, 21-23 April.

56- Whitson, C.H. and Sognesand S.: "Application of the Van Evendingen-Meyer Method for Analyzing Variable-Rate Well Tests," paper SPE 15482 presented at the 1986 SPE Annual Technical Conference and Exhibition, New Orleans, 5-8 October.

57- Coats, K.H., Raport, I.A., McCord, J.R. and Drews, W.P.: "Determination of Aquifer Influence Functions from Field Data," *JPT* (December 1964) 1417-1424.

58- Hutchinson, T.S. and Sikora, V.J.: "A Generalized Water-Drive Analysis," *Trans.* AIME (1959) **216**, 169-178.

59- Hicks, A.L. , Weber, A.G. and Ledbetter, R.L.: "Computing Techniques for Water-Drive Reservoirs," *Trans.* AIME (1959) **216**, 400.

60- Katz, D.L., Tek, M.R. and Jones, S.C.: "A Generalized Model for Predicting the Performance of Gas Reservoirs Subject to Water Drive," paper SPE 428 presented at the 1962 SPE Annual Fall Meeting, Los Angeles, 7-10 October.

61- Gajdica, R.J., Wattenbarger, R.A. and Startzman, R.A.: "A New Method of Matching Aquifer Performance and Determining Original Gas in Place," SPERE (August 1988) 986-993.

62- Molinard, J.E., Le Bitoux, P. and Fasanino, G., Fasanino, G., and Tek, M.R.: "A Generalized Approach To Determine Properly Any Aquifer Influence Function in an Analytical Form," paper SPE 18288 presented at 1988 SPE Annual Technical Conference and Exhibition, Houston, 2-5 October.

63- Wattenbarger, R.A., Ding, S., Yang, W., and Startzman, R.A.: "The Use of a Semianalytical Method for Matching Aquifer Influence Functions," paper SPE 19125 presented at the 1989 SPE Petroleum Computer Conference, San Antonio, Texas, 26-28 June.

64- Menissi M.H., Kenawy, F.A., Mohamed, S.A., and Sallaly, M.: "Development of Aquifer Influence Function for Undersaturated Oil Reservoir Using Semi-Analytical Model," paper SPE 39747 presented at the 1998 SPE Asia Pacific Conference on Integrated Modeling for Asset Management, Kuala Lumpur, Malaysia, 23-24 March.

65- Ding, S.: "The Use of Semi-Analytical Method for Matching Aquifer Influence Function," MS. thesis, Texas A&M U., College Station, Texas, (1990).

66- Petro, D.R., Wei-Chun, C., Burk, M.K., and Rogers, B.A.: "Benefits of Pressure Transient Testing in Evaluating Compaction Effects: Gulf of Mexico Deepwater Turbidite Sands," paper SPE 38938 presented at the 1997 SPE Annual Technical Conference and Exhibition, San Antonio, Texas, 5–8 October.

67- Dranchuk, P.M., and Abou-Kassem, J.H.: "Calculation of Z Factors for Natural Gases Using Equations of State," *J. Cdn. Pet. Tech*. (July-September 1975) 34-36.

68- Sutton, R.P.: "Compressibility Factors for High-Molecular-Weight Reservoir Gases", paper 14265 presented at the 1985 SPE Annual Technical Conference and Exhibition, Las Vegas, Nevada, 22-25 September.

69- Lee, A.L., Gonzalez, M.H., and Eakin, B.E.: "The Viscosity of Natural Gases," *JPT* (Aug. 1966) 997-1000; *Trans.* AIME, **237**.

70- Cullender, M.H. and Smith, R.V.: "Practical Solution of Gas-Flow Equations or Wells and Pipelines With Large Temperature Gradients," *Trans.*, AIME, (1956) **207**.

APPENDIX A

DERIVATION OF SUPERPOSITION TIME FUNCTION FOR OIL RESERVOIR

The general equation used for describing the unsteady state radial flow of slightly compressible fluids in homogeneous porous media can be written as[59]

$$\frac{\partial^2 p}{\partial r^2} + \frac{1}{r}\frac{\partial p}{\partial r} = \frac{\phi\mu c}{k}\frac{\partial p}{\partial t} \quad \text{...(A.1)}$$

The point source solution of Eq. A.1 is:

$$p_w = p_i + \frac{q\mu}{4\pi kh} Ei(\frac{-r_w^2 \phi\mu c}{4kt}) \quad \text{...(A.2)}$$

The pressure drawdown in Eq. A.2 is for a well without damage or improvement. In case of skin effect Eq. A.2 becomes

$$p_i - p_w = \frac{q\mu}{4\pi kh}\ln(\frac{kt}{r_w^2 \phi\mu c}+0.809+2s) \quad \text{..(A.3)}$$

Where

s = skin factor

Rewriting Eq. A.3 in field units, the pressure drop becomes

$$p_i - p_w = \frac{141.2qB\mu}{kh}\log(t) + \frac{141.2qB\mu}{kh}[\log\frac{.00633k}{r_w^2 \phi\mu c}+0.809+2s] \quad \text{............................(A.4)}$$

Assuming

$$m = \frac{141.2B\mu}{kh} \quad \text{..(A.5)}$$

$$b = \frac{141.2B\mu}{kh}[\log\frac{.00633k}{r_w^2 \phi\mu c}+0.809+2s] \quad \text{..(A.6)}$$

Rewriting Eq. A.4 in term of slope and intercept

$$p_i - p_w = mq\log(t) + bq \quad \text{..(A.7)}$$

Rewriting Eq. A.7 after dividing both sides on q, then Eq. A.7 becomes

$$\frac{p_i - p_w}{q} = m\log(t) + b \quad \text{..(A.8)}$$

By plotting $\dfrac{p_i - p_w}{q}$ vs. log(t), we can get straight line with slope m and intercept of b. The permeability and skin factor can be calculated from the slope and intercept respectively.

Variable Rate Radial Flow

The pressure drop for the multi rate (or variable rate) case production is calculated by using superposition method, the pressure drop for certain period of time t_n is calculated as following

$$p_i - p_w = \frac{\mu}{4\pi kh}\{q_1\,(\ln(\frac{kt_n}{r_w^2\,\phi\mu c}+0.809+2s)+(q_2-q_1)(\ln(\frac{k(t_n-t_1)}{r_w^2\,\phi\mu c}+0.809+2s)+........+$$
$$(q_n-q_{n-1})(\ln(\frac{k(t_n-t_{n-1})}{r_w^2\,\phi\mu c}+0.809+2s)$$

....(A.9)

Eq. A.9 can be written in the form of slope and intercept:

$$p_i - p_w = m[q_1\log(t_n)+(q_2-q_1)\log(t_n-t_1)+........+(q_n-q_{n-1})\log(t_n-t_{n-1})]+bq_n ....$$

....(A.10)

By dividing Eq. A.10 by q_n in both sides

$$\frac{p_i - p_w}{q_n} = \frac{m}{q_n}[q_1\log(t_n)+(q_2-q_1)\log(t_n-t_1)+........+(q_n-q_{n-1})\log(t_n-t_{n-1})]+b ....$$

....(A.11)

Eq. A.11 can be written in term of summation of flow rate and time:

$$\frac{p_i - p_w}{q_n} = m\,[\sum_{j=1}^{n}\frac{\Delta q_j}{q_n}\log(t_n-t_{j-1})\,]+b ....(A.12)$$

Eq. A.12 for radial flow.

Eq. A.12 can be written for linear, Bi-linear, and pseudo steady state as

$$\frac{p_i - p_w}{q_n} = m \left[\sum_{j=1}^{n} \frac{\Delta q_j}{q_n} \sqrt{(t_n - t_{j-1})} \right] + b \quad \text{...(A.13)}$$

Eq. A.13 for linear flow

$$\frac{p_i - p_w}{q_n} = m \left[\sum_{j=1}^{n} \frac{\Delta q_i}{q_n} ((t_n - t_{j-1})^{0.25}) \right] + b \quad \text{...(A.14)}$$

Eq. A.14 for bilinear flow

$$\frac{p_i - p_w}{q_n} = m \left[\sum_{j=1}^{n} \frac{\Delta q_j}{q_n} (t_n - t_{j-1}) \right] + b \quad \text{...(A.15)}$$

Eq. A.15 for *PSS* flow

APPENDIX B

DERIVATION OF TANGENT METHOD WITH CURRENT PROPERTIES FOR CONSTANT RATE PRODUCTION

The derivation of tangent method is based on the productivity index, which is constant during the pseudosteady-state period. Production rate during pseudosteady-state period is calculated by using productivity index equation.

$$q_g = J[m(\bar{p}) - m(p_{wf})] \quad \text{...(B.1)}$$

The change in average reservoir pressure with time during *PSS* period can be represented by the following volumetric equation

$$\frac{d\bar{p}}{dt} = \frac{-q_g \bar{B}_g}{\bar{c}_t \bar{V}_p} \quad \text{...(B.2)}$$

Differentiating Eq. B.1 with respect to t for constant rate, we have

$$\frac{dm(\bar{p})}{dt} = \frac{dm(p_{wf})}{dt} \quad \text{...(B.3)}$$

Where

$$m(p) = 2\int_{p_o}^{p} \frac{p}{\mu_g z} dp \text{ is the real gas pseudo-pressure defined by Al-Hussainy } et\ al.^7$$

Where $\dfrac{d\bar{p}}{dt}$ can be calculated as

$$\frac{dm(\bar{p})}{dt} = \frac{2\bar{p}}{\bar{z}\bar{\mu}} \frac{d(\bar{p})}{dt} \quad \text{...(B.4)}$$

We can now substitute Eq. B.4 into Eq. B.2, giving

$$\frac{\bar{z}\bar{\mu}}{2\bar{p}} \frac{dm(\bar{p})}{dt} = \frac{-q_g \bar{B}_g}{\bar{c}_t \bar{V}_p} \quad \text{...(B.5)}$$

We plot $\dfrac{[m(p_i) - m(p_{wf})]}{q_g}$ vs. time in pseudosteady-state period. The slope of this plot is

$$\widetilde{m}_{pss} = \frac{-1}{q_g} \frac{dm(p_{wf})}{dt} \quad \text{..(B.6)}$$

We can substitute Eq. B.3 into Eq. B.6, giving

$$\widetilde{m}_{pss} = \frac{-1}{q_g} \frac{dm(\overline{p})}{dt} \quad \text{..(B.7)}$$

We can substitute Eq. B.7 into Eq. B.5, we have

$$\frac{\overline{z}\overline{\mu}}{2\overline{p}} \widetilde{m}_{pss} = \frac{\overline{B}_g}{\overline{c}_t \overline{V}_p} \quad \text{..(B.8)}$$

The OGIP can be calculated from the following

$$OGIP = \frac{V_{pi} S_{gi}}{B_{gi}} \quad \text{..(B.9)}$$

The change in pore volume due to the change in pressure is giving by the following

$$\overline{V}_p = V_{pi} \exp(-c_f(p_i - \overline{p})) \quad \text{..(B.10)}$$

We can now substitute Eq. B.9 into Eq. B.10, we have

$$\overline{V}_p = \frac{OGIP\, B_{gi}}{S_{gi}} \exp(-c_f(p_i - \overline{p})) \quad \text{..(B.11)}$$

We can now substitute Eq. B.11 into Eq. B.8 and solve for *OGIP*, giving

$$OGIP = (\frac{\overline{B}_g}{\overline{c}_t}) (\frac{S_{gi}}{B_{gi}}) \frac{2\overline{p}}{\overline{z}\overline{\mu}} \frac{1}{\widetilde{m}_{pss}} \exp(c_f(p_i - \overline{p})) \quad \text{...(B.12)}$$

The gas formation volume factor can be calculated as

$$B_g = 0.0282 \frac{T\overline{z}}{\overline{p}} \quad \text{..(B.13)}$$

Eq. B.12 can be written in another form for initial pressure and initial compressibility factor, gives

$$OGIP = \frac{2p_i S_{gi}}{z_i \mu(\overline{p}) c_t(\overline{p})} \frac{1}{\widetilde{m}_{pss}} \exp(c_f(p_i - \overline{p})) \quad \text{...(B.14)}$$

The change in pore volume can be calculated as

$$\phi(\overline{p}) = \phi_i\, e^{-c_f(pi - \overline{p})} \quad \text{..(B.15)}$$

By substituting Eq. B.15 into Eq. B.14, we have

$$\text{OGIP} = \frac{2p_i\, S_{gi}\, \phi_i}{z_i}\left(\frac{1}{\phi(\bar{p})\mu(\bar{p})c_t(\bar{p})}\right)\left(\frac{1}{\tilde{m}_{pss}}\right) \quad\text{...(B.16)}$$

Eq. B.16 gives the accurate OGIP at any value of average reservoir pressure. The OGIP can be calculated by using the initial properties of viscosity and compressibility as.

$$OGIP = \frac{2p_i\, S_{gi}}{(z_i\mu_g c_t)_i}\left(\frac{1}{\tilde{m}_{PSS}}\right)_i \quad\text{...(B.17)}$$

We can now solving Eqs. B.16 and B.17 for the value of the slope at each time step, giving

$$\frac{2p_i\, S_{gi}\, \phi_i}{z_i}\left(\frac{1}{\phi(\bar{p})\mu(\bar{p})c_t(\bar{p})}\right)\left(\frac{1}{\tilde{m}_{pss}}\right) = \frac{2p_i\, S_{gi}}{(z_i c_t B_g)_i}\left(\frac{1}{\tilde{m}_{PSS}}\right)_i \quad\text{...........................(B.18)}$$

Eq. B.18 can be solved for the slope value, gives

$$\tilde{m}_{pss} = \frac{(\phi\mu c_t)_i}{\phi(\bar{p})\mu(\bar{p})c_t(\bar{p})}\left(\tilde{m}_{PSS}\right)_i \quad\text{...(B.19)}$$

The slope in pseudosteady-state is given by

$$\tilde{m}_{pss} = \frac{d}{dt}\left(\frac{m(p_i) - m(p_{wf})}{q_g}\right) \quad\text{...(B.20)}$$

In case of constant rate $m(p_i)$ is constant, then by differentiating Eq. B.20, we have

$$\tilde{m}_{pss} = \frac{-dm(p_{wf})}{dt} \quad\text{...(B.21)}$$

We can now substitute Eq. B.21 into Eq. B.19, giving

$$\frac{-dm(p_{wf})}{dt} = \frac{(\phi\mu c_t)_i}{\phi(\bar{p})\mu(\bar{p})c_t(\bar{p})}\left(\tilde{m}_{PSS}\right)_i \quad\text{...(B.22)}$$

Eq. B.22 can be written as

$$\frac{-dm(p_{wf})}{dt_n} = \left(\tilde{m}_{PSS}\right)_i \quad\text{...(B.23)}$$

Where the t_n is called pseudotime

$$dt_n = (\phi\mu c_t)_i\,\frac{1}{\phi(\bar{p})\mu(\bar{p})c_t(\bar{p})}\,dt \quad\text{...(B.24)}$$

We can integrate Eq. B.24 to calculate the pseudotime (t_n)

$$\int_0^t t_n = (\phi\mu c_t)_i \int_0^t \frac{1}{\phi(\bar{p})\mu(\bar{p})c_t(\bar{p})} dt \quad \dots\dots\dots\dots\dots\dots\dots\dots\dots\dots\dots\dots\dots\dots\dots\dots\dots\text{(B.25)}$$

We can now calculate the pseudotime (t_n) as

$$t_n = (\phi\mu c_t)_i \int_0^t \frac{1}{\phi(\bar{p})\mu(\bar{p})c_t(\bar{p})} dt \quad \dots\dots\dots\dots\dots\dots\dots\dots\dots\dots\dots\dots\dots\dots\dots\dots\dots\text{(B.26)}$$

APPENDIX C
RELATIONSHIP BETWEEN SUPERPOSITION TIME AND MATERIAL BALANCE TIME IN *PSS*

In this section, we show the superposition time and material balance time are equivalent for pseudosteady-state. This is true for constant reservoir properties. This is also true for variable properties with modified definition of material balance pseudo time and superposition pseudo time.

Superposition Equation for Constant Properties

The superposition equation for the variable rate with constant reservoir properties was derived from constant rate solution for any flow regime. The superposition equation for variable rate in pseudosteady-state is given as

$$\frac{[m(p_i)-m(p_{wf})]}{q_{gn}} = m\,[\sum_{j=1}^{n}\frac{\Delta q_{gj}}{q_{gn}}(t_n - t_{j-1})\,] + b \quad\text{...(C.1)}$$

The superposition time for pseudosteady-state

$$Super\_t = \sum_{j=1}^{n}\frac{\Delta q_{gj}}{q_{gn}}(t_n - t_{j-1}) \quad\text{..(C.2)}$$

Where

Super_t = superposition time in *PSS*

Eq. C.2 can be written as

$$Super\_t = \frac{1}{q_{gn}}\sum_{j=1}^{n}(q_{gj} - q_{gj-1})(t_n - t_{j-1}) \quad\text{...(C.3)}$$

Eq. C.3 can be factorizing as

$$Super\_t = \frac{1}{q_{gn}}[\sum_{j=1}^{n}q_{gj}\,t_n - \sum_{j=1}^{n}q_{gj-1}t_n - \sum_{j=1}^{n}q_{gj}\,t_{j-1} + \sum_{j=1}^{n}q_{gj-1}t_{j-1}\,] \quad\text{.......................(C.4)}$$

Grouping first and second term in Eq. C.4, we have

$$Super\_t = \frac{1}{q_{gn}} [\sum_{j=1}^{n} q_{gj-1} t_{j-1} - \sum_{j=1}^{n} q_{gj} t_{j-1} + \sum_{j=1}^{n} (q_{gj} - q_{gj-1}) t_n] \quad \text{...........................(C.5)}$$

The summation of last term in Eq. C.5 will give

$$\sum_{j=1}^{n} (q_{gj} - q_{gj-1}) t_n = q_{gn} t_n \quad \text{...(C.6)}$$

Substitute Eq. C.6 into Eq. C.5, we have

$$Super\_t = \frac{1}{q_{gn}} [q_{gn} t_n + \sum_{j=1}^{n} q_{gj-1} t_{j-1} - \sum_{j=1}^{n} q_{gj} t_{j-1}] \quad \text{................................(C.7)}$$

For j = 1

$$q_{g0} = 0 \quad \text{...(C.8)}$$

$$t_0 = 0 \quad \text{...(C.9)}$$

By using Eqs. C.6 and C.7 and grouping first and second term in Eq. C.5, we have

$$q_{gn} t_n + \sum_{j=1}^{n} q_{gj-1} t_{j-1} = \sum_{j=1}^{n} q_{gj} t_j \quad \text{...(C.10)}$$

Substituting Eq. C.10 into Eq. C.7, we have

$$Super\_t = \frac{1}{q_{gn}} [\sum_{j=1}^{n} q_{gj} t_j - \sum_{j=1}^{n} q_{gj} t_{j-1}] \quad \text{..(C.11)}$$

Eq. C.11 can be written as

$$Super\_t = \frac{1}{q_{gn}} [\sum_{j=1}^{n} q_{gj} (t_n - t_{j-1})] \quad \text{...(C.12)}$$

Material Balance Time for Constant Properties

The material balance time approach proposed to analyze variable rate and pressure in pseudosteady-state. The material balance time equation is given by

$$t_{mb} = \frac{G_p}{q_g} \quad \text{...(C.13)}$$

The cumulative production G_p can be calculated as

$$G_p = \sum_{i=1}^{n} q_{g_i} (t_i - t_{i-1}) \quad \text{...(C.14)}$$

Substituting Eq. C.14 into Eq. C.13, we have

$$t_{mb} = \frac{1}{q_{gn}} \sum_{i=1}^{n} q_{g_i}(t_i - t_{i-1})$$ ....(C.15)

Where

t_{mb} = material balance time

So, the above derivation shows that the superposition time and material balance time is exactly the same. So, we can use the cumulative production to calculate the time function in pseudosteady-state.

Example 1

In this example we applied Eqs. C12 and C.15 for constant reservoir properties with variable rate, the result shown in Table C.1 and as you can see the superposition time *Super_t* and t_{mb} are equal.

TABLE C-1—CALCULATION OF SUPERPOSITION TIME AND MATERIAL BALANCE TIME				
Time	q_g	G_p	t_{mb}	Super_t
days	Mscf/D	Mscf	days	Days
1	10	10	1.0	1.0
2	30	40	1.333	1.333
5	20	100	5.0	5.0
6	60	160	2.667	2.667
8	30	220	7.333	7.333
10	5	230	46.0	46.00

Superposition Equation for Variable Properties

The modified superposition equation is used when the reservoir properties change which give the linear equation. The modified superposition used pseudo time instead of regular time. The pseudo time equation is

$$t_n = (\phi\mu c_t)_i \int_0^t \frac{1}{\phi(\bar{p})\mu(\bar{p})c_t(\bar{p})} dt$$ ....(C.16)

By substituting Eq. C.16 into Eq. C.1, we have

$$\frac{[m(p_i) - m(p_{wf})]}{q_{gm}} = \tilde{m}_{PSS} \left[\sum_{j=1}^{m} \frac{\Delta q_j}{q_{gn}}(t_{nm} - t_{nj-1})\right] + b \quad\text{..(C.17)}$$

The modified superposition time or superposition pseudo time given by

$$Super\_t = \sum_{j=1}^{m} \frac{\Delta q_{gj}}{q_{gm}}(t_{nm} - t_{nj-1}) \quad\text{...(C.18)}$$

Where

By using Eqs. C.3- C.9 Eq. C.18 can be written as

$$Super\_t = \frac{1}{q_{gm}}\left[\sum_{j=1}^{m} q_{gj}(t_{ni} - t_{nj-1})\right] \quad\text{...(C.19)}$$

Material Balance Time for Variables Properties

The material balance pseudo time approach proposed can analyze variable rate and pressure in pseudosteady-state. The material balance pseudo time equation is given by

$$t_{amb} = \frac{G_{ap}}{q_g} \quad\text{..(C.20)}$$

Where

t_{nMC} = material balance pseudo time

G_{ap} = pseudo cumulative production

The pseudo cumulative production G_{ap} can be calculated by using pseudo time instead of time as

$$G_{ap} = \sum_{i=1}^{n} q_{gi}(t_{ai} - t_{ai-1}) \quad\text{...(C.21)}$$

Substituting Eq. 19 into Eq. 18, we have

$$t_{amb} = \frac{1}{q_{gm}}\sum_{i=1}^{m} q_{gi}(t_{ni} - t_{ni-1}) \quad\text{..(C.22)}$$

The superposition pseudo time and material balance pseudo time are equivalent for pseudosteady state period as shown in Eq. C.17 and Eq. C.20.

Example 2

In this example we applied Eqs. C.17 and C.20 for variable reservoir properties with variable rate in pseudosteady-state, the result shown in **Table C.2** and as you can see in **Table C.2** the superposition time *Super_t* and t_{nmb} are equal.

TABLE C-2—CALCULATION OF SUPERPOSITION PSEUDOTIME AND MATERIAL BALANCE PSEUDOTIME					
Time Days	t_n days	q_g MSCF/D	G_{pa} Bcf	t_{ambt} day	$t_{super)PSS}$ day
0.01	0.50	5000.00	0.0025	0.50	0.50
0.02	0.51	5000.00	0.0026	0.51	0.51
0.04	0.53	5000.00	0.0026	0.53	0.53
0.05	0.55	5000.00	0.0027	0.55	0.55
300.80	265.43	2000.00	1.3253	662.66	662.66
303.75	267.66	2000.00	1.3298	664.90	664.90
304.75	268.42	2000.00	1.3313	665.66	665.66
399.38	338.57	2000.00	1.4716	735.80	735.80
400.00	339.02	2000.00	1.4725	736.25	736.25
400.75	339.56	4000.00	1.4747	368.67	368.67
401.65	340.22	4000.00	1.4773	369.32	369.32
402.65	340.94	4000.00	1.4802	370.05	370.05
600.81	472.48	1000.00	2.0049	2004.89	2004.89
601.78	473.07	1000.00	2.0055	2005.48	2005.48

APPENDIX D

DERIVATION OF TANGENT METHOD WITH CURRENT PROPERTIES FOR CONSTANT BOTTOMHOLE FLOWING PRESSURE PRODUCTION

Tangent Slope with Current Properties

The derivation of tangent slope is based on the productivity index, which is constant during the *PSS* period. Production rate can be calculated by

$$q_g = J_{CP}[m(\bar{p}) - m(p_{wf})] \quad \text{...(D.1)}$$

The change in average reservoir pressure with time during *PSS* period can be represented by the following volumetric equation

$$\frac{d\bar{p}}{dt} = \frac{-q_g \bar{B}_g}{\bar{c}_t V_p} \quad \text{...(D.2)}$$

Differentiating Eq. D.1 with respect to *t,* we have

$$\frac{dq_g}{dt} = J_{CP} \frac{dm(\bar{p})}{dt} \quad \text{...(D.3)}$$

The $\dfrac{d\bar{p}}{dt}$ can be calculated as

$$\frac{dm(\bar{p})}{dt} = \frac{2\bar{p}}{\bar{z}\bar{\mu}} \frac{d\bar{p}}{dt} \quad \text{...(D.4)}$$

We can now substitute Eq. D.4 into Eq. D.3, giving

$$\frac{dq_g}{dt} = J_{CP} \frac{2\bar{p}}{\bar{z}\bar{\mu}} \frac{d\bar{p}}{dt} \quad \text{...(D.5)}$$

By substituting Eq. D.2 into Eq. D.5, we have

$$\frac{1}{q_g} \frac{dq_g}{dt} = -J_{CP} \frac{2\bar{p}}{\bar{z}\bar{\mu}} \frac{\bar{B}_g}{\bar{c}_t V_p} \quad \text{...(D.6)}$$

We plot log $\dfrac{[m(p_i) - m(p_{wf})]}{q_g}$ vs. time in pseudosteady-state period. The slope of this plot is

giving by

$$\tilde{m}_{\exp d} = \left| \frac{-d\log(q_g)}{dt} \right| = \left| \frac{-d\ln(q_g)}{2.303dt} \right| \quad\text{...(D.7)}$$

Where

$$m(p_i) - m(p_{wf}) = \text{Constant}$$

By differentiate Eq. D.7, we have

$$\tilde{m}_{\exp d} = \frac{-1}{2.303 q_g} \frac{dq_g}{dt} \quad\text{...(D.8)}$$

We can substitute Eq. D.8 into Eq. D.6, giving

$$-2.303\tilde{m}_{\exp d} = J_{CP} \frac{-2\bar{p}}{\bar{z}\bar{\mu}} \frac{\bar{B}_g}{\bar{c}_t \bar{V}_p} \quad\text{..(D.9)}$$

We solve Eq. D.9 for the current pore volume

$$\bar{V}_p = J_{CP} \frac{2\bar{p}\bar{B}_g}{2.303\bar{z}\bar{\mu}\,\bar{c}_t} \frac{1}{\tilde{m}_{\exp d}} , \text{Mscf}\text{...(D.10)}$$

The change in pore volume due to the change in pressure is giving by the following

$$\bar{V}_p = V_{pi} \exp(-c_f(p_i - \bar{p})) \quad\text{...(D.11)}$$

The *OGIP* can be calculated from the following

$$OGIP = \frac{V_{pi} S_{gi}}{B_{gi}} \quad\text{.. (D.12)}$$

We can now substitute Eq. D.12 into Eq. D.11, we have

$$\bar{V}_p = \frac{OGIP\, B_{gi}}{S_{gi}} Exp(-c_f(p_i - \bar{p})) \quad\text{..(D.13)}$$

We can now substitute Eq. D.13 into Eq. D.9 and solve for *OGIP*, giving

$$OGIP = J_{CP}\left(\frac{\bar{B}_g}{B_{gi}}\right) \frac{2\bar{p}S_{gi}}{2.303\bar{z}\bar{\mu}\,\bar{c}_t} \frac{1}{\tilde{m}_{\exp d}} Exp(c_f(p_i - \bar{p})) \quad\text{..............................(D.14)}$$

The gas formation volume factor can be calculated as

$$B_g = 0.0282 \frac{T\bar{z}}{\bar{p}} \quad\text{..(D.15)}$$

Eq. D.14 can be written in another form for initial pressure and initial compressibility factor as

$$OGIP = J_{CP} \frac{2p_i\, S_{gi}}{2.303z_i \bar{\mu}\, \bar{c}_t} \frac{1}{\tilde{m}_{exp\,d}} Exp(c_f(p_i - \bar{p})) \dots\dots\dots(D.16)$$

Eq. D.17 gives the change in pore volume

$$\phi(\bar{p}) = \phi_i\, Exp^{-c_f(pi - \bar{p})} \dots\dots\dots(D.17)$$

By substituting Eq. D.17 into Eq. D.16, we have

$$OGIP = J_{CP} \frac{2\, p_i\, S_{gi}\, \phi_i}{2.303z_i} \left(\frac{1}{\bar{\phi}\bar{\mu}\, \bar{c}_t}\right)\left(\frac{1}{\tilde{m}_{exp\,d}}\right) \dots\dots\dots(D.18)$$

Where

$\bar{\phi}$ = porosity at average reservoir pressure

$\bar{\mu}$ = viscosity at average reservoir pressure

$\bar{c}_t$ = total compressibility at average reservoir pressure

Eq. D.18 used current properties, which give accurate value of OGIP at any value of average reservoir pressure.

APPENDIX E

ANALYSIS OF TIGHT GAS WELLS BY USING NORMALIZED PSEUDOTIME AND SUPERPOSITION METHOD

Well HR-58

Well HR-58 is from tight gas reservoir with high pressure. The well has produced for 532 days. **Fig. E-1** shows the production history of well HR-58. **Fig. E-2** shows a log-log diagnostic plot of $\Delta(m)p/q_g$ vs. time. The diagnostic plots show half-slope for almost 10 days followed by transition zone and unit slope for late period. So, this well shows the boundary effect after 10 days due to the high production rate and small reservoir size.

Production data is plotted against the Super.t and Super.t_n on the same graph to illustrate the necessity of using normalized pseudotime as shown in **Fig. E-3**. When plotted against Super.t_n the data exhibits a straight line with one slope. In this case the OGIP is calculated to be 9.8 Bcf.

However, when the real-time is used, the production data does not show a straight line; instead it shows a curve with reducing slope, i.e. increasing OGIP. The OGIP calculated from the Super.t was as high as 16.21 Bcf based where the slope were taken. The OGIP is calculated by using the slope from the early point of *PSS* period. This value is used as first trial to calculate the normalized pseudotime. This pseudo-time is then used in the superposition calculation to determine a new OGIP. The process is repeated until it converges as provided in the above procedures to calculate the normalized pseudotime. **Fig. E-4** shows the result of OGIP from iteration procedures that give 9.8 Bcf
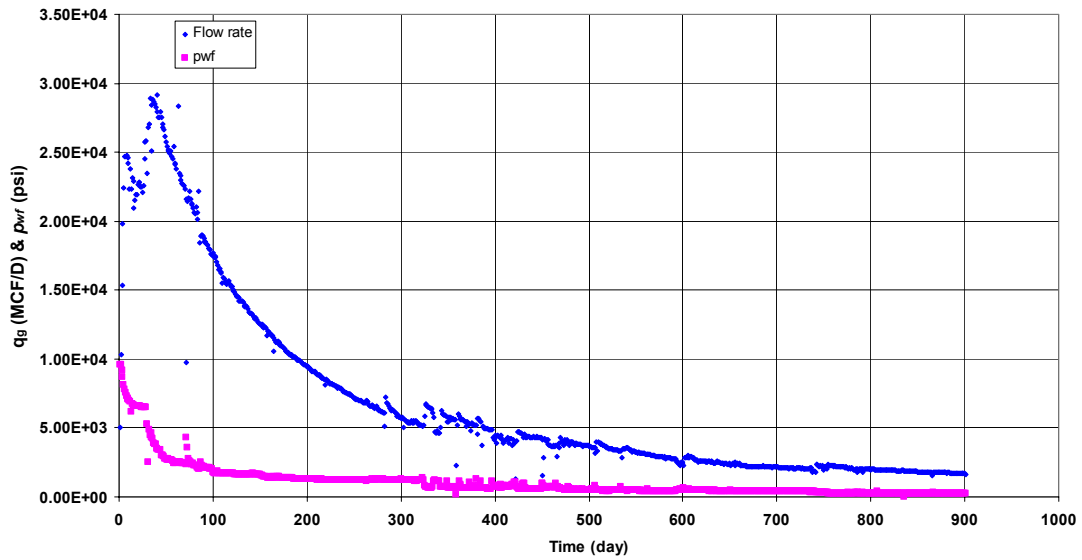
Fig. E-1—Shows production history for Well HR-58.
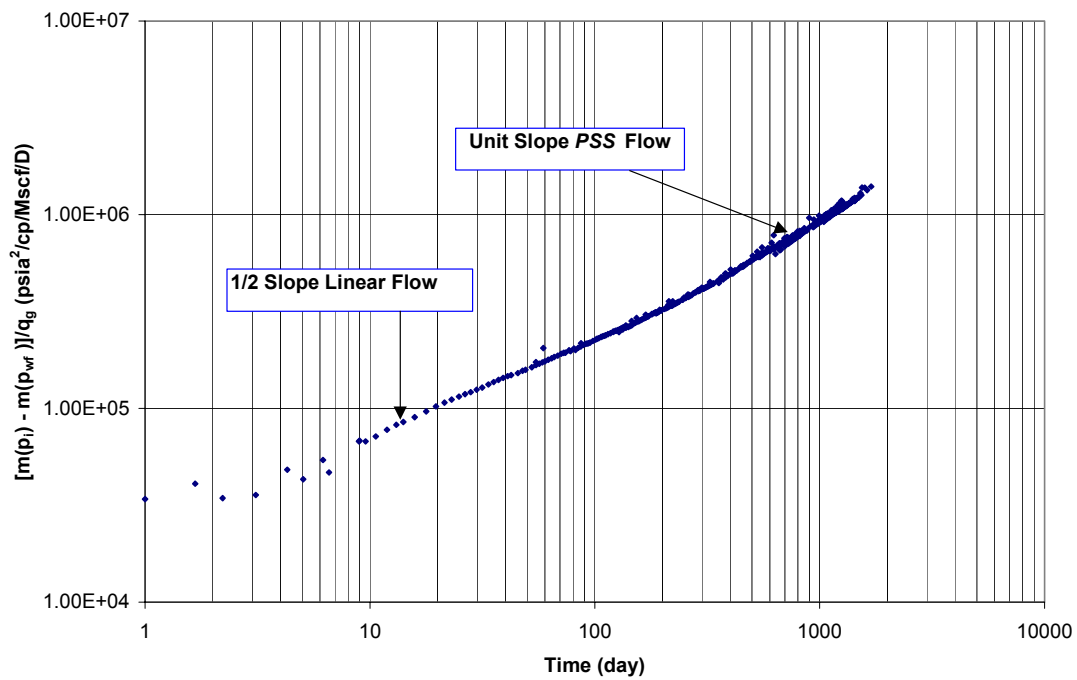
Fig. E-2—Log-log diagnostic plot of $\Delta m(p)/q_g$ vs. *t* for well HR-58 which shows half slopes, transition zone, and unit slope.
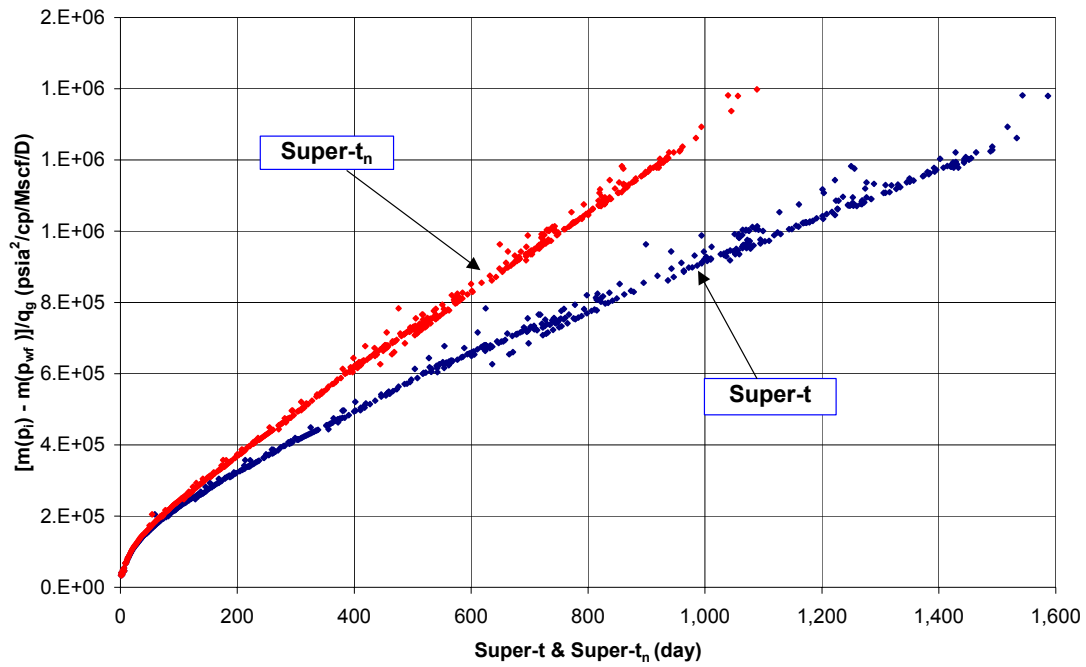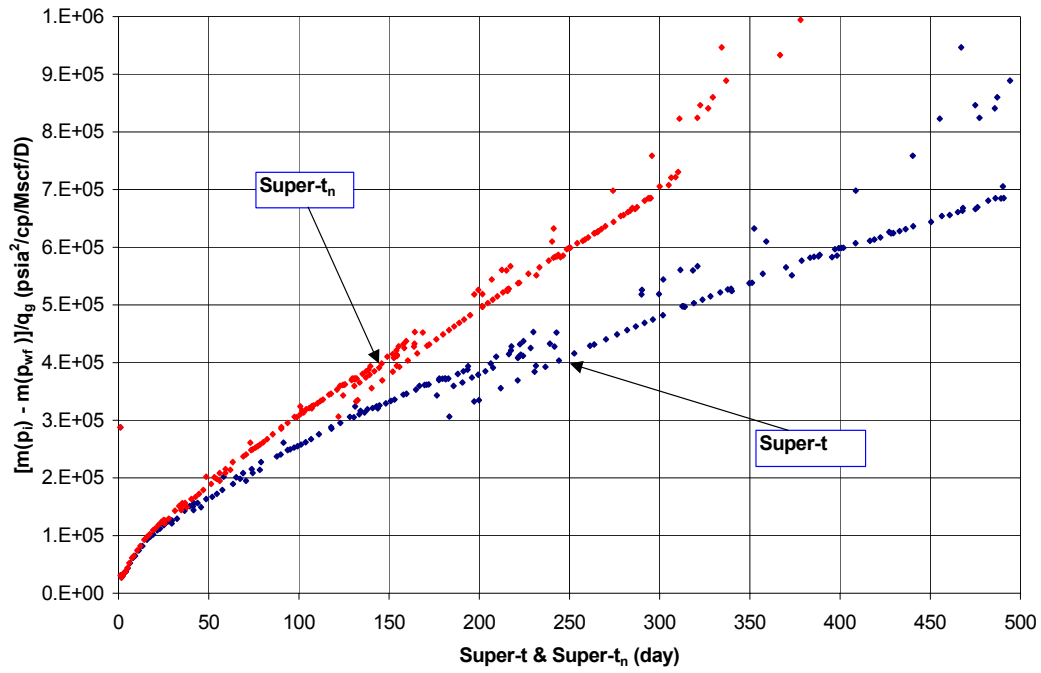
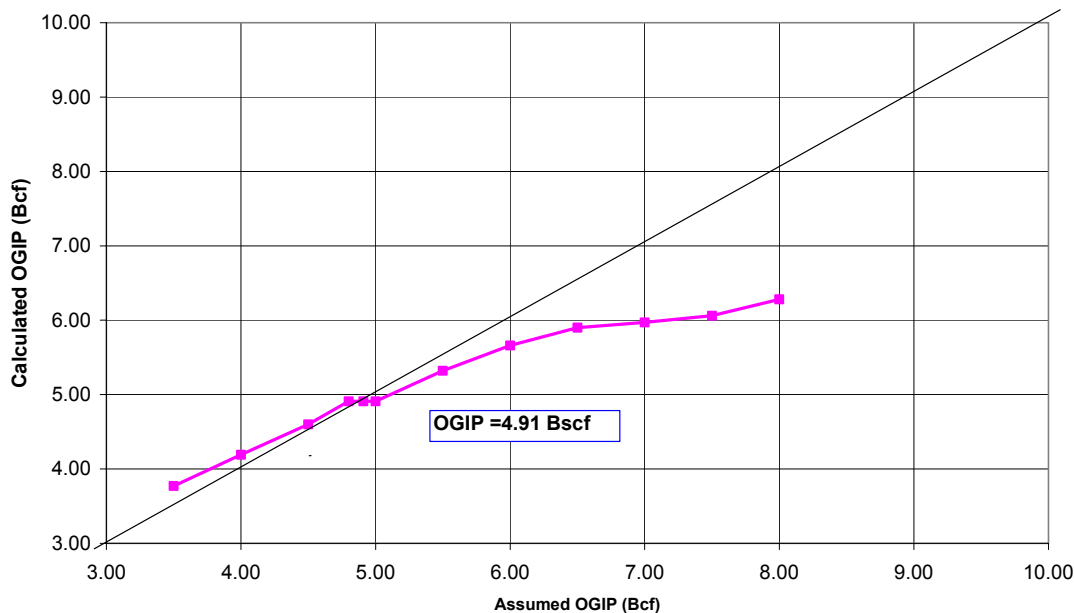**Fig. E-3**—Shows comparison between Super-t and Super-t$_n$ for Well HR-58.
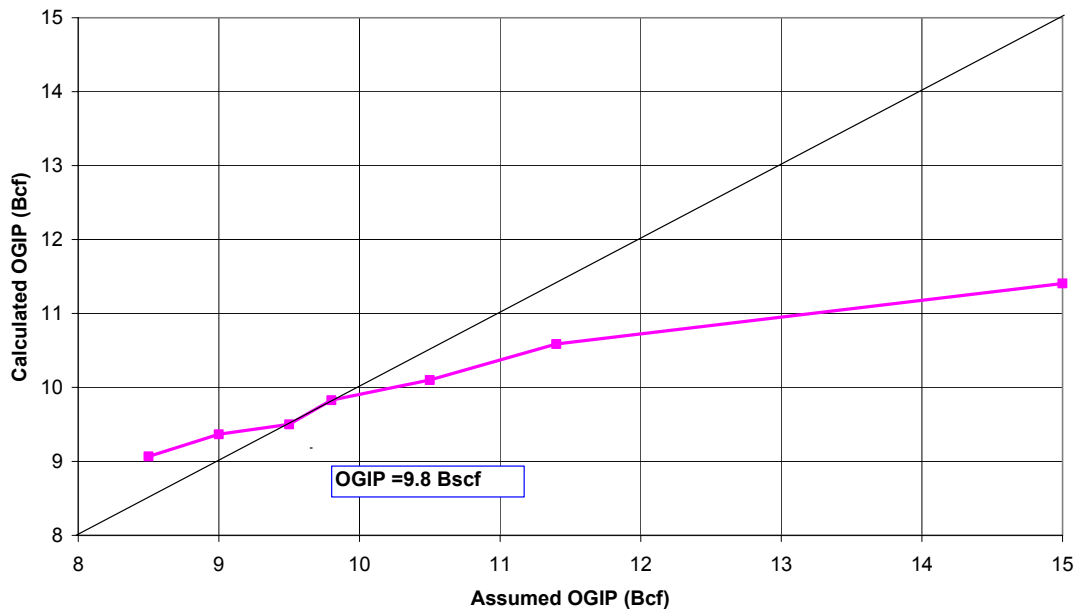
Fig. E–4—Shows the result from iteration procedure for calculating the correct OGIP by using normalized pseudotime method for Well HR-58.

Well HR-60

The third field example is for well HR-60, which produced for 659 days with cumulative production 5.03 Bcf. **Fig. E-5** shows, the production history of well HR-60. **Fig. E-6** shows a log-log diagnostic plot of $\Delta(m)p/q_g$ vs. time. The diagnostic plots show half-slope for almost 20 days followed by unit slope for late period. So, this well shows the boundary effect after 20 days due to the high production rate and small reservoir size. Also, There is a shut-in show a transient period for short time and then the well reach PSS period again.

Production data is plotted against the superposition of both real-time and normalized pseudotime on the same graph after trial for different OGIP value to find the

correct OGIP value as shown in **Fig. E-7**. When plotted against Super_t_n the data exhibits a straight line with one slope. In this case the OGIP is calculated to be 7.15 Bcf.

Fig. E-8 shows the unique answer of OGIP from Super_t_n slope that gives value 7.15 Bcf instead of 12 Bcf from Super_t slope after iteration for different value of OGIP.
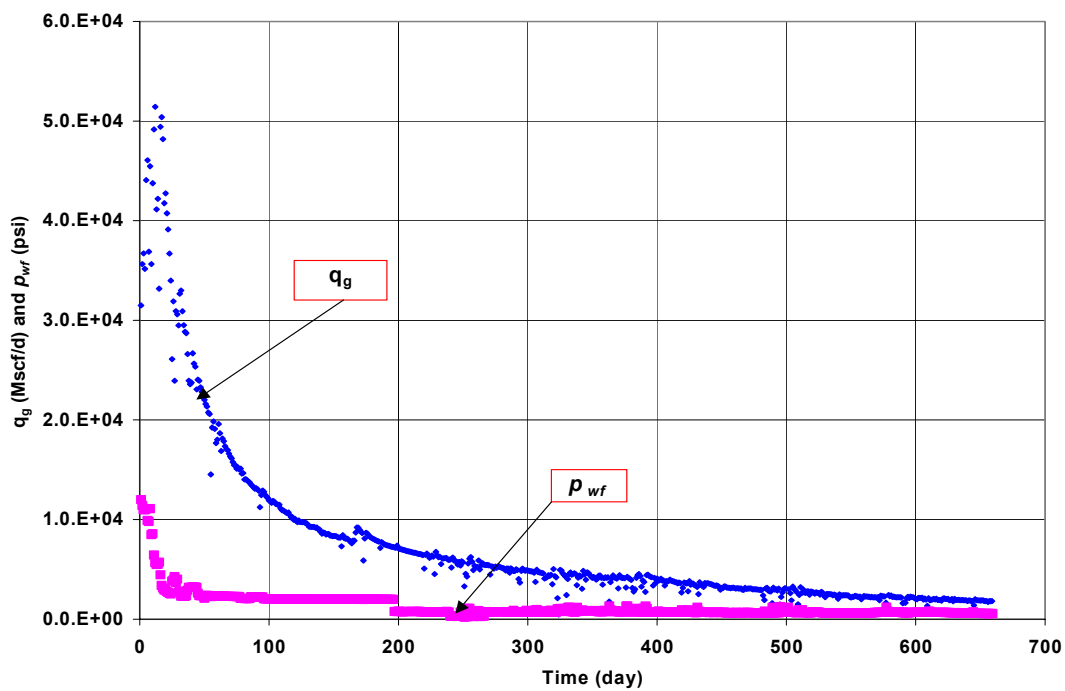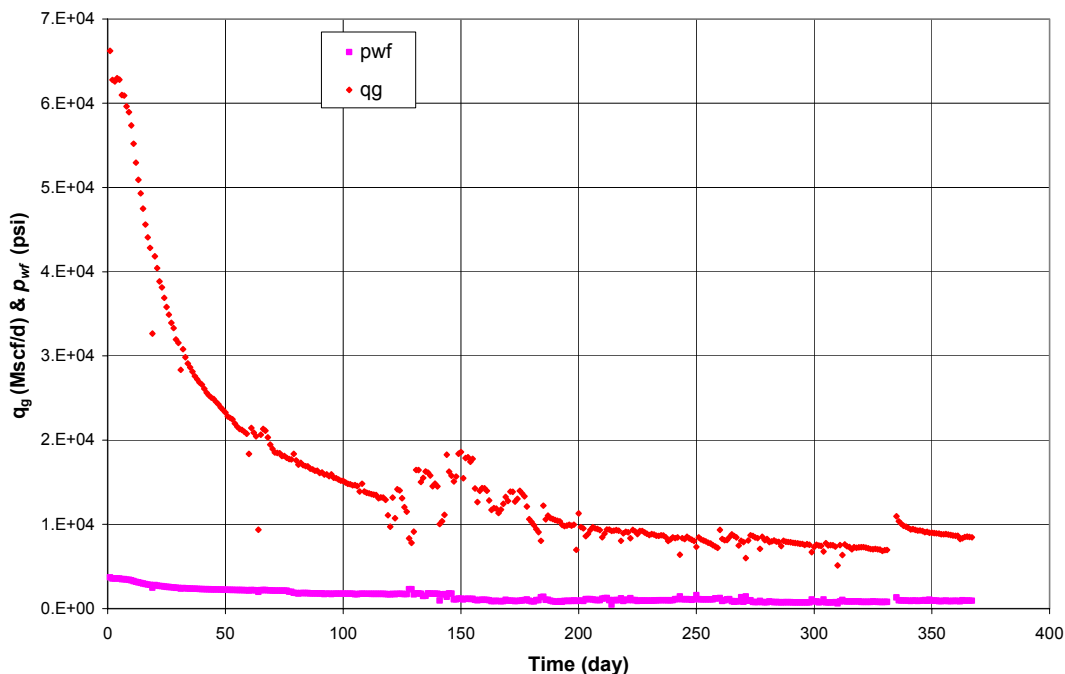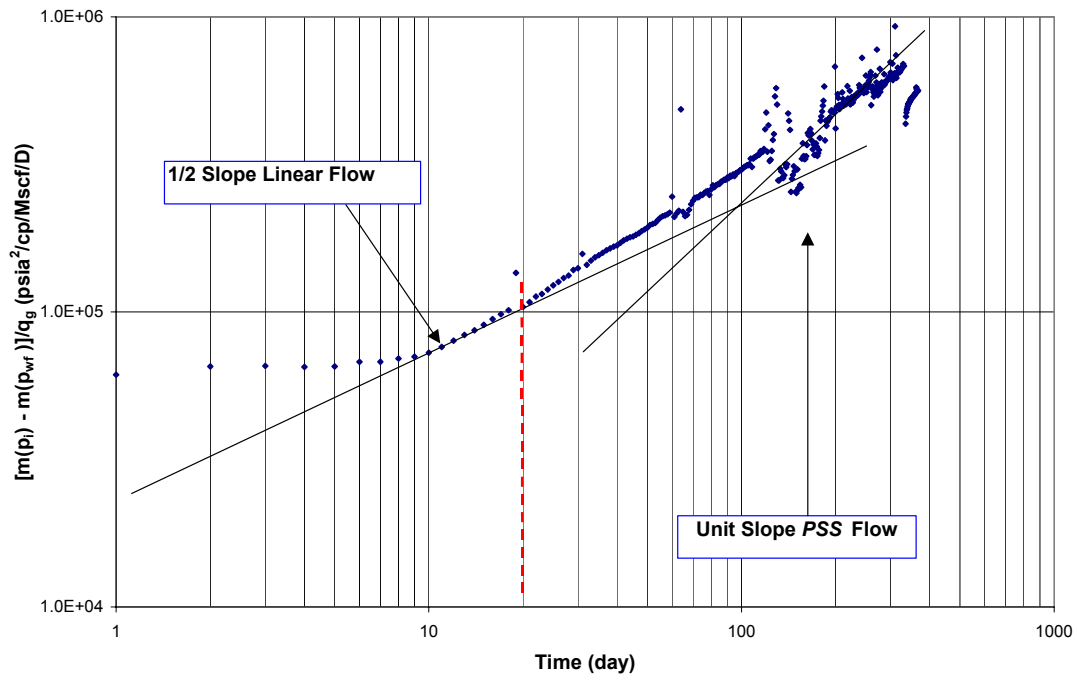

Fig. E-5—Well HR-60 production history.
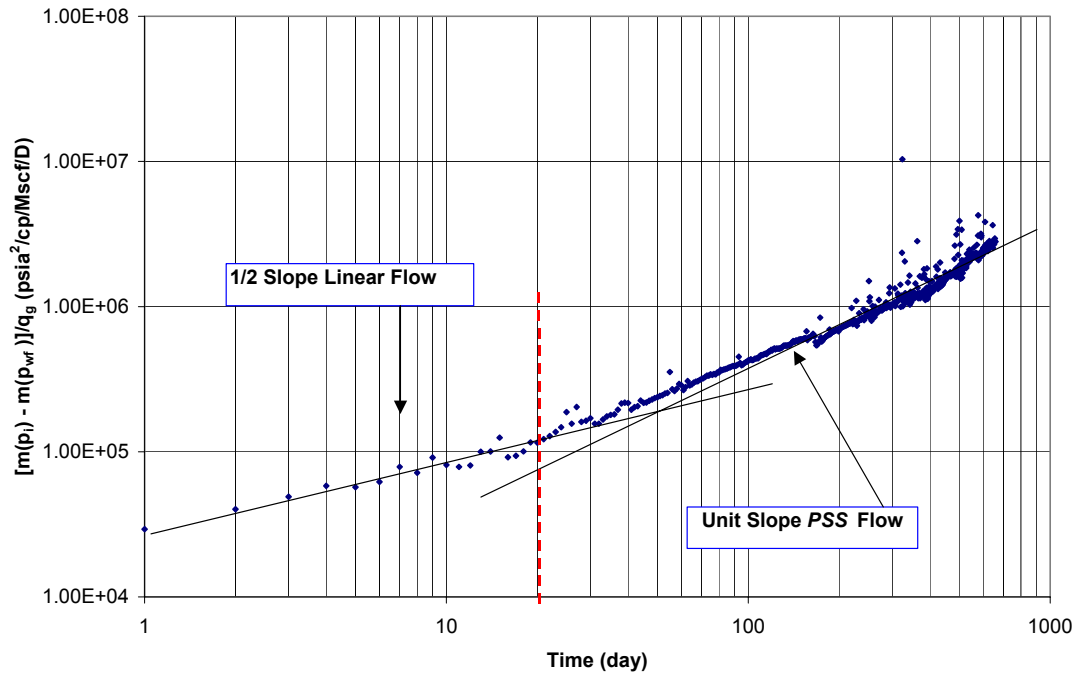
Fig. E-6—Log-log diagnostic plot of $\Delta m(p)/q_g$ vs. t for well HR-60 which shows half slopes and unit slope.
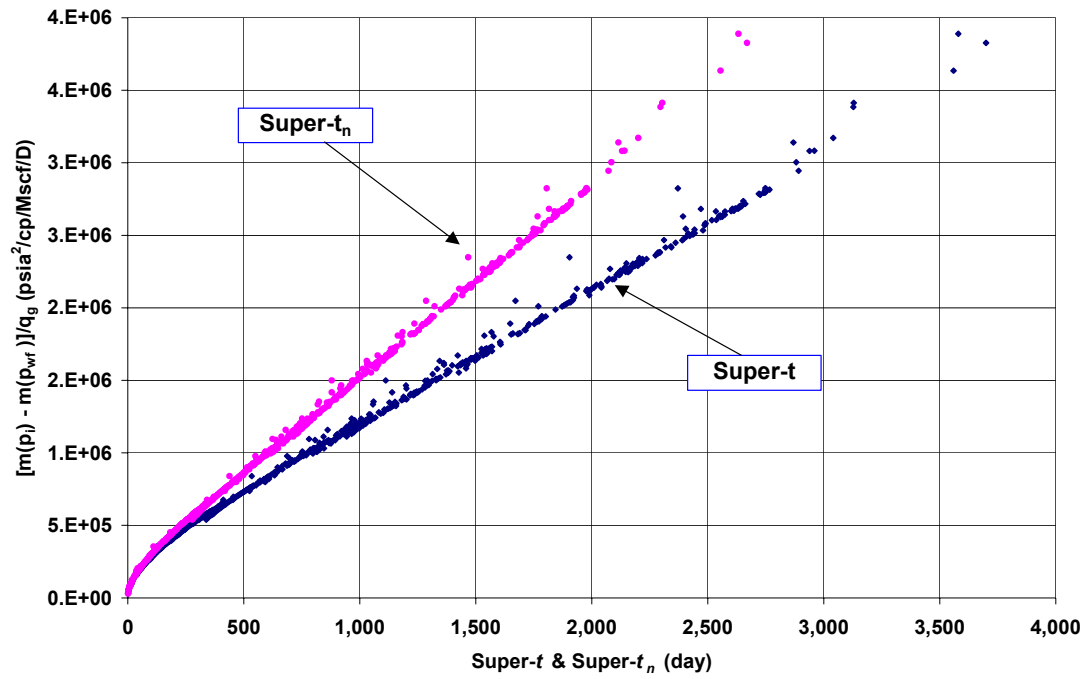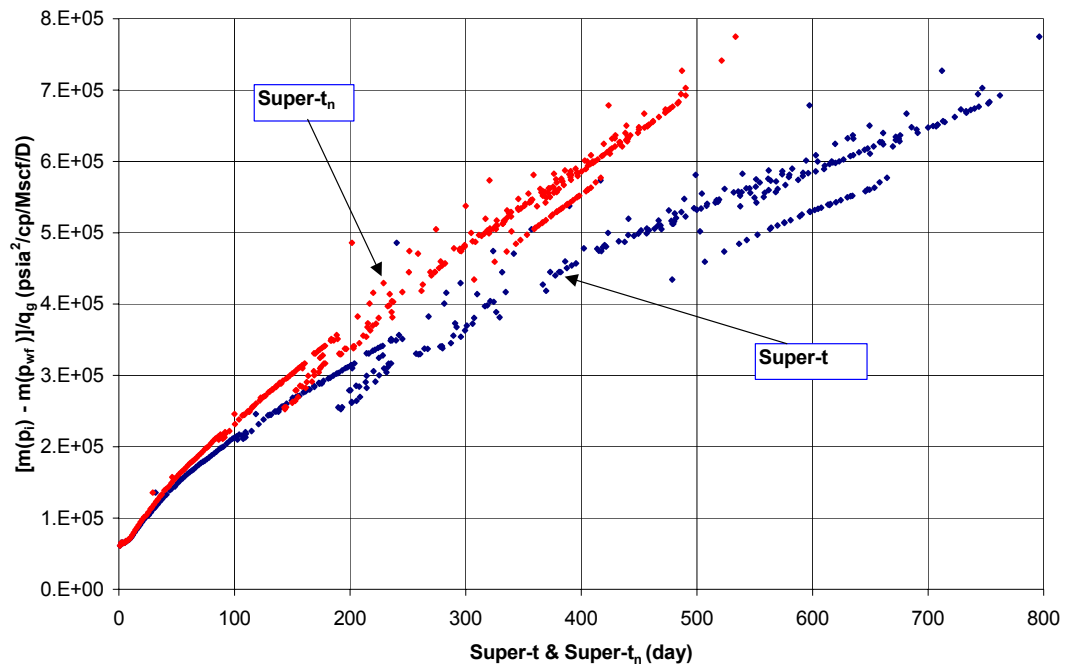
Fig. E-7—Shows comparison between Super-t and Super-t_n for Well HR-60.
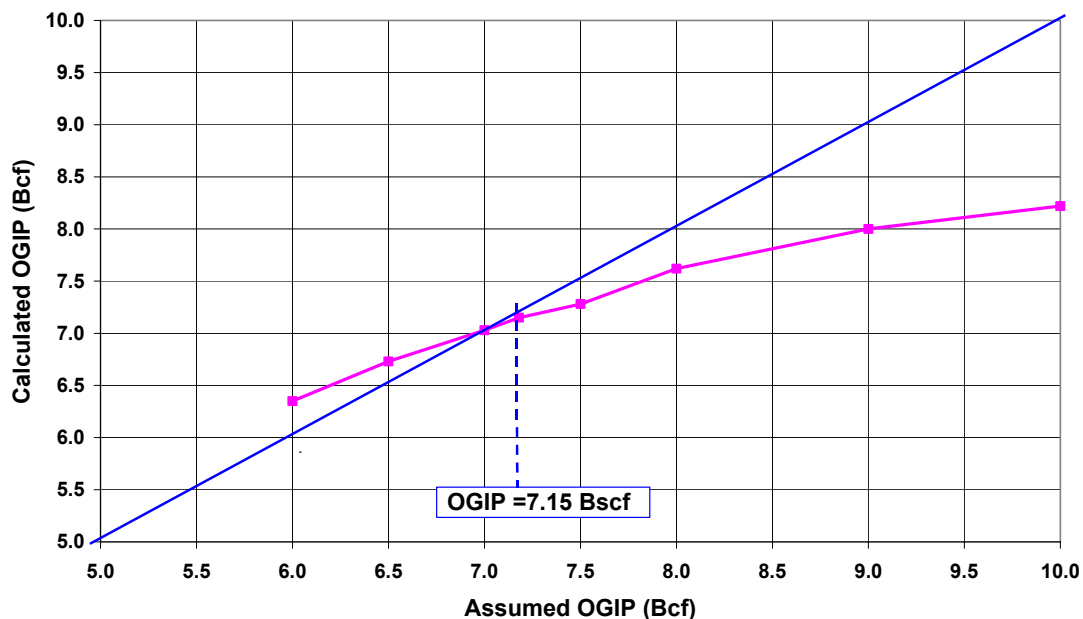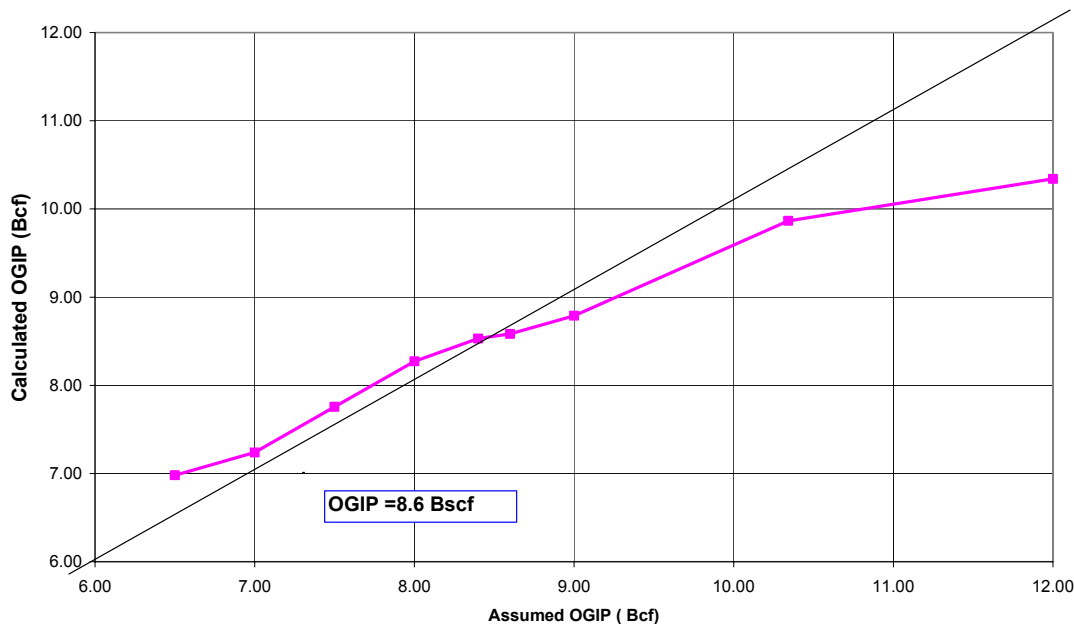
Fig. E-8—Shows the result from iteration procedure for calculating the correct OGIP by using normalized pseudotime method for Well HR-60.

Well HR-61

The fourth field example is for well HR-61, which produced for 218 days with cumulative production 3.38 Bcf. show the reservoir data. **Fig. E-9** shows the production history of well HR-61. **Fig. E-10** shows a log-log diagnostic plot of $\Delta(m)p/q_g$ vs. time. The diagnostic plots show half-slope for almost 6 days followed by unit slope for late period. There are many shut-in periods in the production history of this well, which show a transient period for short time and then followed by *PSS* period again. So, as we can see in **Fig. E-10** there is many *PSS* periods with one slope but due to the effect of properties change these periods does not give straight line as we can see in **Fig. E-11** of Super.t line.

Production data is plotted against the superposition of both real-time and normalized pseudotime on the same graph after trial for different OGIP value to find the correct OGIP value as shown in **Fig. E-11**. When plotted against Super.t_n the data exhibits a straight line with one slope. Also, we can see many parallel lines for Super.t_n in *PSS* period after we correct for properties changes. In this case the OGIP is calculated to be 4.91 Bcf.

Fig. E-12 shows the unique answer of OGIP from Super.t_n slope that gives value 4.91 Bcf instead of 9.0 Bcf from Super.t slope after iteration for different value of OGIP.
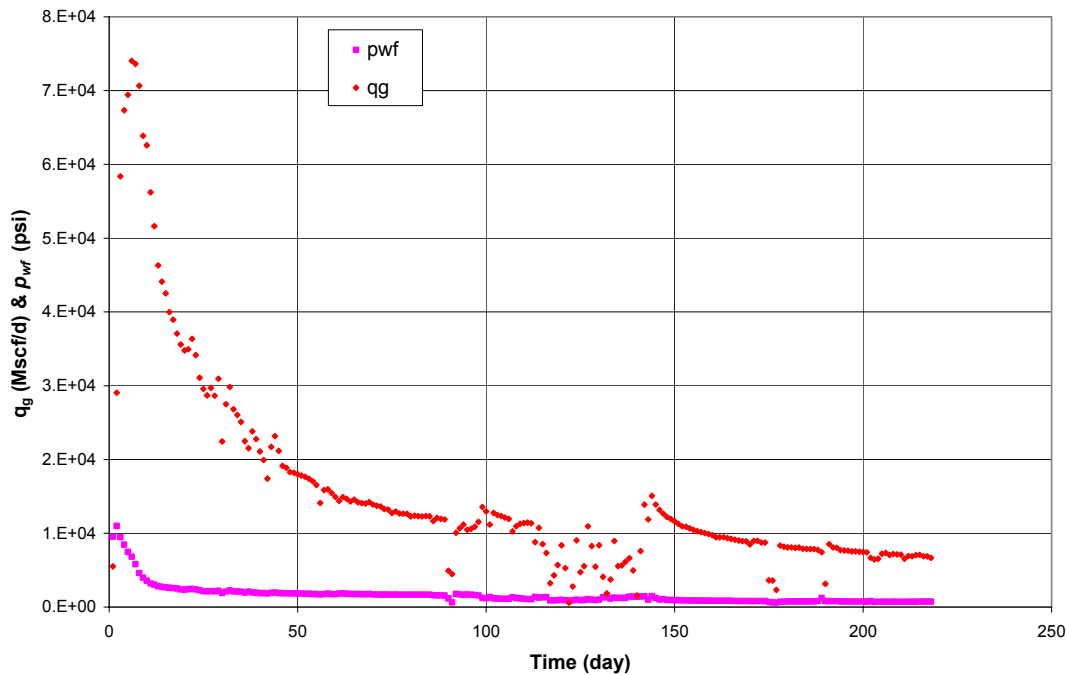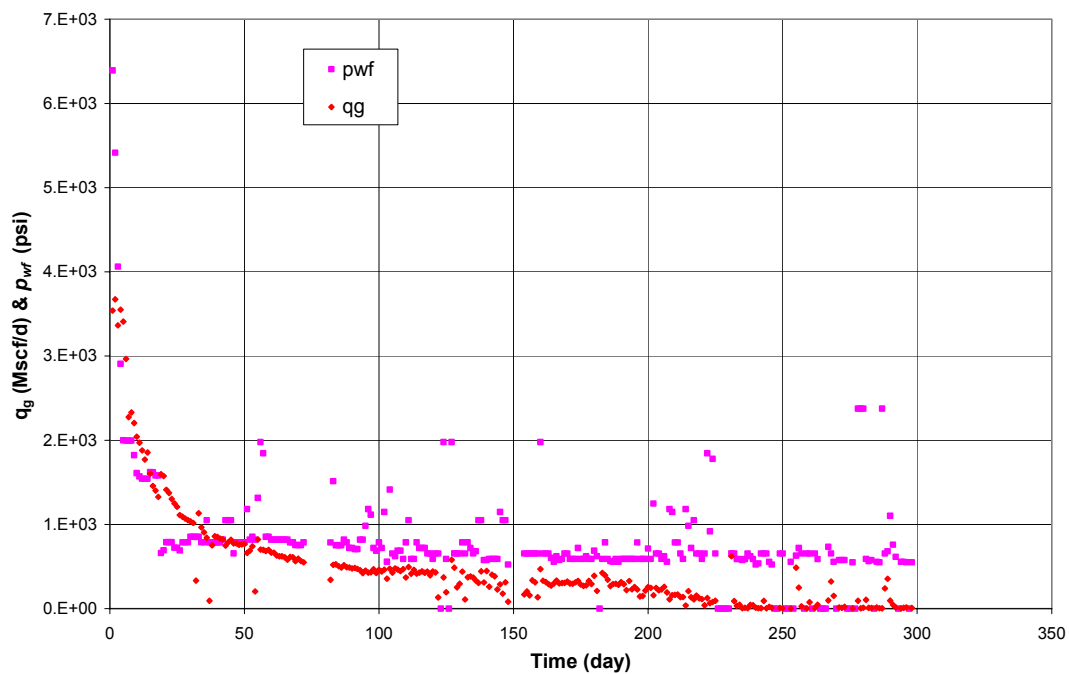

Fig. E-9—Well HR-61 production history.
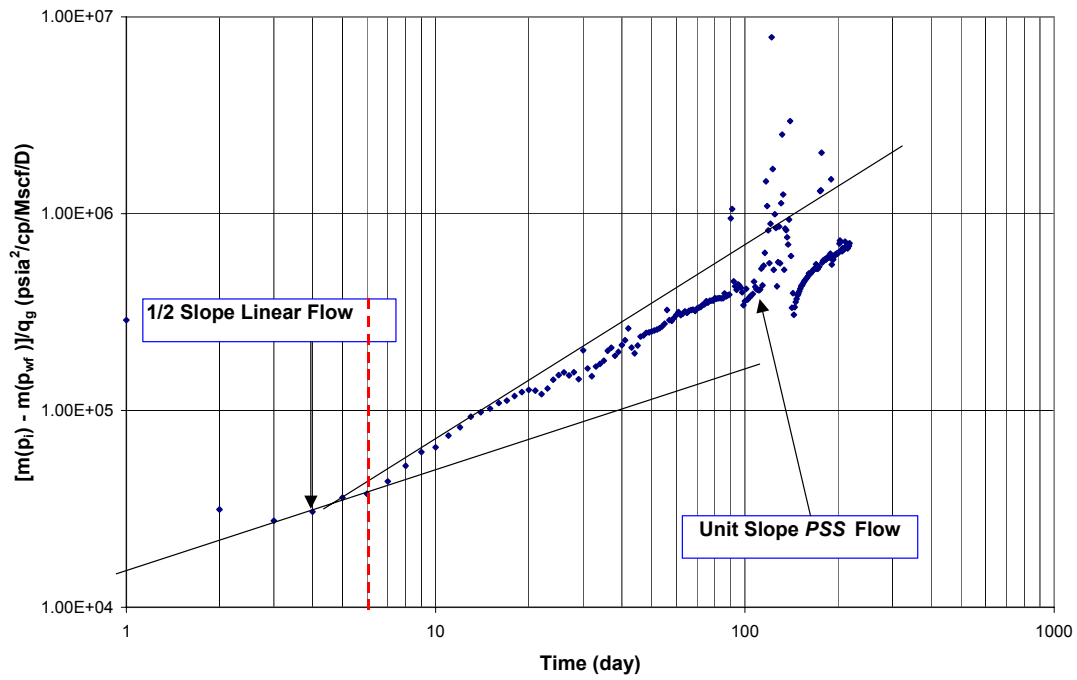
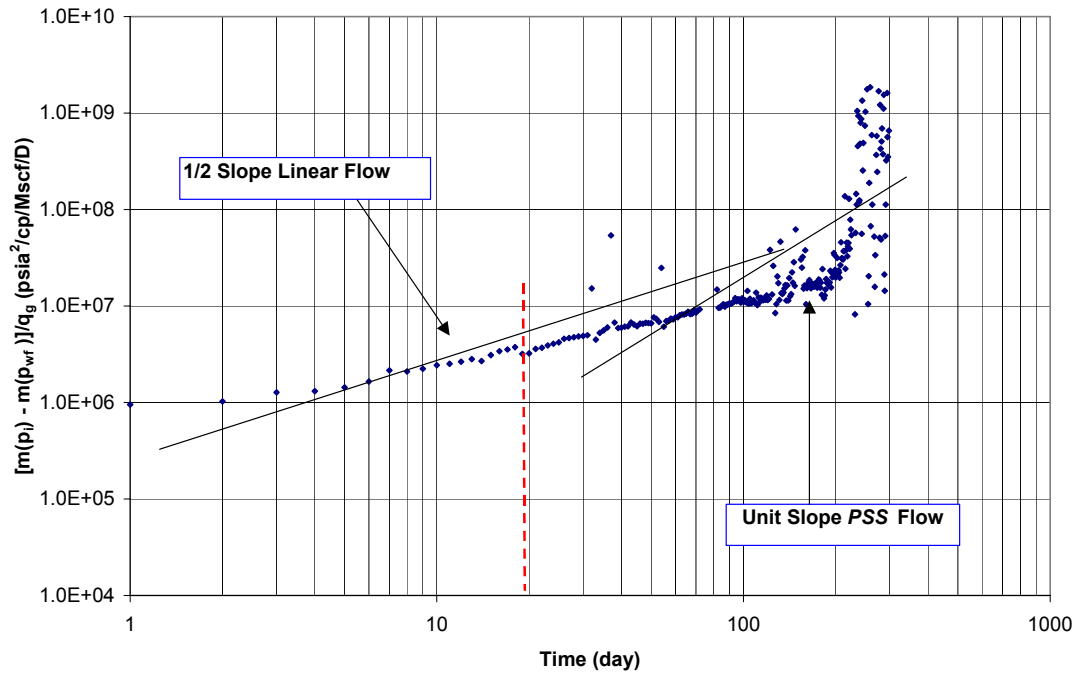**Fig. E-10**—Log-log diagnostic plot of $\Delta m(p)/q_g$ vs. *t* for well HR-60 which shows half slopes and unit slope.
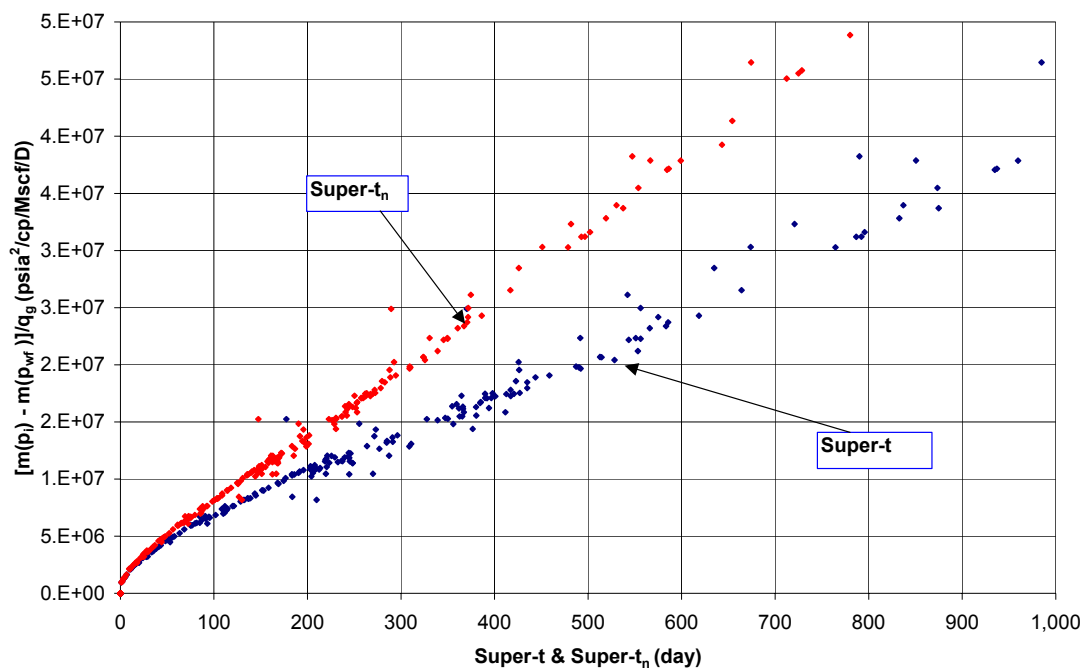
Fig. E-11—Shows comparison between Super-t and Super-t$_n$ for Well HR-61.
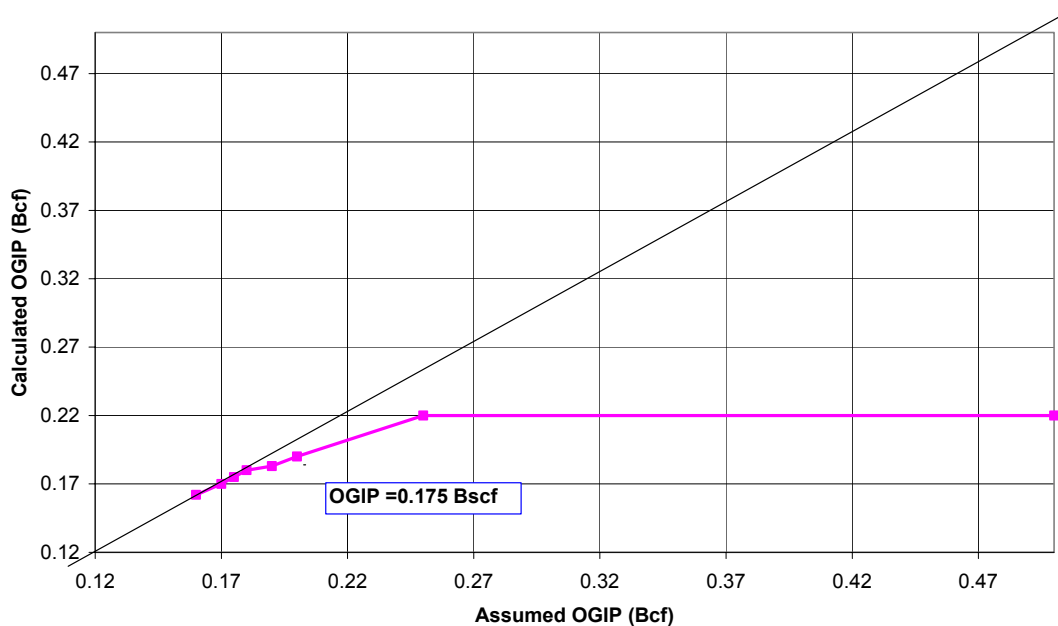
Fig. E–12—Shows the result from iteration procedure for calculating the correct OGIP by using normalized pseudotime method for Well HR-61.

Well HR-62

The fifth field example is for well HR-62, which produced for 367 days with cumulative production 5.53 Bcf. **Fig. E-13** shows, the production history of well HR-62. There are many shut-in periods in the production history of this well as shown in **Fig. E-14**, which Show many periods of *PSS*.

Fig. E-15 shows a log-log diagnostic plot of $\Delta(m)p/q_g$ vs. time. The diagnostic plots show half-slope for almost 20 days followed transition period and then by unit slope for late period. There are many shut-in periods in the production history, which show a transient period for short time and then followed by *PSS* period again.

Production data is plotted against the superposition of both real-time and normalized pseudotime on the same graph after trial for different OGIP value to find the correct OGIP value as shown in **Fig. E-16**. When plotted against Super.t_n the data exhibits a straight line with one slope. Also, we can see many parallel lines for Super.t_n in *PSS* period after we correct for properties changes. In this case the OGIP is calculated to be 8.6 Bcf.

Fig. E-17 shows the unique answer of OGIP from Super.t_n slope that gives value 8.6 Bcf instead of 16.28 Bcf from Super.t slope after iteration for different value of OGIP. The error in using Super-t slope in OGIP is equal 89.3%.
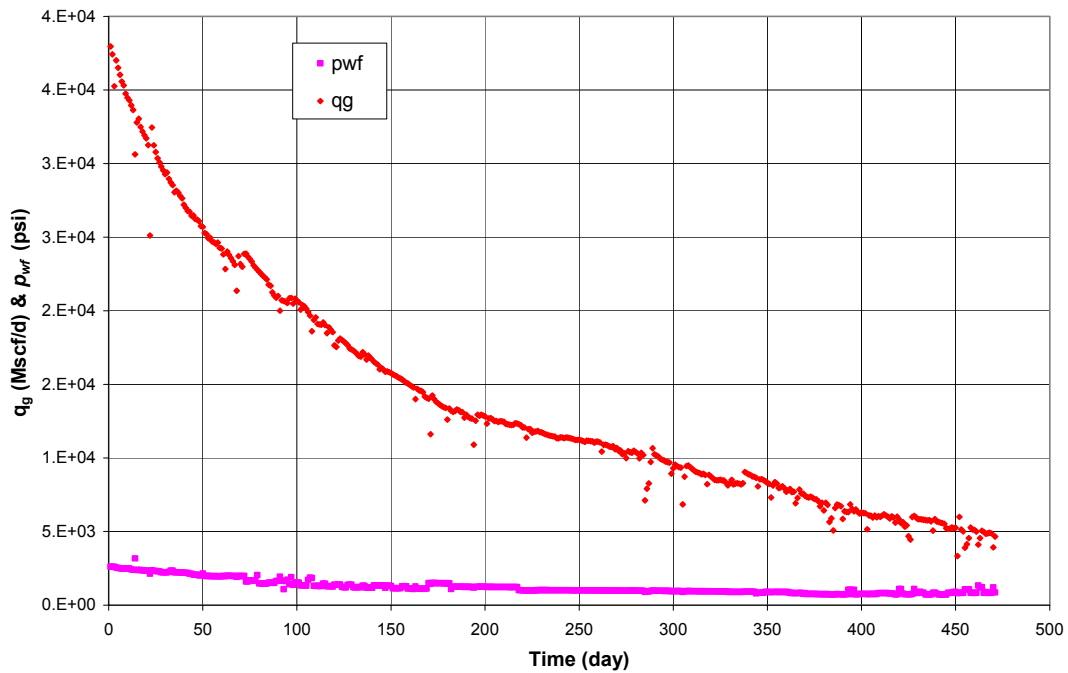

Fig. E-13—Well HR-62 production history.

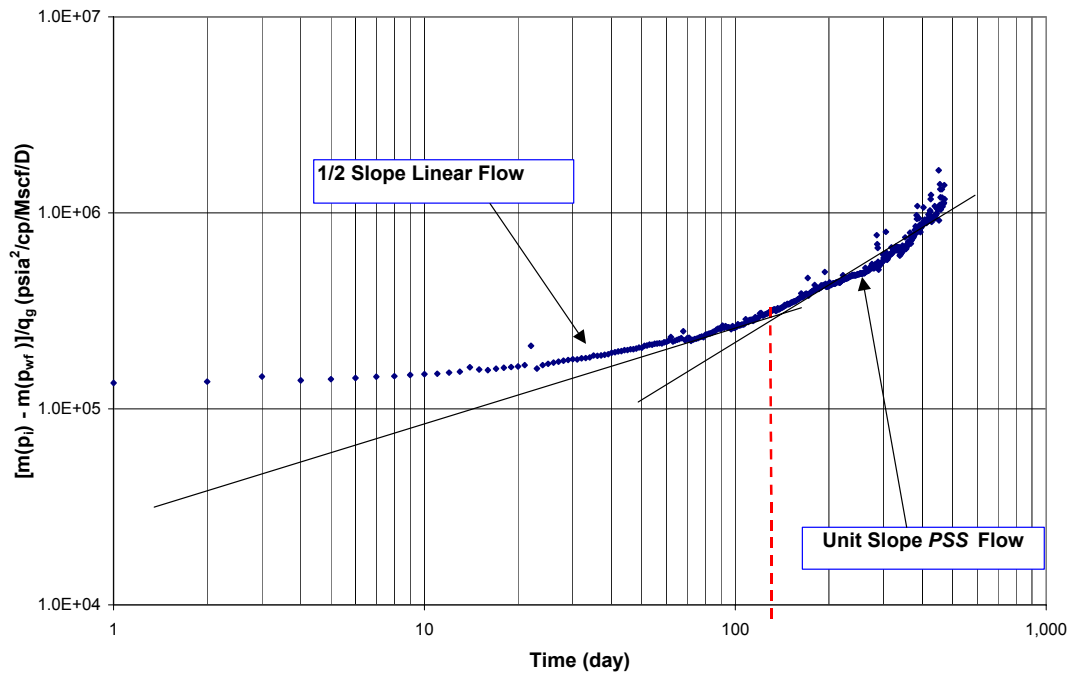**Fig. E-14**—Log-log diagnostic plot of $\Delta m(p)/q_g$ vs. *t* for well HR-62 which shows half slopes and unit slope.
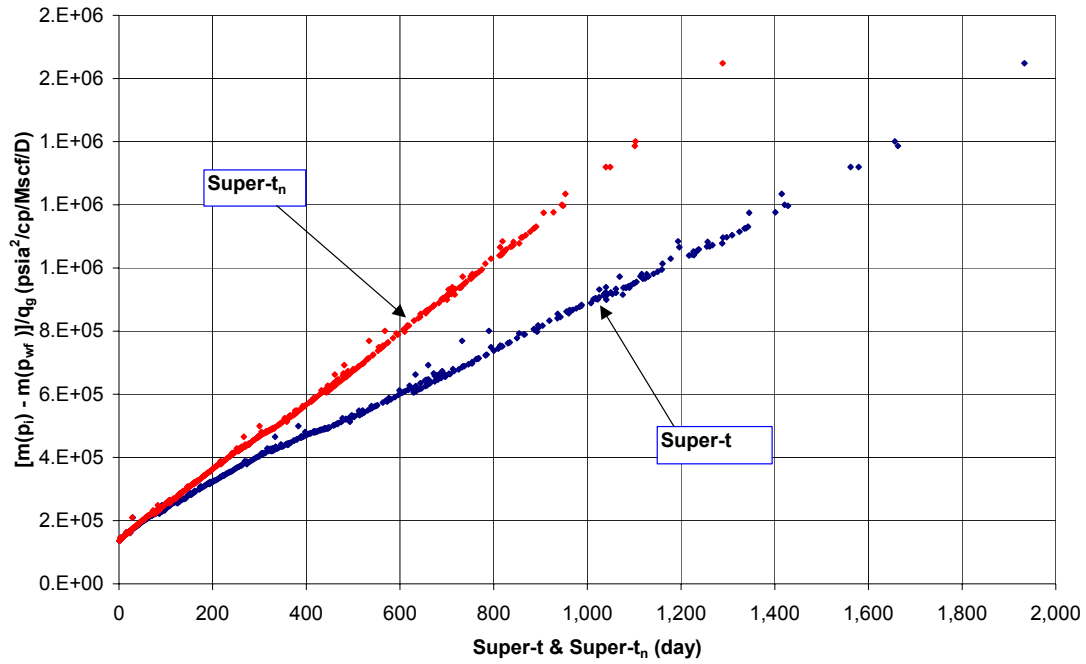
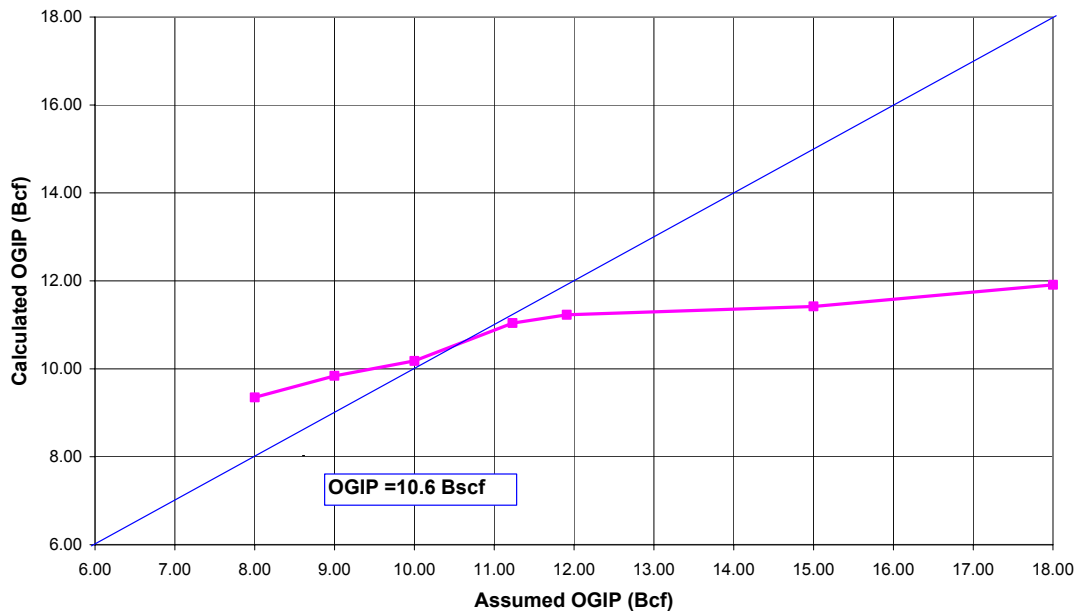**Fig. E-15**—Shows comparison between Super‑t and Super‑t_n for Well HR-62.

Fig. E–16—Shows the result from iteration procedure for calculating the correct OGIP by using normalized pseudotime method for Well HR-62.

Well HR-64

The six-field case is for well HR-64, which produced for 298 days with cumulative production 0.13 Bcf. **Fig. E-17** shows, the production history of well HR-64. This well depleted in short time due to small size of the reservoir and liquid load up problem in late period.

Fig. E-18 shows a log-log diagnostic plot of $\Delta(m)p/q_g$ vs. time. The diagnostic plots show half-slope for almost 20 days followed transition period and then by unit slope for late period. There are many shut-in periods in the production history, which show a transient period for short time and then followed by *PSS* period again.

Production data is plotted against the superposition of both real-time and normalized pseudotime on the same graph after trial for different OGIP value to find the correct OGIP value as shown in **Fig. E-19**. When plotted against Super.t_n the data

exhibits a straight line with one slope. Also, The Super.t line is not straight line due to great change in reservoir properties which is related to the small size of this reservoir. In this case the OGIP is calculated to be 0.175 Bcf.

Fig. E-20 shows the unique answer of OGIP from Super.t_n slope that gives value 0.175 Bcf instead of 0.24 Bcf from Super.t slope after iteration for different value of OGIP. The error in using Super.t slope in OGIP is equal 37.14%.
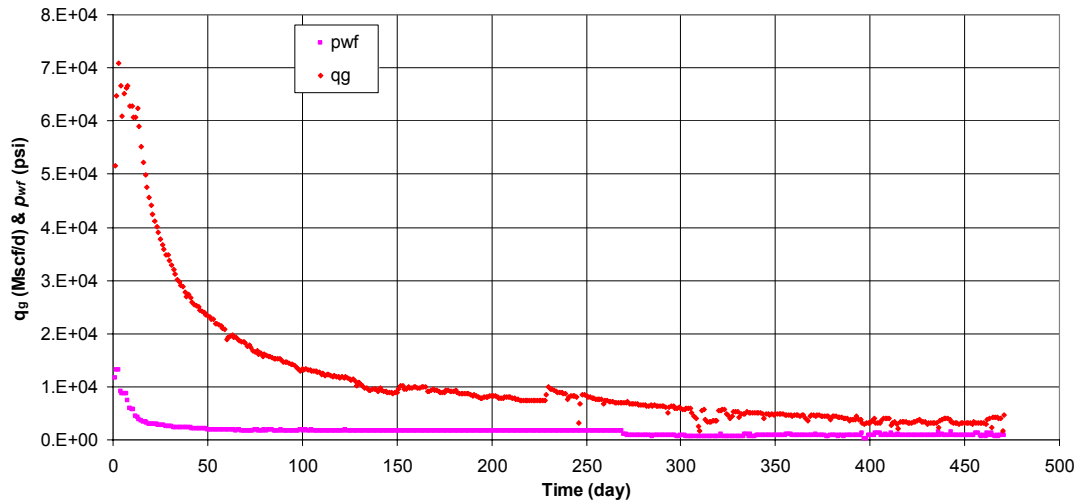

Fig. E-17—Well HR-64 production history.

Fig. E-18—Log-log diagnostic plot of $\Delta m(p)/q_g$ vs. *t* for well HR-64 which shows half slopes and unit slope.

Fig. E-19—Shows comparison between Super-t and Super-t_n for Well HR-64.

Fig. E–20—Shows the result from iteration procedure for calculating the correct OGIP by using normalized pseudotime method for Well HR-64.

Well HR-54

The six-field example is for well HR-54, which produced for 471 days with cumulative production 6.53 Bcf. show the reservoir data. **Fig. E-21** shows the production history of well HR-54.

Fig. E-22 shows a log-log diagnostic plot of $\Delta(m)p/q_g$ vs. time. The diagnostic plots show half-slope for almost 105 days followed transition period and then by unit slope for late period.

Production data is plotted against the superposition of both real-time and normalized pseudotime on the same graph after trial for different OGIP value to find the correct OGIP value as shown in **Fig. E-23**.

Fig. E-24 shows the unique answer of OGIP from normalized pseudotime method that gives value 10.6 Bcf instead of 15.15 Bcf from superposition with real time. The error in OGIP value is 43%.
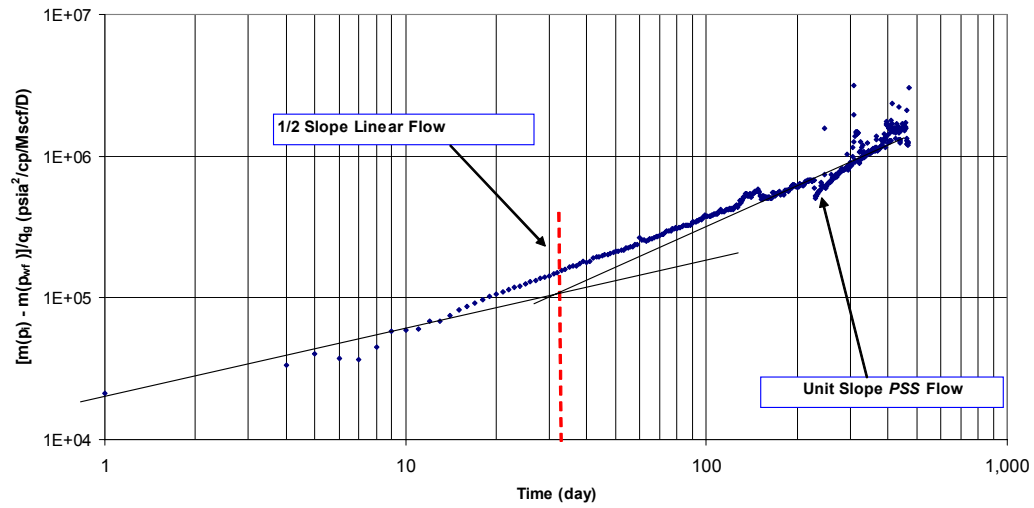

Fig. E-21—Well HR-54 production history.

Fig. E-22—Log-log diagnostic plot of $\Delta m(p)/q_g$ vs. t for well HR-54 which shows half slopes and unit slope.
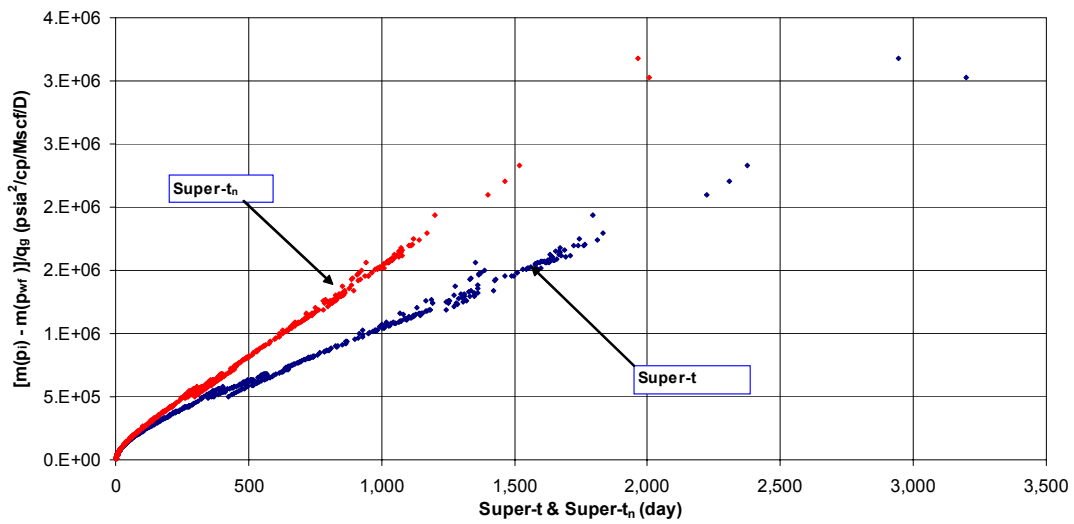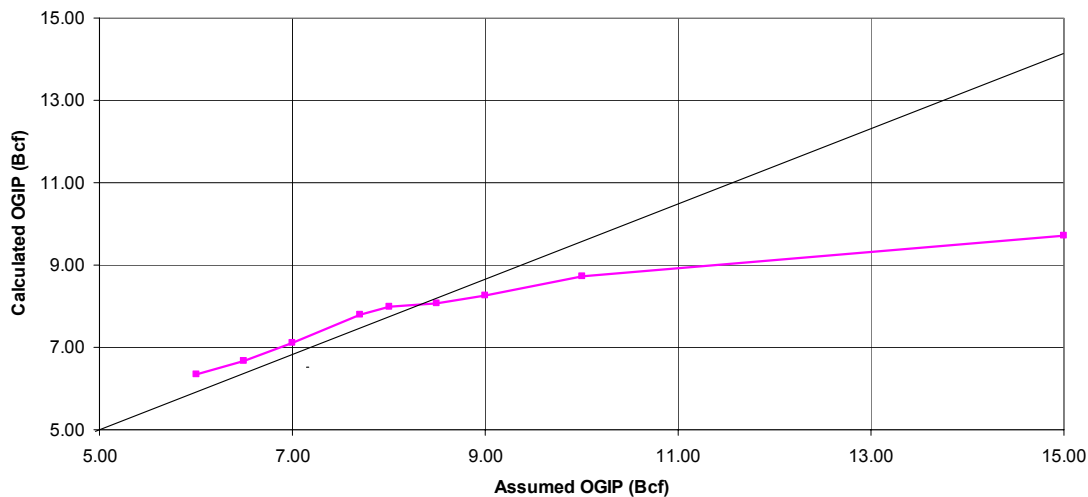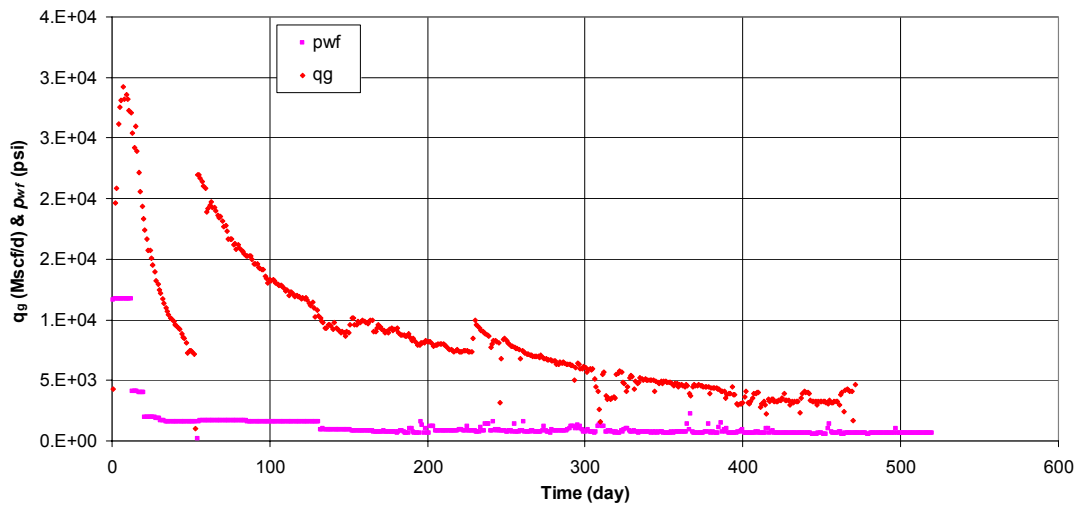
Fig. E-23—Shows comparison between Super‑t and Super‑t_n for Well HR-54.

Fig. E–24—Shows the result from iteration procedure for calculating the correct OGIP by using normalized pseudotime method for Well HR-54.

Well HR-56

The seven-field example is for well HR-56, which produced for 470 days with cumulative production 5.39 Bcf. show the reservoir data. **Fig. E-25** shows the production history of well HR-56.

Fig. E-26 shows a log-log diagnostic plot of $\Delta(m)p/q_g$ vs. time. The diagnostic plots show half-slope for almost 35 days followed transition period and then by unit slope for late period.

Production data is plotted against the superposition of both real-time and normalized pseudotime on the same graph after trial for different OGIP value to find the correct OGIP value as shown in **Fig. E-27**.

Fig. E-28 shows the unique answer of OGIP from normalized pseudotime method that gives value 8.0 Bcf instead of 12.21 Bcf from superposition with real time. The error in OGIP value is 52.63%.


Fig. E-25—Well HR-56 production history.

Fig. E-26—Log-log diagnostic plot of $\Delta m(p)/q_g$ vs. *t* for well HR-56 which shows half slopes and unit slope.

Fig. E-27—Shows comparison between Super-t and Super-t_n for Well HR-56.
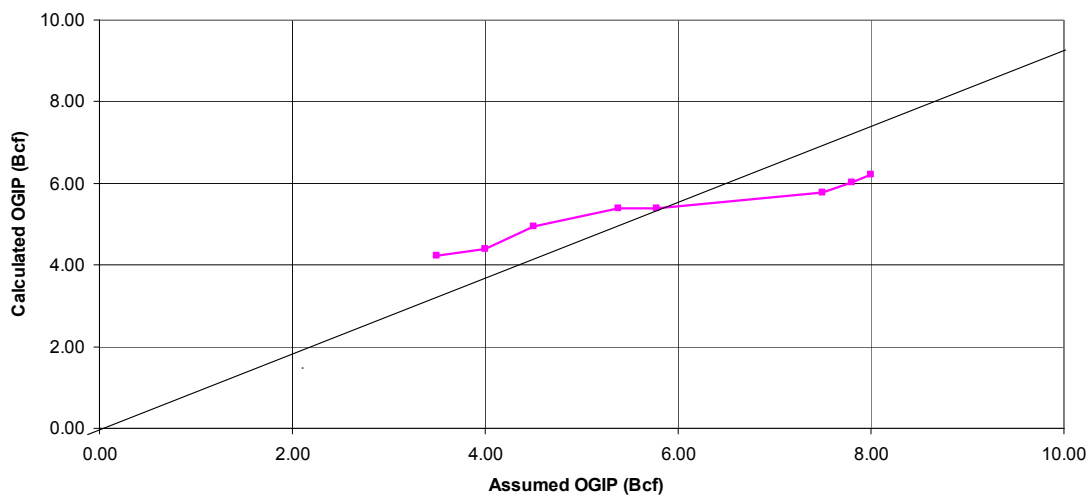
Fig. E–28—Shows the result from iteration procedure for calculating the correct OGIP by using normalized pseudotime method for Well HR-56.

Well CC-5

The eight-field example is for well CC-5, which produced for 520 days with cumulative production 3.24 Bcf. show the reservoir data. **Fig. E-29** shows the production history of well CC-5.

Fig. E-30 shows a log-log diagnostic plot of $\Delta(m)p/q_g$ vs. time. The diagnostic plots show half-slope for almost 10 days followed two-unit slope period for late time. This is due to there is shut in period in the production and well reach PSS in short time as we can see in **Fig. E-30** in unit slope period.

Fig. E-29—Well CC-5 production history.
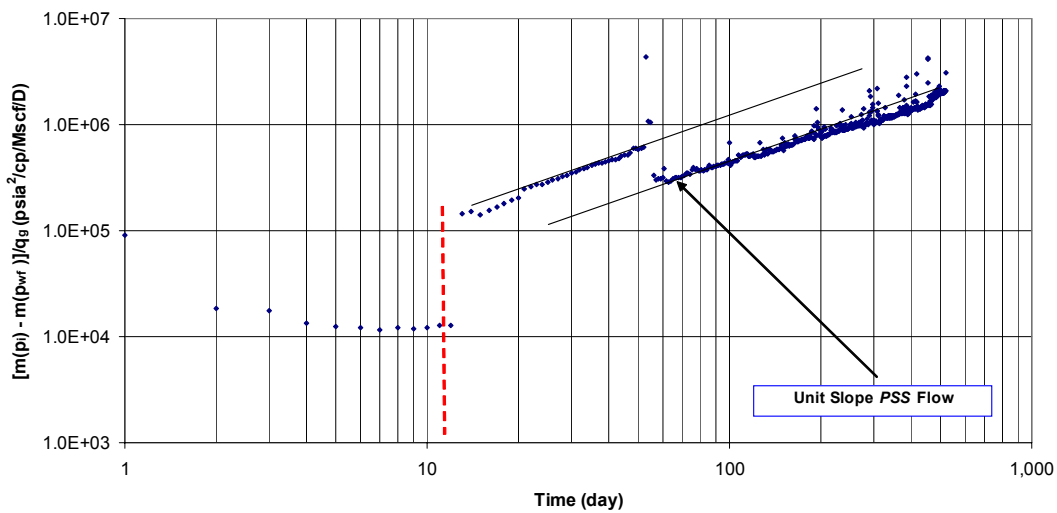
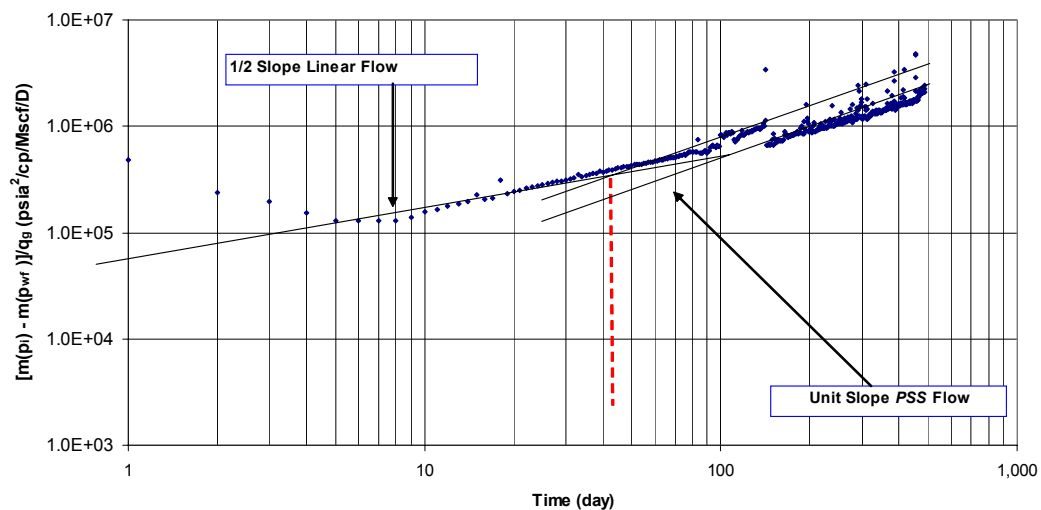**Fig. E-30**—Log-log diagnostic plot of Δm(p)/q$_g$ vs. t for well CC-5 which shows transient period and two unit slope periods.

Production data is plotted against the superposition of both real-time and normalized pseudotime on the same graph after trial for different OGIP value to find the correct OGIP value as shown in **Fig. E-31**. **Fig. E-32** shows the unique answer of OGIP

from normalized pseudotime method that gives value 5.38 Bcf instead of 6.24 Bcf from superposition with real time.
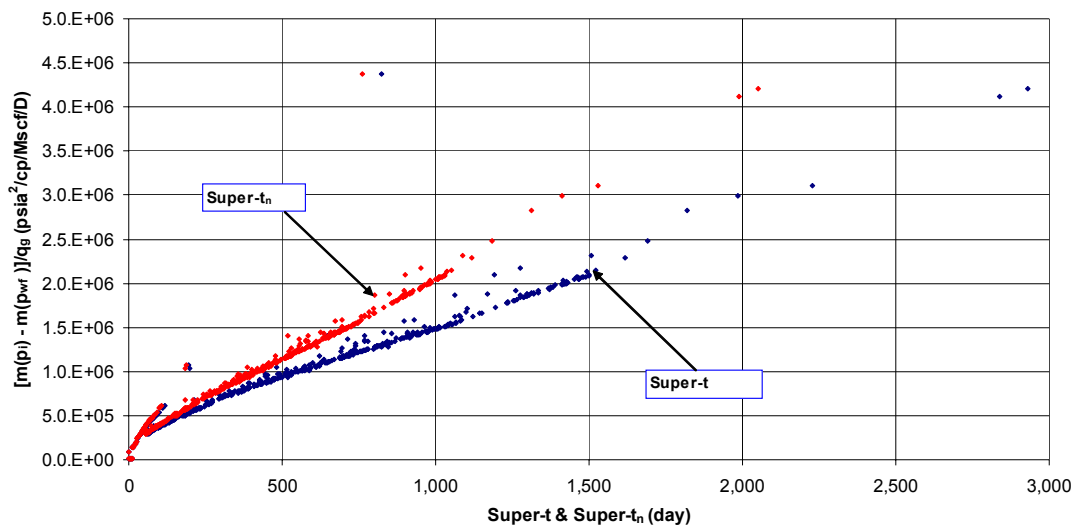
Fig. E-31—Shows comparison between Super-t and Super-t_n for Well CC-5.

Fig. E–32—Shows the result from iteration procedure for calculating the correct OGIP by using normalized pseudotime method for Well CC-5.

Well CC-6

The nine-field example is for well CC-6, which produced for 488 days with cumulative production 2.82 Bcf. show the reservoir data. **Fig. E-33** shows the production history of well CC-6.

Fig. E-34 shows a log-log diagnostic plot of $\Delta(m)p/q_g$ vs. time. The diagnostic plots show half-slope for almost 50 days followed transition zone, and two-unit slope period for late time. This is due to there is shut in period in the production and well reach *PSS* in short time as we can see in **Fig. E-34** in unit slope period.

Production data is plotted against the superposition of both real-time and normalized pseudotime on the same graph after trial for different OGIP value to find the correct OGIP value as shown in **Fig. E-35**.

Fig. E-36 shows the unique answer of OGIP from normalized pseudotime method that gives value 5.5 Bcf instead of 6.71 Bcf from superposition with real time. The error in OGIP from Super.t method is equal 22.0%.
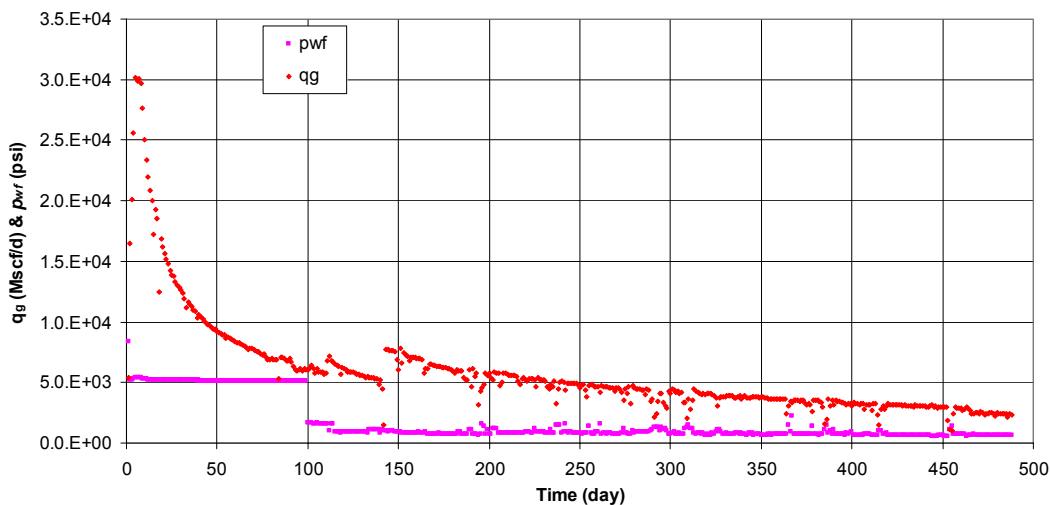
Fig. E-33—Well CC-6 production history.

Fig. E-34—Log-log diagnostic plot of $\Delta m(p)/q_g$ vs. t for well CC-6 which shows transient period and two unit slope periods.
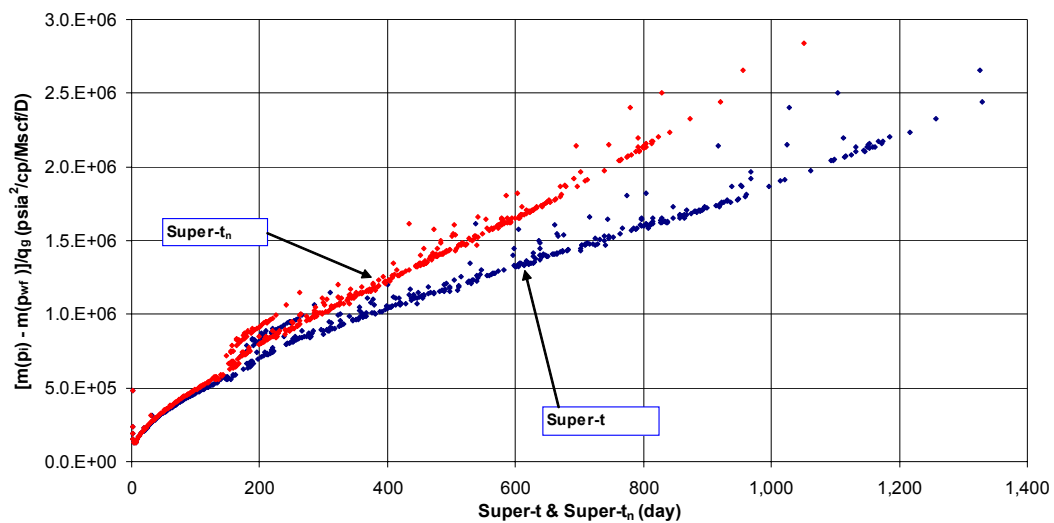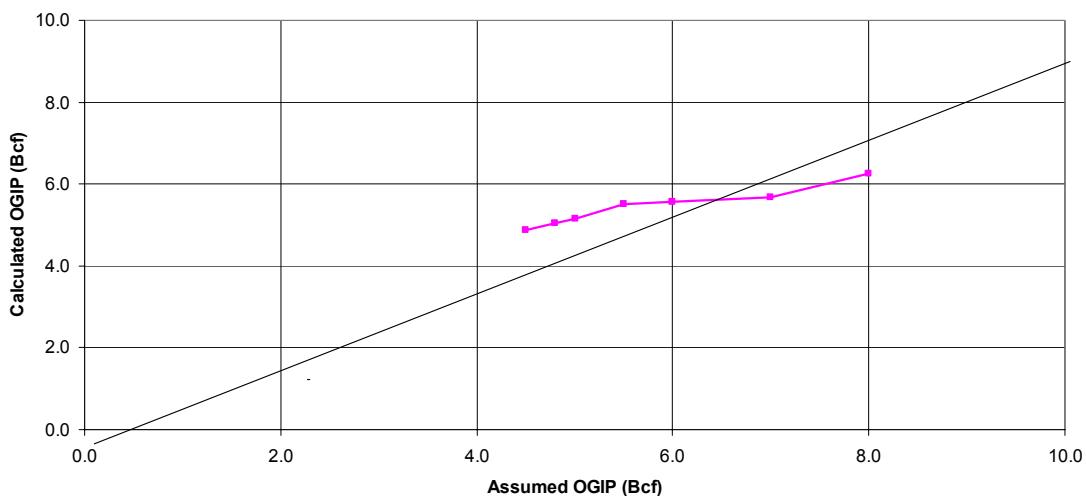

Fig. E-35—Shows comparison between Super-t and Super-t_n for Well CC-6.

Fig. E–36—Shows the result from iteration procedure for calculating the correct OGIP by using normalized pseudotime method for Well CC-6.

Well CC-7

The ten-field example is for well CC-7, which produced for 488 days with cumulative production 2.82 Bcf. show the reservoir data. **Fig. E-37** shows the production history of well CC-7.

Fig. E-38 shows a log-log diagnostic plot of $\Delta(m)p/q_g$ vs. time. The diagnostic plots show half-slope for almost 25 days followed transition zone, and four-unit slope period for late time. This is due to there is shut-in period in the production and the well reach *PSS* in short time as we can see in **Fig. E-38** in unit slope period. So all unit slope period should give one slope but due to the properties change these period become non-linear.

Production data is plotted against the superposition of both real-time and normalized pseudotime on the same graph after trial for different OGIP value to find the correct OGIP value as shown in **Fig. E-39**. The normalized pseudotime superposition correct for properties change and make all *PSS* lines parallel as you can see in **Fig. E-39**.

Fig. E-40 shows the unique answer of OGIP from normalized pseudotime method that gives value 4.75 Bcf instead of 6.71 Bcf from superposition with real time.
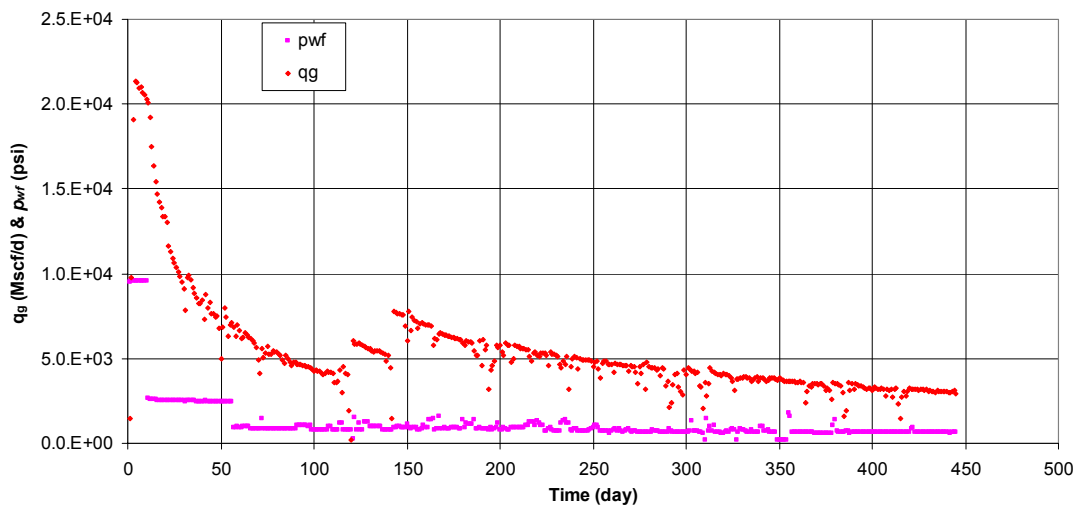

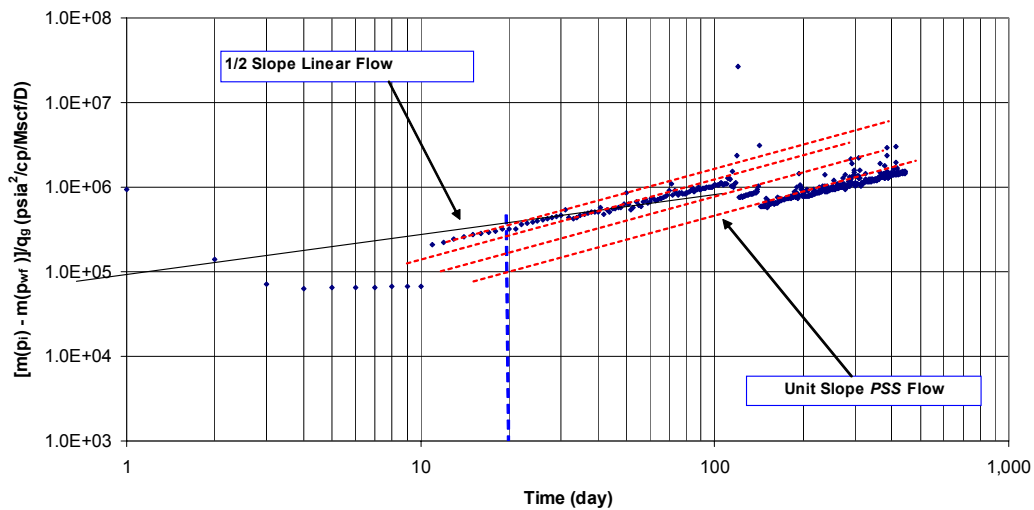
Fig. E-37—Well CC-7 production history.

Fig. E-38—Log-log diagnostic plot of $\Delta m(p)/q_g$ vs. t for well CC-7 which shows transient linear period and four unit slope *PSS* periods.
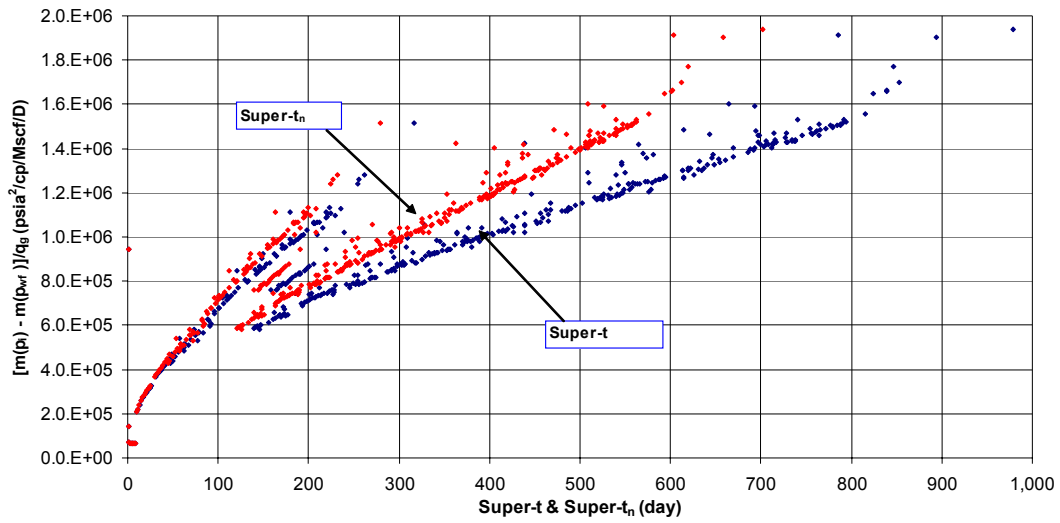
Fig. E-39—Shows comparison between Super‑t and Super‑t$_n$ for Well CC-7.
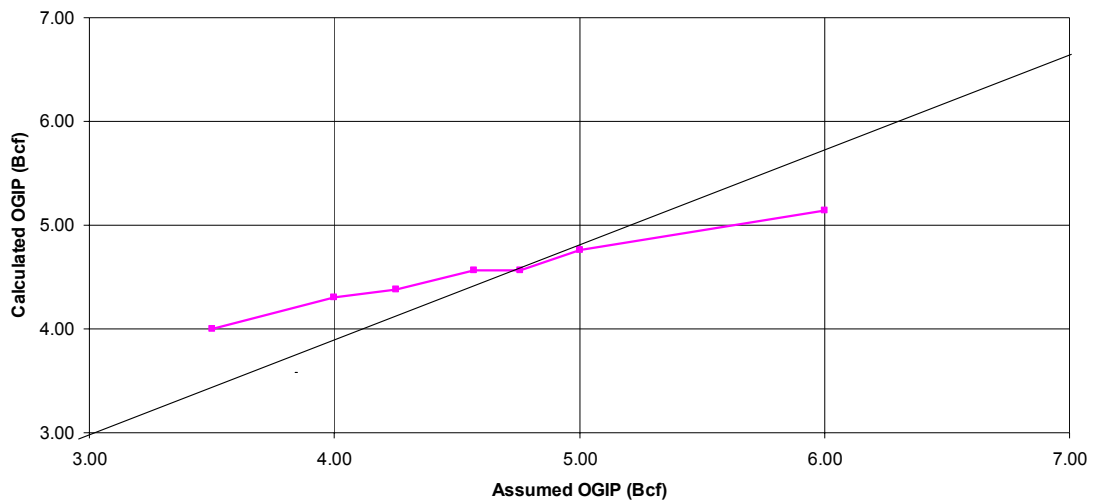

Fig. E–40—Shows the result from iteration procedure for calculating the correct OGIP by using normalized pseudotime method for Well CC-7.

Well CC-2

The eleven-field example is for well CC-2, which produced for 671 days with cumulative production 4.65 Bcf. show the reservoir data. **Fig. E-41** shows the production history of well CC-2.

Fig. E-42 shows a log-log diagnostic plot of $\Delta(m)p/q_g$ vs. time. The diagnostic plots show half-slope for almost 28 days followed transition zone, and unit slope period for late time. This is due to there is shut-in period in the production and the well reach *PSS* in short time as we can see in **Fig. E-42** in unit slope period.

Production data is plotted against the superposition of both real-time and normalized pseudotime on the same graph after trial for different OGIP value to find the correct OGIP value as shown in **Fig. E-43**.

The unique answer of OGIP from normalized pseudotime method that gives value 7.0 Bcf instead of 10.53 Bcf from superposition with real time. The error in OGIP from Super.t is equal to 50.4%.
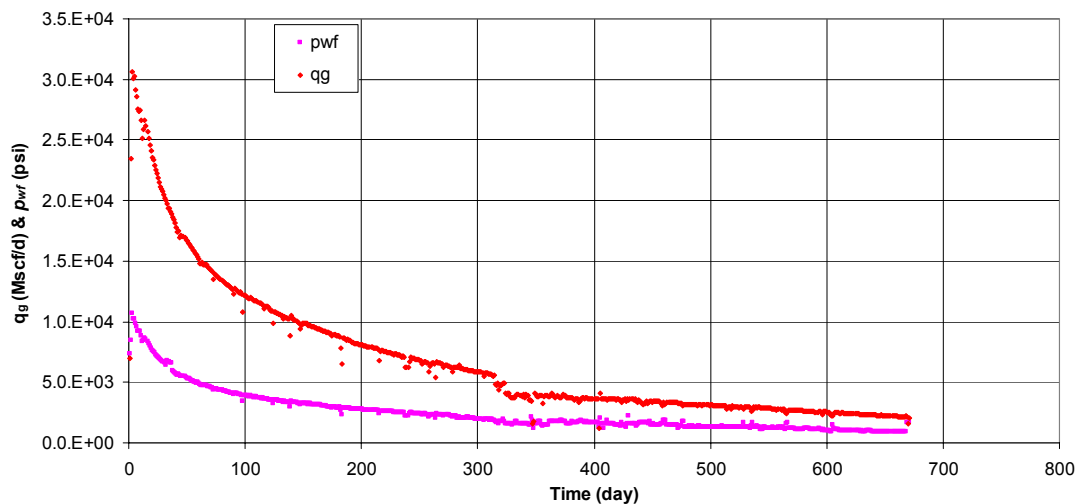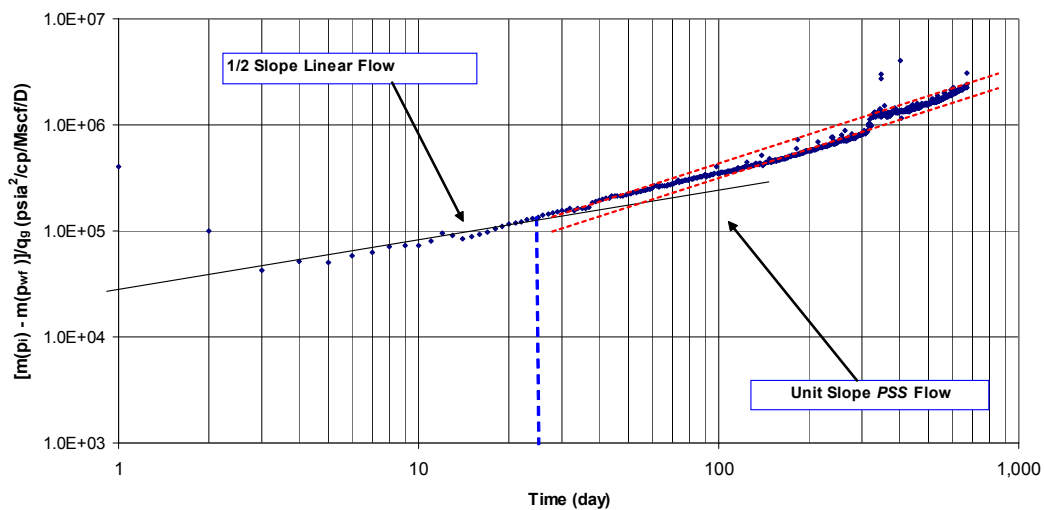

Fig. E-41—Well CC-2 production history.

Fig. E-42—Log-log diagnostic plot of $\Delta m(p)/q_g$ vs. t for well CC-2 which shows transient linear period and two unit slope *PSS* periods.
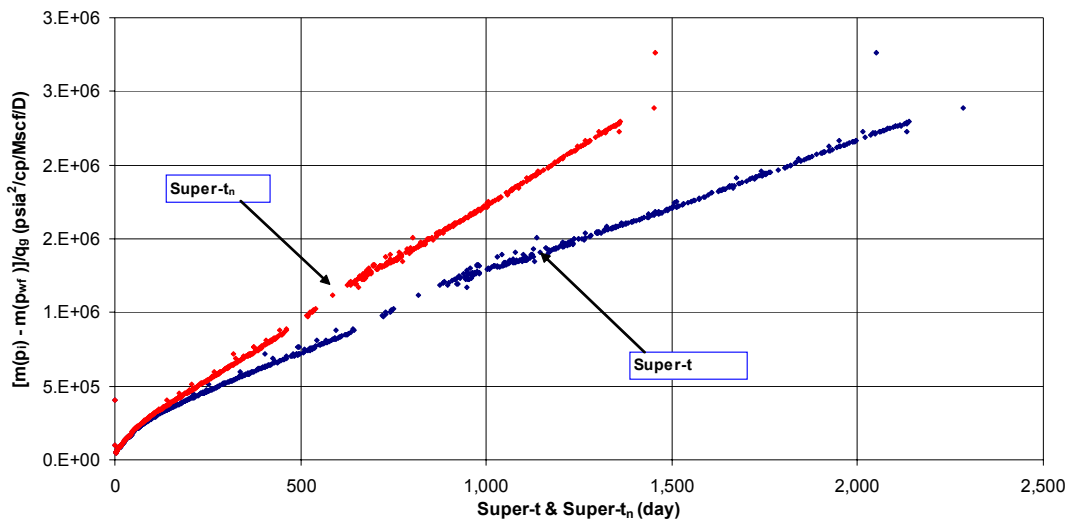

Fig. E-43—Shows comparison between Super-t and Super-t_n for Well CC-2
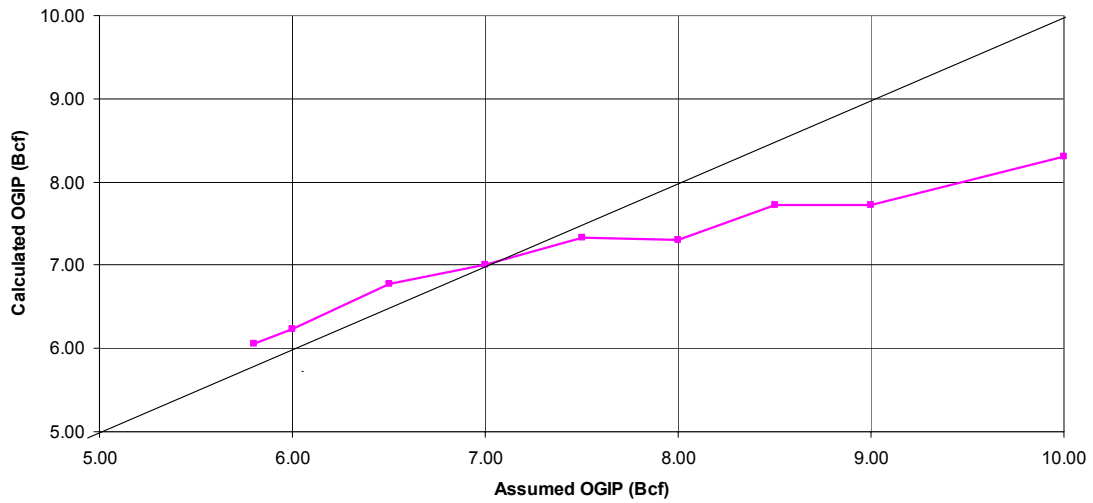
Fig. E–44—Shows the result from iteration procedure for calculating the correct OGIP by using normalized pseudotime method for Well CC-2.

VITA

Name: Mazher Hassan Ibrahim

Permanent Address: 507 Richardson Building

                    College Station, TX 77843-3116

Education: B.S., Petroleum Engineering

                    Suez Canal University

                    Suez, Egypt, 1991

                    M.S., Petroleum Engineering

                    Suez Canal University

                    Suez, Egypt, 1996

                    Ph.D., Petroleum Engineering
                    Texas A&M University,
                    College Station, Texas, U.S.A.
                    (Jan. 2000 - December 2004)